Transient modelling of the flow and heat transfer in a once through helical coil steam generator tube for a Small Modular PWR

G Botha

22161368

Dissertation submitted in partial fulfilment of the requirements for the degree *Magister* in Nuclear Engineering at the Potchefstroom Campus of the North-West University

Supervisor: Prof M van Eldik

May 2016

“Fear is temporary, regret is eternal”

ABSTRACT

With a shortage of electricity experienced worldwide, the modular nuclear reactor has become a viable solution to consider. The main focus when developing a modular reactor is for it to be compact and easily manufactured and transported. This necessitates the redesign of the once bulky steam generator (SG).

New technological developments are therefore being looked into, including integrated once through (IOTSG) and once through helical coil steam generators (OTHSG). This allows for a more compact design than the conventional u-tube steam generators (UTSG), and leads to the SG being able to produce super-heated steam with associated higher generation efficiencies.

Various mathematical models exist to simulate UTSGs, but limited work could be found for the new OTHSG designs. From the literature review it is evident that abundant work has been done on the modelling of single phase flow within tubes, but for two-phase flow boiling within pipes the research is more limited. The different flow regimes, cross-over points and bubble formations make the modelling even more challenging when transient conditions are considered.

The aim of this study is to develop a transient model that can simulate the OTHSG from start-up through boiling and up to super-heated steam conditions. In order to develop a thorough understanding of the fundamentals, a customised transient homogeneous two-phase flow model is first developed using Engineering Equation Solver (EES), and the results compared with that of a model generated using the commercial software package Flownex. Flownex is then used to model more complex transients.

It was shown that the helical coil of the SG can be simplified and represented by equivalent vertical pipes in parallel with an enhanced heat transfer coefficient applied to cater for the coil geometry. The steady state results obtained compare well with experiments done by Cinotti (2002) on the IRIS reactor's OTHSG. When evaluating the Flownex result for the heat transfer rate of the OTHSG, including the coil enhancement factor, the error was 0.48%. The largest error was found to be that of the predicted secondary side pressure loss, namely 2.87%. A simulation of a cold start-up transient was successfully performed and the results also compare well with experimental data. Evidence of such a transient simulation could not be found elsewhere in literature.

Keywords: transient modelling, helical coil, once through steam generator, two-phase heat transfer, coil enhancement factor.

DECLARATION

I, Gerrit Botha (Identity Number: 9110175120086, Student number: 22161368), hereby declare the work contained in this dissertation to be my own. All information which has been gained from various journal articles, text books or other sources has been referenced accordingly.

G. Botha. — 30 October 2015

DATE

Prof. M. van Eldik. — 2 November 2015

DATE

Prof. P.G. Rousseau. — 2 November 2015

DATE

ACKNOWLEDGEMENTS

I would like to extend my utmost gratitude to my study leaders; Professors Martin van Eldik and Pieter Rousseau, for their input, guidance and advice during this study. Another special thank you to Dr Anthonie Cilliers for the opportunities he made me part of that help grow my personal and professional life. To The Department of Science and Technology and The National Research Foundation, thank you for the financial support for the 2014 term of this study, without it, the study would not have been possible. To Miss Francina Jacobs, who was always there when I needed advice and support. To the admin staff of The North-West University`s Mechanical and Nuclear Engineering Department: Dalien Zietsman, Lilian van Wyk, Mientjie Botha and Sue-mari Benson, thank you, for the early morning coffees that helped kick start the day, it was appreciated. To my parents, Louise and Etienne Botha, although they were way back home, they were always there for moral support, prayers and motivation. To my friends for always being there, I appreciate it. Lastly, and most important, my Heavenly Father, for granting me this opportunity, the wisdom and endurance to complete this study. . .

TABLE OF CONTENTS

LIST OF FIGURES

LIST OF TABLES

LIST OF EQUATIONS

NOMENCLATURE

ABBREVIATIONS

BWR	Boiling Water Reactors
CV	Containment Vessel
EES	Engineering Equation Solver
FBNR	Fixed Bed Nuclear Reactor
HTR	High Temperature Reactors
HWR	Heavy Water Reactors
IAEA	International Atomic Energy Agency
IMR	Integrated Modular Water Reactor
IOTSG	Integrated Once Through Steam Generator
IRIS	International Reactor Innovative and Secure
LMCR	Liquid Metal Cooled Reactors
LOCA	Loss of Coolant Accidents
LWR	Light Water Reactors
NPP	Nuclear Power Plant
OTHSG	Once Through Helical Coil Steam Generator
PV	Pressure Vessel
PWR	Pressurised Water Reactor
SCFD	System Computational Fluid Dynamics
SG	Steam Generator
SMART	System-Integrated Modular Advanced Reactor
SMR	Small Modular Reactor
UTSG	U-Tube Steam Generator

DEFINITIONS

Homogenous:	The two phases are considered uniformly mixed and the average values are used.
Medium reactor:	A reactor with an electrical output between 300 and 700 [MWe].
Modular reactor:	A reactor that is designed so that all critical components are contained within the pressure vessel, making the transport and implementation easier and safer.
Primary:	Primary loop that circulates through the reactor core. Fluid is under high pressure and remains single phase.
Pseudo-steady state:	Is the steady state or stabilized solution that a flow network achieves after a transient is initiated. A snap shot of the fluid properties and flow conditions is assumed to be steady state as the change between time steps are neglectable.
Secondary:	Secondary loop that circulates through the turbines and condenser. It is at a lower pressure and undergoes phase change within the cycle.
Small reactor:	A reactor with an electrical output of 300 [MWe] or less.
Super heating:	Heating a fluid above the saturation temperature to produce super-heated steam.
Two-Fluid:	Each phase of the fluid is modelled independently
Two-phase:	The condition where a fluid is a combination of liquid and vapour phase.
Upset phenomena:	Any situation that occurs that is not considered normal operation conditions within a NPP

SYMBOLS

A	Area	$[m^2]$
A_{ff}	Free Flow Area	$[m^2]$
A_p	Perimeter	[m]
C_{th}	Thermal Capacity	[J/K]
C_p	Heat Capacity	[J/kgK]
D	Diameter	[m]
F	Two-phase Multiplier	[-]
f	Friction Factor	[-]
g	Gravitational Acceleration	$[m/s^2]$
H	Height	[m]
h	Enthalpy	[J/kg]
h_c	Heat Transfer Coefficient	$[W/m^2K]$
k	Conductivity	[W/mK]
L	Length	[m]
$\dot{m}$	Mass Flow	[kg/s]
Nu	Nusselt	[-]
P	Pressure	[Pa]
Pr	Prandtl	[-]
Q	Heat	[W]
r	Radius	[m]
Re	Reynolds Number	[-]
S	Two-phase Suppression	[-]
t	Time	[s]
T	Temperature	[K]
~~V~~	Volume	$[m^3]$

V	Velocity	[m/s]
W	Work	[W]
X	Quality	[-]
z	Height	[m]

GREEK SYMBOLS

α	Interrogation Factor	[-]
χ_{tt}	Lockhart-Martinelli	[-]
δ	Curvature Ratio	[-]
Δ	Change in	[-]
ε	Void Fraction	[-]
λ	Non-dimensional Pitch	[-]
σ	Surface Tension	[N/m]
∅	Gas multiplier	[-]
μ	Viscosity	[Ns/m]
ρ	Density	[kg/m^3]

SUBSCRIPTS

e	Outlet
g	Gas
H	Hydraulic
i	Inlet
l	Liquid
Max	Maximum Value
Min	Minimum Value

p	Primary
Sat	Saturation
s	Secondary
0	Total

SUPERSCRIPTS

0	Previous Time Step

CHAPTER 1 - INTRODUCTION

1.1 BACKGROUND

As technology advances and designers strive towards more efficient power plants, the development of new cycle components is at the order of the day. One area of technological advancement is the Small Modular Reactor (SMR), based on either the pressurised water reactor (PWR) or the boiling water reactor (BWR) designs. An important requirement for SMRs is that the steam generator (SG) needs to be very compact and fully integrated within the plant (International Atomic Energy Agency, 2012).

In order to decrease the size of the nuclear island, and make the reactor modular, a different design moving away from the standard U-tube steam generator (UTSG) must be used. New integrated once through steam generators (IOTSG) and once through helical coil steam generators (OTHSG) are being looked into as they have specific advantages when it comes to steam quality, but manufacturing comes at a cost (Bonavigo & De Salve, 2011). These smaller integrated designs allow for more compact reactor designs with less piping and components. Less parts leads to less components that can fail during operations and also results in a decrease in overall construction time (IRSN, 2013).

Seeing that this is new technology, there are currently very few mathematical models available that can predict the dynamic response of an OTHSG. The existing models are only able to model certain scenarios such as loss of coolant accidents or transients where all the boiling regimes are already established (Adballa, 1993). The ability to predict the normal operating conditions is crucial to analyse the design of this type of SG.

As most SMRs are still in a conceptual or design phase it is difficult to evaluate the performance of the plants into which the OTHSGs will be incorporated. However, an accurate dynamic model can assist in making design alterations based on operating scenarios that produce unwanted results during the simulation. The main advantage of such a simulation model is the ability to simulate phenomenon, scenarios or configurations to enable cost effective designs, as a variety of aspects can be changed to optimize for cost and/or efficiency (Hoffer, Sabharwall, & Anderson, 2011).

1.2 PROBLEM STATEMENT

As steam is being produced in the OTHSG of a SMR, there is phase change taking place. The resultant two-phase flow is complex and intricate to simulate. Therefore an applicable mathematical model is needed to simulate the dynamic response of an OTHSG. From a review of the literature it was found that there are currently no readily available dynamic models to simulate the SG behaviour from start-up to full power, as well as through other normal transient operating conditions.

1.3 OBJECTIVES

The objectives of this study are:

- Conduct a literature review to determine what types of SG are envisioned to be used in the current development of SMRs of the PWR type.
- Obtain a deeper understanding of dynamic modelling and two-phase flow in thermal-fluid systems. Then to formulate an appropriate modelling approach for simulating the two-phase flow in a SG of a SMR for transient conditions with the correct conservation, heat transfer and pressure drop equations for the different regimes.
- Develop an appropriate simulation model to simulate the dynamic response of a tube in an OTHSG and to verify the results generated with the model.
- Apply the model to simulate a typical start-up transient that would be encountered in a SMR reactor to show the capabilities and limitations of the model.

This study will not aim to develop or design a complete new type of SG. Furthermore, the transient model will not be used to investigate upset or accident phenomena.

1.4 METHODOLOGY

The primary aim of this study is to develop a dynamic model for an OTHSG tube which adequately captures the transient response and two-phase flow boiling phenomena occurring in the SG, from start-up to normal operating conditions.

In order to accomplish this task, the relevant literature regarding two-phase flow and transient thermal-fluid process modelling needs be studied. As soon as the necessary understanding of two-phase flow heat transfer is obtained, a homogeneous simulation model of a single vertical SG tube will be developed for a numerical thermal hydraulic solver named Engineering Equation Solver (EES).

As the simulation of two-phase flow is complex, the correctness of the numerical implementation has to be investigated. To achieve this, the primary and secondary sides of the SG tube configuration will first be viewed independently to ensure that the model can obtain a realistic solution for both streams. Simplified correlations and fluid properties will be used during the evaluation along with a constant heat flux over the surface. The selected heat flux will be such that the secondary side can undergo the required phase change.

This study will mainly focus on the details of the secondary side, as it is known that the primary side does not undergo any phase change during normal operations. To ensure the numerical integration stability, the transient will need to be evaluated for a few pre-selected time step intervals. The numerical stability of the transient will first be tested for fixed input boundary values and then for a step change in primary inlet temperature.

With the stability achieved, the simplified fluid properties will then be replaced with the correctly calculated properties at these conditions. The combined model is then re-evaluated to ensure that the discontinuities in the fluid properties are handled correctly.

The next step will be to expand the model by incorporating the correct two-phase heat transfer and pressure drop correlations for the secondary side. As there is no phase change on the primary side the normal single phase heat transfer and pressure drop correlations will be used.

The homogeneous two-phase flow model developed in EES, will then be verified with a model developed in Flownex (Flownex, 2012). Due to the numerous advantages, like solution time and stability of using Flownex, the Flownex model will then be expanded to include the more complex helical geometry of an OTHSG. The OTHSG Flownex model will also be verified with steady state results obtained in literature.

For the final part of the study a cold start up transient simulation will be run to inspect the thermal dynamic response of the SG, as existence of a simulation like this could not be found in literature.

CHAPTER 2 – LITERATURE STUDY

2.1 INTRODUCTION

The International Atomic Energy Agency (IAEA) is currently monitoring various SMR developments that have the potential of producing cost-effective commercial modular reactors (International Atomic Energy Agency, 2012). These SMRs include all current reactor designs e.g. Light Water (LWR) of the PWR and BWR types, Heavy Water (HWR), High Temperature (HTR) and Liquid Metal Cooled Reactors (LMCR) designs. For this study, the focus will be placed on SGs for PWRs, due to the fact that these reactors are currently the most widely implemented and operated reactors (International Atomic Energy Agency, 2012). This chapter will cover the following:

- Which SGs are most widely used in modern SMR PWRs
- Two-phase flow modelling
- Single and two-phase heat transfer
- Single and two-phase pressure drops
- Heat transfer enhancement factors

2.2 CURRENT PWR`S IN DEVELOPMENT

According to the IAEA`s document on the current status of SMRs (International Atomic Energy Agency, 2012), there are currently 131 SMR units in operation in 26 member states and 14 new SMRs under construction (International Atomic Energy Agency, 2012). In the sections to follow an in-depth study will be done of the current SGs used in the PWR type SMRs. The countries that are currently operating or developing SMR PWRs will be discussed in the subsequent section:

2.2.1 ARGENTINA

The Argentinean Government is operating a 25 [MWe] prototype PWR called the CAREM-25, which has been operational for a number of years (International Atomic Energy Agency, 2012). This reactor incorporates twelve integral mini-helical OTHSGs. These are situated within the Pressure Vessel (PV) around the upper perimeter. The placement of the SG induces forced convection due to gravitational forces, which in turn induces natural

convection. This resulted in the elimination of active pumping systems. The SG generates steam at 47 [Bar] with 30 [ºC] of super heating (Magana, Delmstro, & Markieqicz, 2010).

2.2.2 BRAZIL

The Brazilian Fixed Bed Nuclear Reactor (FBNR) is a conceptual 72 [MWe] modular unit, which will have special design features. The fuel chamber will be held in place by means of forced circulation, supplied by means of a high volume flow pump (Annonymous, 2011). If the system is interrupted, the core drops into a storage unit due to gravity and is kept below critical mass, which in turn shuts down the reactor. The unit will use a shell-and-tube SG to develop steam at 326 [ºC] and 16 [MPa] (Sahin, 2007).

2.2.3 CHINA

The People's Republic of China has an operational CNP-300 PWR already deployed in 1991. It is capable of producing 325 [MWe] with upright U-tube SGs that produces steam at 51.9 [Bar] and 260 [ºC] (The Hong Kong Institution of Engineers, 2008). The designers are investigating methods to use the current design along with new technologies to upscale the CNP-300 to develop the CNP-600 and CNP-1000 models. These upgrades will be capable of generating 600 and 1000 [MWe] respectively (Yuming, 2010).

2.2.4 FRANCE

The French are currently developing an innovative conceptual modular underwater reactor, FlexBlue, that can produce between 50 and 205 [MWe] depending on the client`s needs (DCNS, 2014). Due to the fact that it is still currently in development, no details regarding the SG have been released. The aim of the system is to produce steam at 15.5 [MPa] and 310 [ºC] (DCNS, 2014).

2.2.5 JAPAN

The conceptual Integrated Modular Water Reactor (IMR), currently under development by Mitsubishi Heavy Industries, will be designed to generate 350 [MWe] with the use of four large integrated OTHSGs. These SGs will generate steam at 5 [MPa] and 296 [ºC]. The design reduces the containment vessel (CV) of the IMR dramatically from that of other PWRs with a similar power rating as the IMR (Mitsubishi, 2011).

2.2.6 KOREA

The Korean System-Integrated Modular Advanced Reactor (SMART) is a 100 [MWe] integrated reactor, that is awaiting final design approval. As with the CAREM-25, the SMART utilises eight OTHSGs that is situated within the circumference of the PV, to produce superheated steam at 15 [MPa] and a superheating of 30 [ºC] (Lee, 2010).

2.2.7 RUSSIAN FEDERATION

According to the IAEA, the Russian Federation is currently developing seven SMR PWRs (International Atomic Energy Agency, 2012). The developments include small modular reactors for the use in modern icebreakers; to larger units developed for commercial power generation. The seven reactors that are currently monitored by the IAEA are as follows:

2.2.7.1 ABV-6M

The ABV-6M reactor, currently in the design phase, is of the floating modular power plant design. The 8.6 [MWe] units will be preassembled on the floating platform and then transported to the designated location. The integrated design ensures a compact reactor with all the components situated within the CV. The design report specifies that an internal OTHSG will be used in the final design (Afrikantov OKB Mechanical Engineering, 2011).

2.2.7.2 SHELF

SHELF is a 6 [MWe] conceptual reactor, intended for underwater energy production, with the same design features as the FlexBlue. This will be used for offshore drilling and exploration missions, where it is difficult to provide power by other means. The reactor will incorporate an integrated OTHSG, to produce steam at 17 [MPa] and 320 [ºC] (International Atomic Energy Agency, 2012).

2.2.7.3 KLT-40S

The KLT-40S is the predecessor of the RITM-200 and this type of reactor was used with the previous generation of icebreakers. The 38 [MWe] unit uses external recuperative helical coil steam generators to produce steam at 290 [ºC] and 3.82 [MPa]. The external steam generators resulted in very bulky reactors, which are the reason for the KLT-40s being phased out (International Atomic Energy Agency, 2012).

2.2.7.4 RITM-200

The RITM-200 is a 55 [MWe] PWR reactor that is currently in the design phase by the Russian company, OKBM Afrikantov, to be used as propulsion for their new fleet of icebreakers. These reactors are scheduled to replace the KLT-40s as soon as the designs and licensing are completed (International Atomic Energy Agency, 2012). More details on the reactor`s steam generator are currently unavailable (UX Consulting Company, 2012).

2.2.7.5 VBER-300

The VBER-300 reactor is another conceptual Russian reactor, designed for use on new age icebreakers. The reactor`s range is dependent on the amount of steam generator loops installed, from 150 [MWe] generated using a two-loop up to 600 [MWe] from a six-loop reactor cycle. The loops use modular OTHSGs to produce steam (International Atomic Energy Agency, 2012). More details about the pressure and temperature of the generated steam are currently not available.

2.2.7.6 VVER-300

Another Russian floating reactor, which is in the design phase, is the VVER-300, a 300 [MWe] two-loop system being designed for use at small power grids in remote locations. The in-line shell-and-tube steam generator is being designed to produce dry saturated steam (Gidropress, 2011).

2.2.7.7 UNITHERM

The Unitherm is an unmanned concept design for marine applications capable of delivering 2.5 [MWe]. The integrated design allows for a small and compact reactor, suitable for unmanned submarines and drilling explorations. The reactor will use a vertical tube IOTSG to produce steam at 3 [MPa] and 234 [ºC] (International Atomic Energy Agency, 1995).

2.2.8 INTERNATIONAL CONSORTIUM

The International Reactor Innovative and Secure (IRIS) is an integral PWR reactor, currently being developed by the International Consortium and are in the basic design phase. The 335 [MWe] unit provides steam at 15.5 [MPa] and 330 [ºC] by means of modular OTHSGs. The main aim of the IRIS reactor is to provide safe electricity by means of a small integral reactor

(Carelli, 2004). The design data states that the SG will have an annular design with the coil passing through the annulus. Test data for the SG of this reactor was found and will be used as the bench mark and verification of the model in the preceding chapters.

2.2.9 UNITED STATES OF AMERICA

The United States of America, just like the Russian Federation, is developing a number of reactors, which has the aim for electricity production in Nuclear Power Plants (NPP). They are focussing on increasing the power output of the SMRs to be able to build modular NPPs.

2.2.9.1 MPOWER

The mPower is an integrated PWR, in the basic design phase, capable of producing 180 [MWe] and situated in an underground CV. The mPower reactor utilises an integrated straight tube IOTSG to produce steam at 14.1 [MPa] and 300 [ºC] (Ales, 2012).

2.2.9.2 NUSCALE

The NuScale NPP, likewise in the basic design phase, is based on a submerged modular design. The modules are placed in a centralized cooling bath to remove excess heat. The integrated unit produces 45 [MWe] and utilizes an integrated OTHSG to produce steam at 8.72 [MPa] and 290 [ºC] (US Nuclear Regulatory Commission, 2014).

2.2.9.3 WESTINGHOUSE

The larger Westinghouse SMR reactor will be designed to develop 225 [MWe] by the process of integrated recirculating, straight tube IOTSGs (Westinghouse SMR, 2011). Once the design moves from the basic design phase, more details regarding the steam generated will be known.

From this section it can be concluded that the current trend in SG design for SMR PWRs are that of the OTHSG layout. In the subsequent section a study regarding different IOTSG types will be done along with the advantages of each.

2.3 STEAM GENERATORS

Steam possesses immense power, this power is revealed when witnessing the eruption of a geyser or the steam bursts from water that is exposed to red hot metal (Lamb, 2013). From the beginning of the nineteenth century, man tried to utilize this power with technology, from a basic steam kettle to the modern nuclear reactor.

The first machinery that utilised the power of steam was steam powered pumps, which were developed in the 1700`s, to pump water from mines. From there steam powered locomotives, boats, and airplanes arose (Teir, 2002). To date steam is one of the main working fluids used for energy generation worldwide (Invernizzi, 2013).

From the Industrial Revolution, coal fired power plants were the main provider of electricity. However, due to the environmental impact other sources including renewable and nuclear applications have been researched (Lamb, 2013).

In PWR NPP applications, pressurised water is used to cool the core. This water is heated in the core and contracts radioactive particles. As this water contracts radiation, it must be contained in the containment building and cannot be used to drive the turbines directly and a secondary system needs to be installed to develop pure steam to drive the turbines (Green & Hetsroni, 1995). The secondary system leaves the containment area and as a result must be free of any radioactive particles. Hence, to isolate the radioactive primary system from the secondary system a SG is used. Consequently, SGs are used to isolate the primary and secondary water loops from one another and to ensure that no radiation leakage can occur.

2.3.1 U-TUBE

In order to separate the primary and secondary water loops, an inverted UTSG is used (Bonavigo & De Salve, 2011). Bundles of U-tubes are submerged in a pool of the secondary water. The high-pressure primary water flows through the tubes and transfers its heat to the secondary pool by method of conduction (Fletcher & Schultz, 1995).

The secondary water enters an annular area, Figure 1, and travels downwards. It is preheated, by mixing it with water coming from the separator deck, and enters at the base of the U-tube. As the secondary pool water starts to heat, it begins to boil and steam travels to the top of the SG, where the saturated steam and water droplets are separated with driers and the steam is

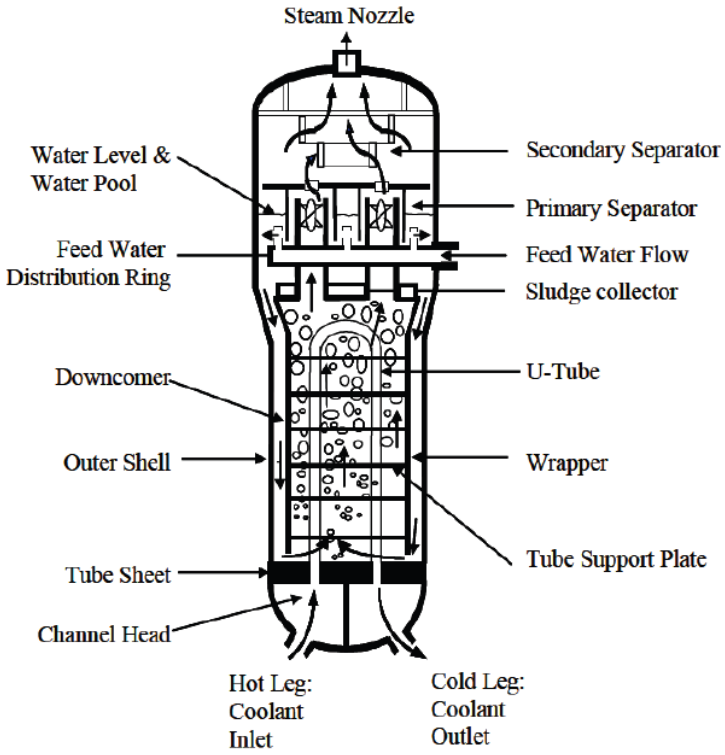

Figure 1 - U-tube steam generator (Green & Hetsroni, 1995).

bled off (Fletcher & Schultz, 1995). As steam is removed the secondary water pool level reduces and make up water, entering via the annulus, keeps this level constant while boiling is maintained. This layout is illustrated in Figure 1. UTSG are only capable of producing saturated steam and do not possess the ability to produce super-heated steam. UTSG usually produces saturated steam at 268.9 - 294.1 [°C] (Fletcher & Schultz, 1995).

2.3.2 ONCE THROUGH CONFIGURATION

In order to increase the outlet vapour quality of the steam generated, a once through design is used. This can be seen as a concentric, tube-in-tube in shell counter-flow heat exchanger (Castleberry, 2012). Two types of once through generators are currently in use, namely straight tube and helical tube SGs.

2.3.2.1 STRAIGHT TUBE

In the straight tube OTSG the hot primary cycle water enters the header at the top of the SG and passes through the tube sheet. The primary fluid flows down through the inner tube as well as the area between the external tubes as shown in Figure 2. It then flows through the lower tube sheet and back to the reactor core, as illustrated by Figure 3. The secondary water

enters the SG though an annular distributor, which flows down the annular area and enters the lower tube sheet. The secondary water in turn enters the annular area between the two concentric tubes. There exist four distinct heat transfer regions within the SG, namely (Rousseau, 2014):

- Feed water heating: Steam is bled off from the turbines to increase the temperature of the feed water and increase the production unit's efficiency. Feed water heating also occurs in the annulus of the SG, as the secondary water flows down the annulus to the tube sheet.

- Nucleate boiling: Vapour bubbles start to form in the lower region of the tubes as the primary water travels up in the annular area between the two tubes.

- Film boiling: As the tubes are in contact with warmer primary water higher up in the SG, film boiling occurs. The vapour begins to form a film on the tube surface as the bubbles increase in size.

- Superheating: As the steam rises to the top, the even warmer tubes dries and super heats the steam.

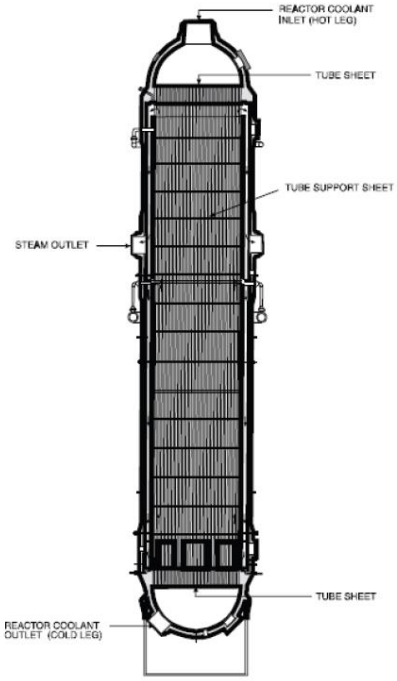

Figure 2 - Straight tube once trough steam generator (Castleberry, 2012).

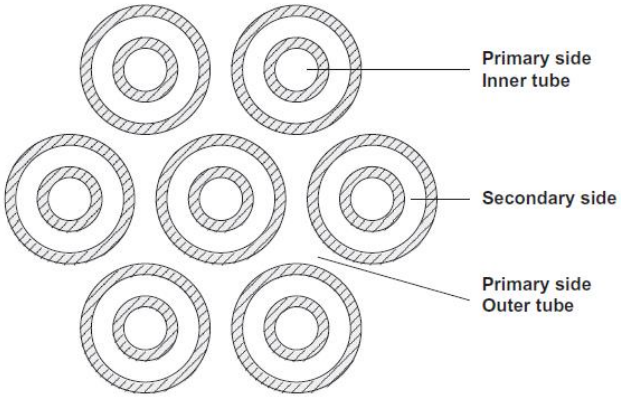

Figure 3 - Flow path in a Straight tube once trough steam generator (Castleberry, 2012).

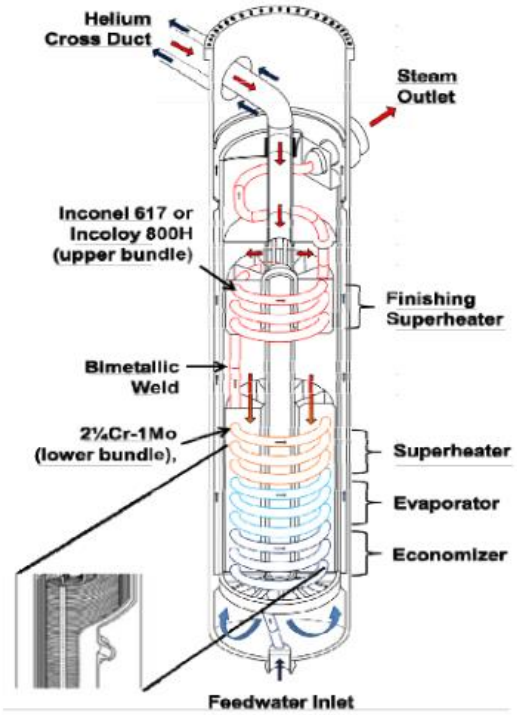

Figure 4 - Once through helical coil steam generator (Hoffer, Sabharwall, & Anderson, 2011).

2.3.2.2 HELICAL COIL

To further increase the contact area of the SG, helical coils are used as illustrated by Figure 4 above. OTHSGs are used with next-generation nuclear reactors that operate at higher temperatures of up to 750 [°C] (Olson, Li, & Wu, 2013). The OTHSG is a very compact heat exchanger due to the helical tubes and no concentric pipes present. The OTHSG is currently at the forefront of SG technology, with the heat transfer efficiency up to 43% more than for a straight tube IOTSG (Hoffer, Sabharwall, & Anderson, 2011).

2.4 FLOW REGIMES

Before the development of a mathematical model for a SG can commence, the different types of flow inside the tubes needs to be comprehended. As water is brought to super-heated levels, the vapour and liquid phases will be present in different ratios throughout the SG (Wolverine Tube, Inc., 2007). This ratio, with liquid-vapour distributions, affects the heat transfer along the length of the tube. As IOTSGs are usually vertical, the flow patterns for vertical tubes will be reviewed. For the simultaneous upward flow of gas and liquid in a vertical tube the developed gasses will produce distinct flow patterns as seen in Figure 5 below (Stevanovic & Prica, 2007).

- Bubbly flow: Bubbles start to nucleate at the tube walls as the fluid moves. The discrete bubbles are nearly spherical in shape and are much smaller that the tube diameter.

- Plug flow: As the void fraction increases adjacent bubbles increases and converges into bigger bubbles. This result in bubbles with dimensions similar to that of the tube. Slug flow has the characteristic flow shape of a hemispherical nose and blunt tail as seen in Figure 5. These bubbles are referred to as Taylor Bubbles after the instability phenomenon of the same name. Slugs of water separate the bubbles from one another. A small film of liquid surrounds the bubbles, as the bubble raises the liquid runs down the tube wall, but the net flow of the mass is still upward.

- Churn flow: As the gas velocity increases the bubbles becomes unstable with the counter-flow of gas and liquid that leads to an oscillating movement with a net upward flow. The gravity and shear forces acting on the bubbles and film layer result in the instability.

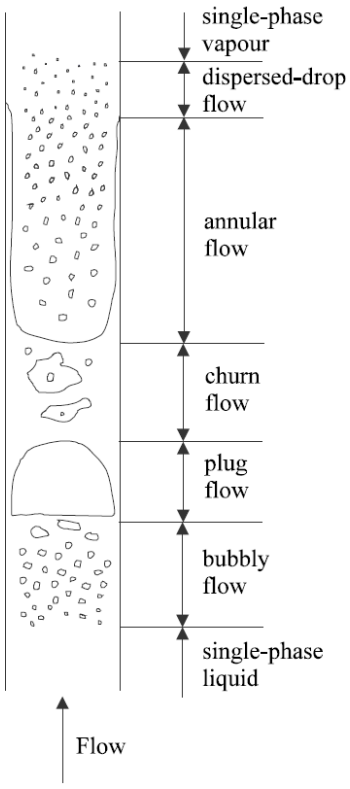

Figure 5 – Two-phase flow regimes in vertical tubes (Wolverine Tube, Inc., 2007).

- Annular flow: The liquid film is expelled to the tube wall given that the interfacial shear, due to the high velocity, overcomes the effect of gravity. This forms an annular ring of liquid around the internal surface of the tube, while the gas forms a continuous phase at the centre. This flow regime is very stable and desired in two-phase flow due to the annular liquid cooling the tube wall and steam with entrapped liquid droplets coincide in the middle.

- Dispersed-drop flow: As the temperature is increased, the film layer starts to decrease. More steam is present and the danger of the film layer drying out and resulting in tube metal excursions may occur.

- Super-heated vapour: As the mist is dried out, super-heated steam is produced. This is then seen as single-phase flow.

2.5 MODELLING

The term ‘model’ refers to the use of engineering and fundamental equations to predict or represent physical phenomena encountered in daily problems. These models can be simple just to verify the magnitude of factors, or can be very complex to simulate a phenomenon in detail.

The modelling of two-phase flow has been intriguing scientists and engineers for numerous of years. It has been noted that different levels of complexity can be used to model this flow within tubes (Ishii & Hibiki, Drift-Flux Model, 2011), as will be discussed below.

2.5.1 TWO-FLUID MODEL

The complexity of the two-fluid model is due to the separate evaluation of the momentum, mass, and energy equations for each of the two fluids present (Fick, 2013). Because two fluids are identified, different velocities, temperatures and flow conditions exist in the fluid stream. Due to the constant changing of the flow within a two-phase mixture a number of closure equations are required to balance the mass, momentum, and heat transfer between the gas and liquid phases (Ishii & Hibiki, Two-Fluid Model, 2011).

As the geometry of the interfacial boundary between the two fluids is irregular and dynamic, it results in numerous closing equations. In addition to the six conservation equations, see Figure 6, the closing equations describe the relations of the mass, energy and momentum

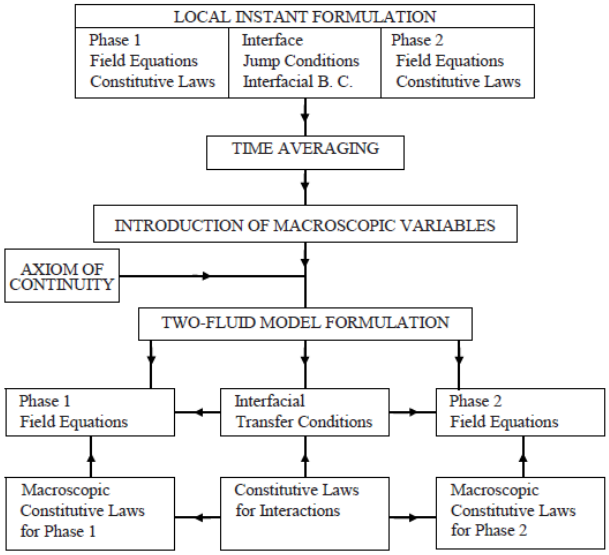

Figure 6 - Two-fluid model (Ishii & Hibiki, Two-Fluid Model, 2011).

transfer as phase changes are taking place (Ishii & Hibiki, Two-Fluid Model, 2011). Most of these equations are gathered from empirical results and contribute to the complexity of the model (Wulff, 2010). This formulation results in 29 equations used to solve the simplest case of the two-fluid model.

It has been found that the formulation of the two-fluid model presents difficulties, even within modern models. As mentioned, the complexity of the ever-changing geometry and contact areas that govern the transfer equations results in difficulty solving the equations. Wulff (2010) emphasises that the closure equations are received from empirical data and that there are still important closure laws that are omitted. This results in errors and solution problems when large changes in parameters or boundary conditions are introduced.

For System Computational Fluid Dynamics (SCFD) it is ideal to solve the equations for each node before progressing to the next node. Unfortunately, due to the closure equations it is mathematically impossible to solve the two-fluid model in this manner, as it describes the complete localised flow. For this, it needs to suppress certain aspects and incorporate assumptions to allow for solving the two-phase model (Levy, 1999). Some of these assumptions are considered to apply averaging techniques as stated in textbooks. The averaging can be classified into space averaging, time averaging, or statistical averaging. The literature describes in detail the techniques applied (Ishii & Hibiki, Two-Fluid Model, 2011), but there are still quite a number of concerns regarding the formulation of the two-fluid model (Stadtke, 2006).

2.5.2 DRIFT-FLUX MODEL

Due to the complexities introduced by the two momentum conservation equations in the two-fluid model, these complicating aspect needs to be solved. By retaining the two mass and energy conservation equations and simplifying the momentum equations, some of these complexities can be mitigated (Ishii & Hibiki, Drift-Flux Model, 2011) and the Drift-Flux model, as shown in Figure 7, was developed.

The Drift-Flux model is built on the assumption that the two fluids have mechanical equilibrium. This states that the two phases are at the same pressure resulting in the two conservation of momentum equations to be simplified into one (Ishii & Hibiki, Drift-Flux Model, 2011). This model takes the different fluid velocities of the two phases into account, resulting in a non-homogeneous model. In order to use the Drift-Flux approach, a slip ratio equation needs to be introduced. A slip ratio is used to relate the different phase velocities in the system. This allows for the use of a single representative momentum conservation equation, even though the velocities differ (Fick, 2013).

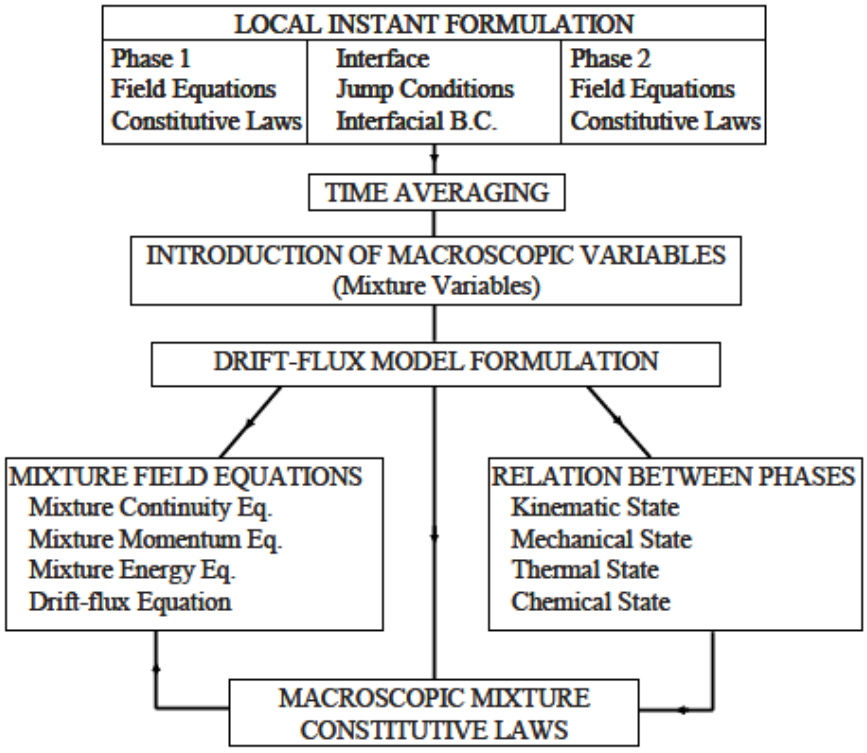

Figure 7 - Drift-Flux model (Ishii & Hibiki, Two-Fluid Model, 2011).

Because the Drift-Flux model describes the flow as a mixture of the two phases, it is also referred to as the mixture model. The term tightly (strongly or closely) coupled refers to the phases` relative velocities towards one another. In tightly coupled mixtures, the relative velocities between the two phases are small. This leads to the Drift-Flux model being better adapted to closely coupled phases, than the two-fluid model. The rapidly changing geometry is neglected by means of the mixture assumption in the Drift-Flux model (Wulff, 2010).

It is mentioned in literature that the main assumption of the Drift-Flux model is the relaxation of the conservation of momentum. If non-thermal equilibrium is assumed the Drift-Flux model reduces to five conservation equations and one coupling slip equation (Levy, 1999). If thermal equilibrium is assumed between the two phases, the two energy conservation equations can also be reduced to one, resulting in only four conservation equations (Levy, 1999).

With the thermal equilibrium, the Drift-Flux model is defined by an energy mixture conservation equation, two mass conservation equations, a mixture momentum equation, and coupled by the slip equation in terms of the relative velocities of the phases (Ishii & Hibiki, Two-Fluid Model, 2011). The two conservation of mass equations account for the transfer of mass over the boundary layer as this is a dependant on the phases' velocities. As the amount of closure and conservation equations are decreased along with the simplification of the mixture approach the Drift-Flux models is more stable and solves faster that the two-fluid model (Wulff, 2010).

2.5.3 HOMOGENEOUS NON-EQUILIBRIUM

If the phase velocities of the Drift-Flux model are assumed to be equal, we obtain the homogeneous non-equilibrium model (Morin, 2013). Even though the non-equilibrium model assumes equal velocities, the two phases can be at different temperatures hence the model name (Aakenes, 2012). This model approach also assumes that the two phases are homogeneous, thus combining the two momentum equations into an equivalent mixture momentum equation (Stadtke, 2006).

2.5.4 HOMOGENEOUS WITH EQUILIBRIUM

The last simplification that can be made from the Drift-Flux model is to assume that both phases have thermal equilibrium (Aakenes, 2012). This is the simplest model used to predict two-phase flow systems and consists of the most simplified assumptions.

When viewing the boundary layer between the two phases we assume that there is no slip present, thus an equal phase velocity along with the thermal equilibrium (Ambroso, Chalons, & Coquel, 2009). The model also requires that both phases be subjected to the same local pressure (Rousseau, 2014). If it is assumed that the boundary layer is infinitely thin, it can be deduced that the transfer rate between mass, momentum and energy is instantaneously resulting in a single pseudo fluid. This implies that there is no interfacial-coupling present, since all the transfers are defined by the mechanical and thermal equilibrium between the phases (Stadtke, 2006). As mentioned, this is a further simplification of the four-equation model and the thermal equilibrium assumption results in a reduction to three equations, namely the conservation of mass, energy, and momentum.

As this model is so simplified it was found that the computation time is much faster than with other models, but lacks the power to fully predict the detail of the flow (Levy, 1999). Computer software can use the equilibrium model to generate preliminary boundary values and fluid properties for more detailed models which would result in an overall decrease in computation time and increased accuracy (Levy, 1999).

In the next sections, the different methods of modelling two-phase flow will be cover, followed by the relevant theory and correlations.

2.6 STEAM GENERATOR MODELS

The complexity of a model greatly depends on the purpose of the results to be obtained. For example, the model to predict the amount of feed water needed to produce a certain amount of power in a NPP will be much less complicated than a model that predicts the flow of the water through the core. Due to the increase in complexity of the model, the computing time required increases accordingly. Therefore, when developing a dynamic model, the computing time and power needs to be kept to a minimum, while still retaining an accurate answer.

2.6.1 TWO-FLUID MODEL

Li *et al* (2008) developed a lumped parameter dynamic model using movable boundaries for a 10 [MW] HTR. This model is used for the prediction of the control system and verification of numerical results. The model was designed to have three zones, namely pre-heating, boiling, and super heating. To simplify the model, the entire tube bank was modelled as a single equivalent tube. From the results, it concluded that the model predicted the dynamics of a SG accurately; hence the change in boundary values was kept small.

Due to the six conservation equations, it is very time consuming to solve the two-fluid model. If the closure equations are not well defined or the step changes fluctuate too rapidly the model loses its stability and accuracy (Ishii & Hibiki, Two-Fluid Model, 2011). These results in the model being used for single pipe flow models where the maximum changes are known and does not occur too rapidly.

2.6.2 DRIFT-FLUX MODEL

The dynamic moving boundary model developed by Adballa (1993) used the drift-flux formulation to model an OTHSG. This formulation groups the coils as a single representative straight tube. The author discretised the SG into four regions for the different phases, namely preheating, nucleate boiling, film boiling, and super-heated region. This model unfortunately requires that all four regions be present to function properly and maintain stability.

The drift-flux approach is also used for the analysis of vertical pipe flow, fluidised beds, and pool boiling. For all these examples, the drift-flux model provides accurate results without taking up too much computing time (Zuber, Drift-Flux, 2014). The simplifications introduced to the drift-flux model results in a better stability and less effort to solve the models with a higher accuracy. This in turn makes the drift-flux model the most functional for modelling two-phase flow systems.

Levy (1999) proposed that the Drift-Flux model is the best balance between accuracy, stability and computing time, due to the simplification of closure equations and the assumptions being made. Most commercial thermal-fluid software packages use some form of the Drift-Flux model. The model recognizes to a certain extent the flow distribution within a channel and incorporate flow patterns. It also has the ability to handle co-current and counter current flow (Levy, 1999).

2.6.3 HOMOGENEOUS

From literature, the homogeneous non-equilibrium model is used for Loss of Coolant Accidents (LOCA) in nuclear reactors or the breaks in pressurised tubes. The accurate modelling of these situations is critical in the design of safety systems (Yuming, 2010). These models are used to model entire systems and do not focus on the details of the components. This approach handles components as black boxes and only calculates the output results (Levy, 1999). For both equilibrium and non-equilibrium approaches, the results can be obtained much faster, but the error of the solution might be quite prominent. Thus, this approach is suitable for system modelling; nevertheless for detailed component modelling the error might be such that it cannot be ignored.

2.7 HEAT TRANSFER AND PRESSURE DROP CORRELATIONS

Over the years flow phenomenon has been studied by multiple scientists for a wide variety of scenarios. The results from these studies were different correlations, each with a certain level of complexity and boundary conditions. In order to develop an accurate model one needs to evaluate these correlations for the phenomena that will be present in this study. In the rest of this section the different correlations will be discussed in more detail. The correlations discussed will be divided into the following groups (Incropera *et al.*, 2011):

- Heat transfer.
- Friction pressure drop.
- Void fraction.

2.7.1 HEAT TRANSFER CORRELATIONS

From thermodynamics it is known that even though a system is in equilibrium there is constant interaction with its surroundings (Incropera *et al.*, 2011). This transfer of energy can be in the form of work or heat. For the purpose of this study the contribution of heat transfer within tubes will be investigated.

2.7.1.1 SINGLE PHASE CONVECTIVE HEAT TRANSFER

The most commonly used correlation for the prediction of fully developed turbulent heat transfer is that of Dittus-Boelter (Incropera *et al.*, 2011). It is a function of the Reynolds and Prandtl number and is used for smooth round tubes. Through experimental tests the maximum error of the correlation has been confirmed to about ± 25 [%]. The Dittus-Boelter correlation has been validated for the following ranges of conditions: $0.7 \leq Pr \leq 160$, $Re \geq 10^4$ and $\frac{L}{D} \geq 10$, where L is the length of the tube segment.

Another widely used correlation is that of Sieder and Tate (1936), who suggested that the heat transfer is largely coupled to the ratio between the viscosity of the bulk and wall regions. The correlation is valid for the following conditions: $0.7 \leq Pr \leq 16000$, $Re \geq 10^4$ and $\frac{L}{D} \geq 10$.

A more accurate correlation was developed by Petukhov (1970). It has a maximum error of ± 10 [%] and is valid for: $0.7 \leq Pr \leq 2000$ and $10^4 \leq Re \geq 5\text{x}10^6$. This correlation uses the friction factor calculated from the Moody diagram (Petukhov, 1970).

Gnielinksi (1976) extended the Petkuhov correlation to include the transition regime. This correlation has an ± 10 [%] error for the same tested flow conditions as Petkuhov.

Jayakumar (2012) proposed that the torsional forces that act on a helical coil will increase the heat transfer. He added an enhancement factor to the trusted Dittus-Boelter correlation to account for the geometry of the coil.

Research by Coronel and Sandeep (2008) focused on the effect of the helical coil on the Nusselt number and further expanded on the work done by Seban and McLauglin (1963) to show that the coil effect increases the heat transfer significantly from that of a straight tube.

2.7.1.2 TWO-PHASE FLOW BOILING HEAT TRANSFER

Chen (1966) proposed the first correlation for flow boiling in vertical tubes. He stated that the two-phase heat transfer is a summation of nucleate and convective heat transfer. The result of this is that a steep temperature gradient is achievable in this section, relative to purely conductive heat transfer (Gungor & Winterton, 1986). As mentioned the vapour formed from the evaporation process increases the liquid velocity thus increasing the convective heat

transfer, although the liquid`s mass flow reduces (Wolverine Tube, Inc., 2007). To take these effects into account, Chen suggested that a suppression and multiplication factor be implemented in the summation.

For the multiplication factor of the two-phase flow found in the Chen correlation (Wolverine Tube, Inc., 2007), the Lockhart-Martinelli parameter is used (Wolverine Tube, Inc., 2007). It is defined as the ratio of the quality, density and viscosity between the saturated liquid and vapour properties. The Chen boiling suppression factor is a function of the two-phase Reynolds number (Rousseau, 2014). The two-phase Reynolds number is a function of the liquid Reynolds number and the multiplication factor.

Forster and Zuber (2004) developed a correlation for nucleate pool boiling. This correlation incorporates the local wall superheat, pressure difference and the saturation pressure and temperature of the fluid (Rousseau, 2014). The widely used Dittus-Boelter correlation forms the convective heat transfer term of the Chan correlation that was used to derive the Forster and Zuber correlation (Incropera *et al.*, 2011).

Shah also did work on boiling in vertical channels and he proposed the use of a chart (Shah, 1982). His correlation take both, convection and boiling, heat transfer modes into consideration, but only uses the larger of the two, to calculate his two-phase transfer coefficient (Wolverine Tube, Inc., 2007). His correlation uses a dimensionless parameter the Froude number for all values of vertical tubes. The Froude number is equal to the local vapour quality and density ratio (Shah, 1982). The Dittus-Boelter correlation is used to characterize the convection of the liquid-phase and from this the boiling heat transfer is calculated. The boiling number represents the effect of the heat flux on nucleate boiling and gives the ratio to the maximum heat flux achievable by complete evaporation. Depending on the values of the boiling number and Froude the heat transfer is then calculated (Kandlikar, 1983). The most notable weakness of this correlation is that the only physical property of the fluid used in the boiling number is the latent heat of the fluid (Wolverine Tube, Inc., 2007). It was found that the latent heat decreases with an increase in pressure, where the heat transfer typically increases with pressure (Aakenes, 2012).

Gungor and Winterton (1986) took the Chen model and compiled a larger database for vertical tubes. They also suggested that the two-phase flow heat transfer should be a combination of the convective heat transfer and nucleate boiling. The Dittus-Boelter

correlation is used to calculate the convective heat transfer, while the Cooper correlation is used to calculate the nucleate boiling. The nucleate boiling is a function of the molecular weight, heat flux and the difference between the saturation and critical pressure of the fluid. The multiplication factor incorporates the Lockhart-Martinelli and boiling number parameters (Wolverine Tube, Inc., 2007). Similar to the Chen correlation, the boiling suppression factor is a function of the liquid Reynolds number. A simpler version of the correlation was proposed which is only based on the convective heat transfer. The convection multiplier is however a bit more complex than before (Wolverine Tube, Inc., 2007).

2.7.1.3 DRY-OUT

The last mode of heat transfer is that of post dry-out. This regime is defined when the heated wall becomes dry before superheating is achieved (Wolverine Tube, Inc., 2007). When the liquid film dries out and the remaining liquid is entrained as droplets, but the quality is still below that of saturated vapour, dry-out has occurred. This regime is also referred to as the liquid deficient regime or mist flow heat transfer, but the last two naming conventions lack accurate description when this occurs at low vapour qualities due to the critical heat flux (Wulff, 2010).

Post dry-out can be achieved in one of the following manners:

- Critical heat flux: The wall heat flux or degree of wall superheat is so high that a vapour film is formed on the wall.
- Dry out of the liquid film: The annular liquid film evaporates completely and water droplets, that still need to evaporate, remain in the gas stream.
- Liquid film entrainment: The shear stress between liquid droplets and the vapour film is so strong that the liquid is completely removed from the wall surface.

For typical values of heat transfer, the coefficients in the post dry-out regime are between ten and thirty times lower than that of the wetted region (Wolverine Tube, Inc., 2007). Care should be taken as the wall temperatures in this region can become significantly high and cause the tube metal to melt or metallurgical changes to take place.

2.7.2 FRICTION PRESSURE DROP

As a fluid flows through a tube, momentum is lost due to surface friction at the boundaries and viscous forces acting on the fluid. To calculate the pressure drop for different flow regimes the following correlations can be used.

2.7.2.1 SINGLE PHASE FLOW

The Darcy-Weisbach friction factor calculates the pressure drop due to friction along a length of a pipe based on the average velocity (Okiishi, 2006). The pressure drop is calculated by means of the Darcy friction factor, which is a function of the Reynolds number. This function is different for laminar and turbulent flow.

2.7.2.2 TWO-PHASE FLOW

Due to the behaviour of two-phase flow the calculation of the friction pressure drop becomes more intricate (Rousseau, 2014). A homogeneous approach can be used that incorporates the two-phase density and velocity to calculate the friction factor. This correlation is only suitable for mass velocities larger than 2000 [kg/m^{2}s] (VDI - Gesellschaft Verfahrenstechnik und Chemieingenieurwesen, 2010).

Another approach is to use a separated flow model. Friedel (1979) calculated the friction pressure drop from the liquid and vapour pressure drops. The liquid pressure drop is calculated using the Darcy-Weisbach friction factor and the liquid Reynolds number. From the liquid dynamic viscosity the Friedel two-phase multiplier uses five dimensionless parameters to obtain the vapour pressure drop (Freidel, 1979).This method is recommended for viscosity ratios of less than 1000 and vapour qualities between 0 and 1.

A method to calculate the two-phase pressure drop was introduced by Lockhart and Martinelli in 1949 (Rousseau, 2014). They suggested that the pressure drop is based on a two-phase multiplier for the liquid and vapour-phase respectively. The multiplication factor uses a constant that is calculated using a combination between the liquid and vapour laminar and turbulent flows (Wolverine Tube, Inc., 2007).

Chisholm (1973) had an extensive empirical method to calculate the two-phase flow for a wide operating range. He suggested that the pressure drop gradients should be calculated separately for the vapour and liquid phases, as a function of the total mass flow and the

density of the respective phases (Wolverine Tube, Inc., 2007). For Reynolds numbers larger than 2000, turbulent flow is assumed and a parameter is obtained by the ratio of the two friction pressure gradients. Chisholm`s two-phase multiplier is a function of this ratio parameter, Chisholm`s parameter and the Blasius expression. The Chisholm parameter is calculated depending on the mass flow and the range of the ratio parameter (Wolverine Tube, Inc., 2007), (Chisholm, 1973).

2.7.3 VOID FRACTION

One of the most important parameters in two-phase flow is that of the void fraction (Ishii & Hibiki, Drift-Flux Model, 2011) and is used to calculate numerous other parameters like physical properties, flow patterns and heat transfer. The void fraction of two-phase flow can be calculated using numerous ways including the chordal, the cross-sectional and the volumetric approaches (Wolverine Tube, Inc., 2007).

The chordal void fraction is defined as the length of the vapour phase to that of the total length and is measured by absorption of a radioactive beam. The cross-sectional void fraction is measured by optical means and is defined as the cross sectional area occupied by the gas over the total cross section. Finally the volumetric cross section is defined by the volume of the gas over the total volume of the section (Wulff, 2010). From these three the most widely used approach is that of the cross-sectional volume fraction.

For a homogeneous void fraction the vapour quality, mass flow and fluid density are used. With this calculation it is assumed that the vapour and liquid travels at the same velocity. This results in the summation of the two void fractions delivering a single equation. The homogeneous void fraction model is only accurate for a limited range of conditions (Wolverine Tube, Inc., 2007). It is furthermore only valid for bubbly and mist flow as the two phases has the same velocity. Another restriction of this approach is that the void fraction cannot be calculated at pressures near the critical point. Here the phase densities are close to identical and no clear distinction between liquid and vapour can be made (Wolverine Tube, Inc., 2007).

When different phase velocities are assumed a slip factor has to be implemented. This is a ratio between the vapour and liquid velocities (Hewitt, 2011). If the phase velocities are equal the slip ratio reverts to unity and the slip to the homogenous void fraction equation. For upward co-current flow the vapour velocity is greater than that of the liquid and the slip

factor will be larger than unity. As for downward flows the gravitational effect increases the liquid velocity and results in a slip factor less than unity (Wulff, 2010).

2.7.3.1 ANALYTICAL MODELS

Some simplifying assumptions have been made in order to predict the void fractions by analytical means (Wolverine Tube, Inc., 2007). The Momentum Flux Model calculates the flux from the homogeneous specific volume of the fluid. It is assumed that the void fraction is obtained when the momentum flux is minimized. Thus the void fraction is obtained when the derivative of the momentum flux equation is set equal to zero. For the simple model the slip factor is the square root of the density ratio (Wolverine Tube, Inc., 2007).

For annular flow the Zivi (1964) void fraction model assumes no liquid is entrained in the central vapour core. This approach is based on the assumption that the total kinetic energy of the two phases will be a minimum. The total kinetic energy equation is the summation of the individual phases` energy equations. This equation is then differentiated and the result is set equal to zero. From this it is found that the void fraction is only dependant on the density ratio of the fluids (Wolverine Tube, Inc., 2007).

In 1967 Levy derived a momentum void fraction model for forced convective boiling for water (Levy, 1999). He assumed that the sum of the frictional and static head losses in the momentum equation for each phase are equal. This assumption implies that the momentum exchange between the phases is under constant flux to maintain this equality (Wolverine Tube, Inc., 2007). A comparison between Levy`s model and experimental data had a very good correlation, but only for high pressures.

2.7.3.2 EMPIRICAL MODELS

In 1969, Smith proposed that separated flow consisting of a vapour phase with a fraction of liquid entrained must be investigated. His investigation implied that the vapour and entrained liquid`s momentum equations should be equal (Wolverine Tube, Inc., 2007). Smith calculated an entrainment factor ($0 < \varepsilon < 1$) empirically and investigated the extremes, where the entrainment factor equalled one and zero. Smith calculated results for an entrainment value of 0.4 by computing three sets of void fractions and comparing them to three different experimental techniques. From these findings it was concluded that a good

correlation exists irrespective of the pressure, mass, velocity, flow regime and enthalpy change with only a $\pm$ 10 [%] error (Wolverine Tube, Inc., 2007).

Chisholm (1972) derived a correlation for the velocity ratio. The expression uses the homogeneous fluid density and a simplified annular flow theory to produce frictional pressure gradients in each phase (Wolverine Tube, Inc., 2007). This approach gives similar entrainment values as Smith (1969), with minor deviations at high vapour qualities. At very low void fractions the vapour velocity approaches that of the liquid, as the buoyancy of the small bubbles are negligible (Wolverine Tube, Inc., 2007).

In 1964 Zuber and Findlay developed the drift flux void fraction model (Zuber & Findlay, 1964), after which Ishii and Wallis also made a large contribution in 2011 (Ishii & Hibiki, Drift-Flux Model, 2011). The model was developed for both vertical and horizontal tubes and the effect of radial void fractions and velocity profiles were also taken into consideration. The drift flux, U, is a representation of the volumetric rate at which the vapour, U_g, is flowing over a unit plane, U_v, that is traveling normal to the channel at a flow velocity of $U = U_v + U_g$ (Wolverine Tube, Inc., 2007). These velocities are the superficial velocities of the two phases defined by the local velocity and the local void fraction (Wolverine Tube, Inc., 2007). The cross-sectional averages are taken over the flow channel and the mean quantities are taken as the weighted averages. The model can only be used if the drift velocity is significantly larger than the volumetric flux (Ishii & Hibiki, Drift-Flux Model, 2011).

2.8 INSTABILITIES IN TWO-PHASE FLOW

The phenomenon of instabilities in two-phase flow is of great importance for the design and operation of a SG (Kakac & Bon, 2007). These instabilities can cause oscillations that can result in mechanical vibrations, control system problems and cycling thermal stresses. Catastrophic failure can occur as a result and thus the effects of these instabilities in two-phase boiling should be considered during the modelling of SG (Ruspini, 2013).

2.8.1 DENSITY-WAVE OSCILLATIONS

Lorents (Kakac & Bon, 2007) investigated the hydrodynamics of two-phase flow in pipes by treating the mixture as homogeneous. From this the Ledinegg instability resulted which can be described as a sudden change in mass flow to a lower value, due to the propagation of a density change wave in the fluid (Kakac & Bon, 2007). This occurs when the slope of the

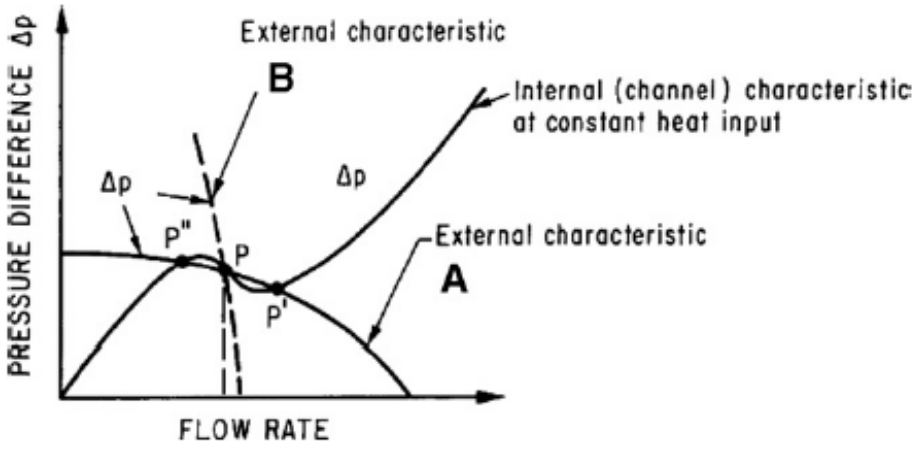

Figure 8 - Ledinegg instability (Kakac & Bon, 2007).

channel`s pressure drop vs. flow rate curve is negative and steeper than the component characteristic curve and multiple intersection points occur, see Figure 8 (Kakac & Bon, 2007). When the external curve (A) is less steep than the internal curve, the operating point (P) is impossible to obtain. A small variation in the mass flow will result in a condition where a larger pressure drop is required and the mass flow will decrease further in order for the system to reach a new operation point. When a numerical model is run the solution can oscillate between the three intersecting points resulting in a numerical instability (Ruspini, 2013). To overcome the Ledinegg instability it is proposed to increase the negative slope of the internal curve (B) so the multi-variable intersection points are eliminated (Kakac & Bon, 2007).

2.8.2 PRESSURE-DROP OSCILLATIONS

Pressure-drop oscillations occur in a compressible fluid, see Figure 8 (Kakac & Bon, 2007). While the system operates on the negative slope (P) a slight increase in the surge tank pressure will result in the accumulation of fluid, as less fluid is leaving than entering (Kakac & Bon, 2007). Due to the accumulation of fluid the pressure in the surge tank will increase the resulting mass flow (A to B).

At the maximum point B only a jump in mass flow can result in a higher pressure (C). At C the mass flow need to decrease to try and reach the operating point until the minimum is reached at D. If a lower pressure is require the system needs to jump to A again, thus resulting in an oscillation in the volume of ABCDA (Kakac & Bon, 2007). This phenomenon results in an oscillation of the mass flow throughout the system which results in a pressure

drop-wave propagating through the medium. As mentioned, this can only occur when a system contains a compressible fluid (Ruspini, 2013).

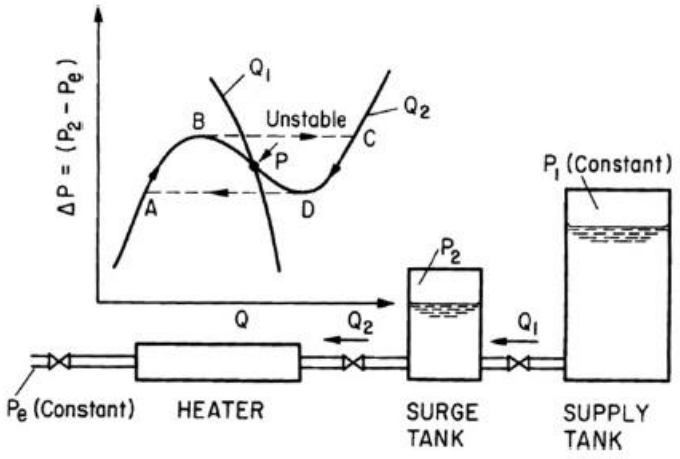

Figure 9 - Pressure-drop oscillation (Kakac & Bon, 2007).

In SGs this occurs in the two-phase boiling region, but at higher void fraction and superheating conditions. The propagation of the pressure waves can be seen as water hammers or acoustic wave propagation (Kakac & Bon, 2007). For high power density systems the amount of compressible fluid needed to initiate this oscillation is very low (Ruspini, 2013).

These oscillations can be initiated by the following mechanisms:

- Gravity: This oscillation was found in vertical systems with a long unheated section downstream of the heated section. It was found that the hydrostatic head was very sensitive at low pressures (Ruspini, 2013). This feedback between the flow, void fraction and head pressure leads to cycling.

- Friction: The different speeds of propagation in the single and two-phase regions results in this instability. Any change in the void fraction or flow will affect the pressure drop (Ruspini, 2013). This can introduce an out-of-phase oscillation between the single and two-phase pressure drops.

- Momentum: With compressible flow the propagation of the pressure drop is delayed and this affects the thermal hydraulic properties of the fluid (Ruspini, 2013).

2.8.3 THERMAL OSCILLATIONS

Thermal oscillations refer to situations where there are fluctuations in the temperatures of a solid in contact with a fluid. These fluctuations of the temperature can be interpreted as the oscillation of the thermal heat transfer during boiling (Kakac & Bon, 2007). It was found that the thermal oscillations were triggered by density-wave oscillations. It is coupled by the movement of the dry out and nucleate boiling boundaries (Ruspini, 2013). If it is triggered by low frequency oscillations the results are the movement of the boiling boundaries. If triggered by high frequency oscillations then there are two distinct modes (Ruspini, 2013):

- High frequency, small amplitude: This is due to the movement of the boundaries (Ruspini, 2013).
- Low frequency, large amplitudes: This is due to the wall thermal capacity, axial conduction and transition boiling (Ruspini, 2013).

2.9 CONCLUSION

From the literature study conducted it can be concluded that the most popular type of SG for the current SMR PWR type reactors being developed/build, is that of the OTHSG design. This kind of SG will most likely be used in all new designs due to its compactness, efficiencies, and degree of superheating.

The simulation model to be developed in this study needs to be able to simulate the dynamic response of the SG from start-up and also handle the transitions between phases. With the gathered results it was identified that a homogenous model will be accurate enough for the detail to be simulated, as we are only interested in the transient response of the system and not the detail interactions between the phases. The simplifications of the model results in less closure and conservation equations that needs to be solved. The formulation of the model will thus have adequate accuracy and stability to predict normal transient situations, as we are interested in the overall dynamics of the SG.

The relevant correlations that can be used were investigated and the regions in which they are accurate. The heat transfer enhancement factor will play a vital role in the accuracy of the model. From the literature it is clear that the instabilities that exist in the two-phase region may pose a problem for the numerical solver used. Care will be taken to identify the properties that are responsible for these instabilities and an adequate approach will be taken.

CHAPTER 3 – TECHNICAL STUDY

3.1 INTRODUCTION

A review of the heat transfer correlations and the different modelling approaches used to simulate thermal-hydraulic systems set the corner stone for the development of a flow boiling simulation. This chapter will focus on an understanding of the necessary mathematical approaches and equations needed to model the transient operations of an OTSG based on a homogeneous approach.

The model development is based on using a SCFD approach. An overview of why this approach was selected will be given, along with a review of the required fundamental fluid properties used to simulate the two-phase thermal fluid system. The conservation equations for mass, momentum and energy applied will also be discussed. Finally the conservation equations to ensure continuity on the boundaries are also investigated.

3.2 SCFD MODELLING

A SCFD simulation entails solving the differential equations for energy, mass and momentum conservation using a system or network approach. This is a collection of one-dimensional elements that are connected by nodes as shown in Figure 10. The elements are represented by the circles and the nodes by squares (Rousseau, 2014). The elements consist of any thermal-hydraulic component such as a pipe, pump, fan, compressor, turbine or heat exchanger element. The nodes connect the elements and have either no physical significance or it can have volume to represent a reservoir.

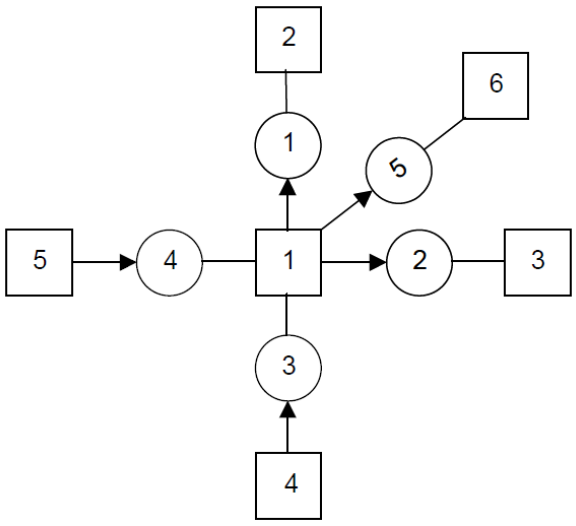

Figure 10 - Systems CFD node-element approach (Rousseau, 2014).

In this approach, it is assumed that the properties of the fluids, at each node are represented as a single averaged value. Thus the conservation of mass and energy are given for the nodes whereas the conservation of momentum is written for the elements that connect the nodes. For the model to be developed as part of this study, one-dimensional flow within the network will be assumed.

For a simulation model, be it a single component or an integrated complex system, four basic fundamental types of equations are required to properly formulate the problem, namely:

- Conservation laws: mass, momentum and energy.
- Component characteristics: heat transfer, pressure drops, friction factors etc.
- Fluid properties: thermodynamic properties.
- Boundary values: temperatures, pressures, mass flow and friction.

3.3 CONSERVATION EQUATIONS

A discussion of the conservation of mass, energy and momentum equations for a generic infinitesimal control volume will follow in this section. In Figure 11 a schematic of the control volume used for the derivation of the equations are given. The conservation equations for a generic homogeneous fluid problem will be discussed to show the relevant formulation. The theory below is based on that of Rousseau (2014).

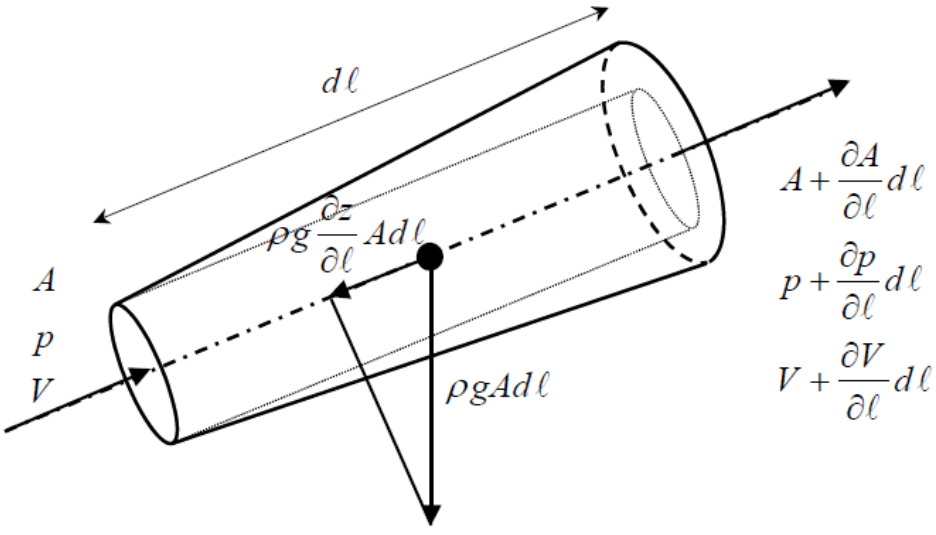

Figure 11 - Schematic of a control volume (Rousseau, 2014).

We assume the flow is one-dimensional and that the properties are averaged over the cross-section of the control volume. It is assumed that the properties only change in the direction of the flow, with the control volume having a length of δL. The component forces that act on the fluid within the control volume also need to be taken into account. These forces can be frictional, gravitational or work exerted on the fluid. Friction has an effect opposite of that of the flow and gravity perpendicular, if the elevation does not change.

As the focus will be on the homogeneous model, the phasic void fraction gives a ratio of the total volume of gas vs. the total volume of the control volume. The correlation to calculate the void fraction will be discussed later.

$$\varepsilon = \frac{\forbar{V}_g}{\forbar{V}} \quad [1]$$

3.3.1 CONSERVATION OF MASS

From work done by Isshi (2011) and refined by Rousseau (2014) the integral form of the conservation of mass equation for a finite control volume is given by:

$$\frac{d}{dt}\iiint \rho d\forbar{V} + \oiint \rho \bar{V}\, \overline{dA} \quad [2]$$

Where $\forbar{V}$ is the control volume, ρ the average fluid density in the control volume and $\bar{V}$ the fluid relative velocity. For clarity all symbols noted with a bar is the averaged value over the control volume. The first term is the rate of change of mass within the control volume over time and the second term is the rate at which mass flows over the boundaries into or out of the control volume. The differential form of the equation is given by:

$$\forbar{V}\frac{d\rho}{dt} + \dot{m}_e - \dot{m}_i = 0 \quad [3]$$

This can be rewritten as:

$$\frac{d\rho}{dt} = \frac{1}{\forbar{V}}(\dot{m}_i - \dot{m}_e) \quad [4]$$

The first term describes the rate at which the mass in the control volume change due to a change in density over time. The right-hand term describes the flow of mass out of and into

the control volume. For steady state conditions there is no change in density over time and the left-hand term is equal to zero. As a homogeneous model will be developed the mass flow and density are that of the homogeneously mixed two-phase fluid.

3.3.2 CONSERVATION OF ENERGY

The integral form of the conservation of energy equation is given by:

$$\dot{Q} + \dot{W} = \frac{d}{dt}\iiint (u + \frac{1}{2}V^2 + gz)\rho d\forall + \oiint \left(h + \frac{1}{2}V^2 + gz\right)\rho \bar{V}\overline{dA} \qquad [5]$$

Where $\dot{Q}$ is the rate at which energy is added to the fluid, and $\dot{W}$ the rate at which work is done on the fluid. The first term on the right hand side is the rate at which the internal, dynamic and potential energy changes within the control volume, and the second term is the rate at which the internal, dynamic and potential energy flows over the control volume boundary.

The differential form of the equation is given by:

$$\dot{Q} + \dot{W} = \cancel{\forall}\frac{d}{dt}(\rho h_0 - p) + \dot{m}_e h_{0e} - \dot{m}_i h_{0i} + \dot{m}_e g z_e - \dot{m}_i g z_i \qquad [6]$$

Rearranging the equation results in:

$$\frac{d}{dt}(\rho h_0 - p) = \frac{1}{\cancel{\forall}}\left(\dot{Q} + \dot{W} - \dot{m}_e h_{0e} + \dot{m}_i h_{0i} - \dot{m}_e g z_e + \dot{m}_i g z_i\right) \qquad [7]$$

The rate of change can be written as:

$$\frac{d}{dt}(\rho h_0 - p) = \rho\frac{\delta h_0}{\delta t} + h_0\frac{\delta \rho}{\delta t} - \frac{\delta \rho}{\delta t} \qquad [8]$$

So the conservation equation becomes:

$$\rho\frac{\delta h_0}{\delta t} + h_0\frac{\delta \rho}{\delta t} - \frac{\delta \rho}{\delta t} = \frac{1}{\cancel{\forall}}\left(\dot{Q} + \dot{W} - \dot{m}_e h_{0e} + \dot{m}_i h_{0i} - \dot{m}_e g z_e + \dot{m}_i g z_i\right) \qquad [9]$$

It can be further simplified to:

$$\frac{\delta h_0}{\delta t} = \frac{1}{\rho\cancel{\forall}}\left(\dot{Q} + \dot{W} - \dot{m}_e h_{0e} + \dot{m}_i h_{0i} - \dot{m}_e g z_e + \dot{m}_i g z_i + \cancel{\forall}\left(\frac{\delta \rho}{\delta t} - h_0\frac{\delta \rho}{\delta t}\right)\right) \qquad [10]$$

The term on the left hand side is the rate at which energy changes due to the change in enthalpy over time. The change of energy due to mass flowing in and out of the control volume is given by terms three and four inside the brackets on the right hand side. The change of potential energy due to the elevation difference of the inlet and outlet is given by terms five and six. The last term gives the change in energy due to the change in the fluid`s density as energy is being absorbed. For steady state calculations no change in enthalpy occurs and the rate term equals zero.

3.3.3 CONSERVATION OF LINEAR MOMENTUM

The integral from of the momentum conservation equation is given by:

$$\oiint \tau \overline{dA} + \iiint \bar{B}\rho \overline{dA} = \frac{\delta}{\delta t}\left(\iiint \bar{V}\rho d\forall\right) + \oiint \bar{V}\left(\rho \bar{V} \overline{dA}\right) \quad [11]$$

The first term represents the forces acting on the surface of the control volume and the second term represents the body forces within the control volume. The rate at which momentum change within the control volume is given by the next term and the last term represents the rate at which momentum is transferred over the control volume`s boundaries. If we integrate over the length of the control volume and assume the liquid is incompressible we get:

$$\rho L \frac{\delta V}{\delta t} + (P_{0e} - P_{0i}) + \rho g(z_e - z_i) + \Delta P_{0L} = 0 \quad [12]$$

Rearranging Equation 12 result in:

$$\frac{\delta V}{\delta t} = \frac{1}{\rho L}\left((P_{0i} - P_{0e}) + \rho g(z_i - z_e) - \Delta P_{0L}\right) \quad [13]$$

It is easier to work with the mass flow rate than the velocity, so the left hand side needs to be rewritten. For this the fundamental mass flow equation is used to rewrite the velocity to mass:

$$\frac{\delta V}{\delta t} = \frac{\rho}{A}\frac{\delta \dot{m}}{\delta t} - \frac{V}{\rho}\frac{\delta \rho}{\delta t} \quad [14]$$

This results in:

$$\frac{\delta \dot{m}}{\delta t} = \frac{A}{L}\left((P_{0i} - P_{0e}) + \rho g(z_i - z_e) - \Delta P_{0L} + VL\,\frac{\delta \rho}{\delta t}\right) \quad [15]$$

This gives the rate of momentum change due to the change in mass flow rate over time. The difference between the inlet and outlet pressures and the pressure change due to elevation is given by the next two terms. The second last term is the pressure drop due to friction forces acting on the liquid boundary interface. The last term is the momentum change of the control volume the density change over time.

3.4 TRANSIENT MODELING

For the steady state conditions the left hand side of the conservation equations is zero as there can be no mass or energy accumulation. When transients are calculated the change of conditions over set time steps need to be considered. From the conservation of mass the rate of change is equal to a source term:

$$\frac{d\rho}{dt} = S_c(t) \qquad [16]$$

The variables can be separated and integrated over a time step Δt from the previous time t^0 to the new time t. The superscript 0 refers to the previous time step values.

$$\int_{t^0}^{t} d\rho = \int_{t^0}^{t} S_c(t)dt \qquad [17]$$

Since the source term is a function of time the right hand side of the equation cannot be integrated without the knowledge of how it varies over time and therefore the shape of the function needs to be assumed.

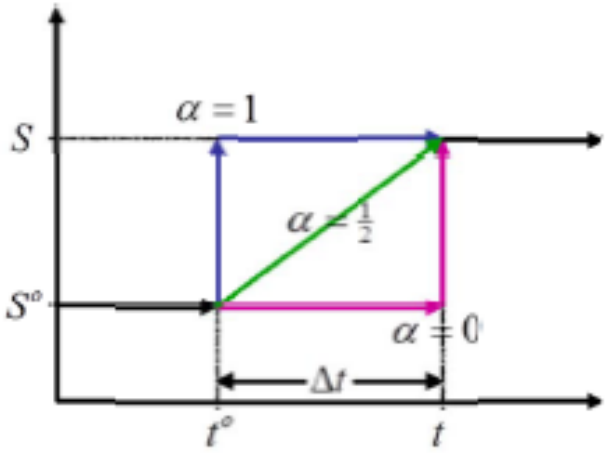

Figure 12 - Time-wise integration (Rousseau, 2014).

Figure 12 shows the possible assumptions taken for the source term. The first approach is to assume that the source term stays constant at the old value for the full length of the time step and then instantaneously jump to the new value ($\alpha = 0$), known as the fully explicit approach:

$$\frac{d\rho}{dt} = S_c^0 \quad [18]$$

If the source term changes instantaneously to the new value and then stays constant ($\alpha = 1$), it is known as the fully implicit approach:

$$\frac{d\rho}{dt} = S_c \quad [19]$$

Although both of these approaches are valid they are not the best and most accurate methods. These will only provide an accurate result if the time step is infinitely small so the change in the variables approaches a smooth line and not a stepped function. This leads to a combination of the two ($\alpha = \frac{1}{2}$). This results in an assumption that the source term maintains an average value between the old and new values for the entire time step and is known as the Crank-Nicholson approach. The generic approach can be written as:

$$\frac{d\rho}{dt} = \alpha S_c + (1-\alpha) S_c^0 \quad [20]$$

This leads to the time-wise integration of the transient term becoming:

$$\frac{\rho - \rho^0}{\Delta t} = \alpha S_c + (1-\alpha) S_c^0 \quad [21]$$

$$\frac{h_o - {h_0}^0}{\Delta t} = \alpha S_c + (1-\alpha) S_c^0 \quad [22]$$

$$\frac{m - m^0}{\Delta t} = \alpha S_c + (1-\alpha) S_c^0 \quad [23]$$

3.5 GEOMETRY

When modelling complex geometries, it can usually be simplified and replaced by an equivalent element that has the same behaviour.

3.5.1 HYDRAULIC DIAMETERS

A flow channel of any geometry can be replaced by an equivalent circular pipe with a specific diameter. This is known as the hydraulic diameter and results in the same flow characteristics as the original geometry. The hydraulic diameter can be calculated by Equation 24, where the free flow area is divided by the total wetted perimeter of the tube.

$$D_H = 4 * \frac{A_{ff}}{A_{p\,wetted}} \quad [24]$$

3.5.2 COIL GEOMETRY

In Figure 13 the geometry of a helical coil is given, this will be used to calculate the enhancement factor to be discussed later in this chapter. The pipe has an inner diameter of 2r and the coil diameter is given by $2R_c$and is the maximum distance between the centres of the pipe on the same plane. The coil diameter is also defined as the pitch diameter. The ratio of the pipe to coil diameter (r/R_c) is called the curvature ratio δ. The non-dimensional pitch, λ, is the ratio of the pitch to the developed length of the coil ($H/2\pi R_c$). The helix angle, α, is the angle at which the coil leaves the xy-plane (Jayakumar, 2012). The helix angle should not be confused with the time-wise integration factor of equations [20-23].

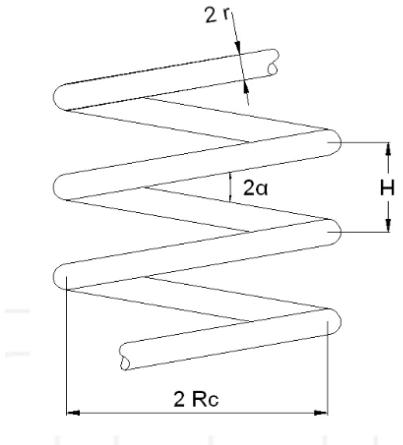

Figure 13 - Helical coil geometry (Jayakumar, 2012).

3.6 HEAT TRANSFER

Due to the nature of two-phase boiling and the transient behaviour of a SG there are numerous zones present along the length of the heat transfer surface. For each of these zones a different heat transfer coefficient has to be used.

3.6.1 SINGLE PHASE FLOW

For the single phase heat transfer, that is sub-cooled liquid or super-heated steam, the Dittus-Boelter equation is the most widely used for turbulent flow. Before the Dittus-Boelter equation can be listed the non-dimensional constants have to be explained.

The Nusselt number provides a measure of the convection heat transfer that can be achieved. It is also known as the non-dimensional temperature gradient at the liquid surface interface.

$$Nu = \frac{h_c D_H}{k} \quad [25]$$

For fully developed laminar flow the Nusselt number is equal to 3.66 and for turbulent flow it is calculated with the Dittus-Boelter equation. Whether or not the flow is turbulent or laminar is given by the Reynolds number.

The Reynolds number is the ratio of the internal to viscous forces in the velocity boundary layer. It gives an indication to whether the flow inside a pipe is laminar of turbulent.

$$Re = \frac{\rho V D_H}{\mu} \quad [26]$$

For values below 2000 the flow is considered to be laminar and above as turbulent.

In order to use the Dittus-Boelter another non-dimensional parameter namely the Prandtl number needs to be defined. It gives the fluid`s ability to transport momentum vs the ability to transport energy and is given by:

$$\mathrm{Pr} = \frac{C_p \mu}{k} \quad [27]$$

The fluid`s heat capacity, viscosity and thermal conductivity is used to calculate this parameter.

Now that the required parameters are defined, the Dittus-Boelter equation is given by:

$$Nu = 0.023Re^{0.8}Pr^{n} \quad [28]$$

In Equation 28 n is 0.4 and 0.3 for heating and cooling respectively. From this formulation the heat transfer coefficient for single phase heat transfer in vertical tubes can be calculated.

Equation 28 was modified by Jayakumar (2012) to incorporate the added effect of heat transfer inside the tube due to the coil effect. This added enhancement factor is a function of the helix`s curvature ratio δ and the enhanced Nusselt number is then given by:

$$Nu_{enhanced} = 0.116Re^{0.71}\mathrm{Pr}^{n}\,\delta^{0.11} \quad [29]$$

This equation is accurate for the following ranges:

- 14000<Re<70000
- 3.0<Pr<5.0
- 0.05< δ<0.2

When viewing the external flow over the tubes of an OTHSG it is a combination of counter and cross flow. For large helix angles the counter flow has a large influence and for smaller angles the cross flow has a larger effect. According to Incropera et al. (2006) the arrangement of the tubes influences the external conductive heat transfer, Equation 30.

$$Nu = \ C_1 Re^{m} Pr^{0.36} \left(\frac{Pr}{Pr_s}\right)^{0.25} \quad [30]$$

Figure 14, shows the arrangement, aligned or staggered, and the geometry required to calculate C_1. The final model will assume that the tubes are staggered for increased heat transfer due to turbulent flow. Turbulent flow is initiated due to the staggering of the tube banks and this increases the heat transfer over the tube banks. Table 1 shows how to calculate the constants according to the alignment and flow over the tubes.

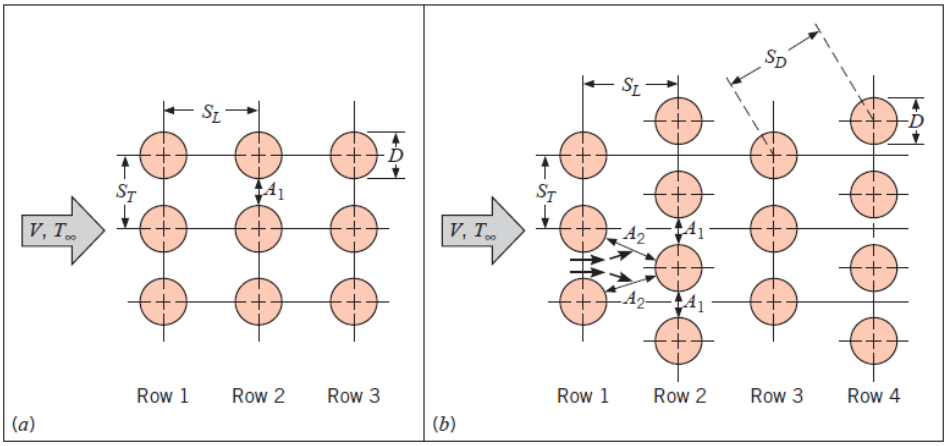

Figure 14 - Tube alignment (Incropera *et al.*, 2011).

Table 1 - Constants of Nusselt for tube bank cross flow.

Configuration	Re	C_1	m
Aligned	$10\text{-}10^2$	0.8	0.4
Staggered	$10\text{-}10^2$	0.9	0.4
Aligned	$10^2\text{-}10^3$	Approximate as a single cylinder	
Staggered	$10^2\text{-}10^3$		
Aligned (S_T/S_L >0.7)	$10^3\text{-}2x10^5$	0.27	0.63
Staggered (S_T/S_L <2)	$10^3\text{-}2x10^5$	$0.35(S_T/S_L)^{0.2}$	0.60
Staggered (S_T/S_L >2)	$10^3\text{-}2x10^5$	0.4	0.60
Aligned	$2x10^5\text{-}2x10^6$	0.021	0.84
Staggered	$2x10^5\text{-}2x10^6$	0.022	0.84

3.6.2 TWO-PHASE FLOW

For two-phase flow the Foster Zuber correlation was used (Incropera *et al.*, 2011) As mentioned in section 2.7.1.2 this correlation incorporates a combination of Equation 28 with a multiplication and suppression factor. The two-phase heat transfer coefficient is given by:

$$h_{ctp} = Fh_c + Sh_{FZ} \quad [31]$$

In this equation the single phase Dittus-Boelter heat transfer coefficient is that of the remaining liquid and the Frost-Zuber coefficient is given by:

$$h_{FZ} = \frac{0.00122(\Delta T_{sat})^{0.24}(\Delta P_{sat})^{0.75} C_{pl}^{0.45} \rho_l^{0.49} k_l^{0.79}}{\sigma^{0.5} h_{lg}^{0.24} \mu_l^{0.29} \rho_g^{0.24}} \quad [32]$$

The Frost-Zuber heat transfer coefficient is calculated by taking the difference between the saturation pressure at the wall temperature and the bulk temperature into account. Then also the fluid`s heat capacity, density and thermal conductivity at the bulk temperature. The surface tension of the fluid at the bulk temperature, the latent enthalpy, liquid viscosity and gas density is used respectively.

Due to the turbulent nature of boiling, the convective heat transfer increases and this effect is calculated by the multiplication factor F:

$$F = 2.35(\chi_{tt}{}^{-1} + 0.213)^{0.736} \quad [33]$$

The multiplication factor is calculated by means of the Lockhart-Martinelli parameter. If $\chi_{tt}^{-1} < 0.1$ then the multiplication factor is set to 1.

$$\chi_{tt} = \left(\frac{1-x}{x}\right)^{0.9} \left(\frac{\rho_g}{\rho_l}\right)^{0.5} \left(\frac{\mu_l}{\mu_g}\right)^{0.1} \quad [34]$$

The last term to be discussed in Equation 31 is that of the suppression factor. The argument behind it is that the presence of the convective heat transfer results in a temperature gradient through the liquid film that is greater than that of pure boiling. This results in slightly lower wall temperatures that in turn suppress the formation of bubbles on the wall surface and therefore the suppression factor is always less than one.

$$S = \left(1 + 2.53x10^{-6}\left(Re_f F^{1.25}\right)^{1.17}\right)^{-1} \quad [35]$$

As mentioned in section 2.7.1.2, nucleate boiling starts when the wall reaches a critical temperature, calculated by:

$$T_{wall_{crit}} = \frac{8\sigma T_{sat} Q`}{\rho_g(h_{gl})k_f} + T_{sat} \quad [36]$$

This critical wall temperature is the nucleate initiation point and uses the surface tension, saturation temperature and heat flux at the wall along with the gas density thermal conductivity and the latent enthalpy.

3.7 PRESSURE DROP

Due to the friction between the fluid and the surface interface energy is lost. This loss is measured in the pressure loss that occurs over the length of the pipe segment. According to the phase of the fluid the pressure drop can be calculated for either single phase or two-phase flow.

3.6.1 SINGLE PHASE PRESSURE DROP

The single phase pressure drop friction factor for laminar flow through a pipe or duct can be calculated by:

$$f = \frac{C}{Re} \quad [37]$$

The constant C varies for different geometries. When the Reynolds number is above 2000 the flow is considered turbulent and due to the erratic movement the pressure drop is calculated by (Rousseau, 2014):

$$f = 0.25\left(Log\left(0.27\frac{\varepsilon}{D_h} + \frac{5.74}{Re^{0.9}}\right)\right)^{-2} \quad [38]$$

The friction factor inside helical coils is given by Kridhna (2012). Where the helical friction factor is a function of the Dean number, but when rearranged it is a function of the curvature ratio of the coil and the friction factor of the uncoiled tube.

$$f_{coil} = f\left(1 - \left(1 - \left(\frac{11.6}{Re\,\delta^{0.5}}\right)^{0.45}\right)^{0.45}\right)^{-1} \quad [39]$$

Once the friction factor has been calculated the pressure drop is given by:

$$\Delta P_{0L} = \frac{1}{2}\frac{f_{coil}L}{D}\rho V^2 \quad [40]$$

3.6.2 TWO-PHASE PRESSURE DROP

The two-phase pressure-drop can be related to a single phase pressure drop, but increased with a gas-based two-phase multiplication factor.

$$\Delta P_{0Ltp} = \emptyset_g^2 (\Delta P_{0L})_g \quad [41]$$

The single phase pressure drop is calculated due to frictional losses if the pipe was only filled with the vapour phase:

$$(\Delta P_{0L})_g = \frac{\left(\frac{f_g L}{D_H}\right)|\dot{m}_g|\dot{m}_g}{2\rho A^2} \quad [42]$$

The friction factor is based on the gas flow only and is calculated with the gas Reynolds number. The length, free flow area and hydraulic diameter are that of the pipe segment. The pressure drop can also be written in terms of a liquid only two-phase multiplier and single phase pressure drop. The equations are the same as for the gas approach, but the mass flow rate and properties of the liquid phase are used. These two approaches should yield the same answer and when combining the equations it is found that:

$$\frac{(\Delta P_{0L})_f}{(\Delta P_{0L})_g} = \frac{\emptyset_g^2}{\emptyset_f^2} \quad [43]$$

From empirical values Soliman (Levy, 1999) correlated the two-phase gas multiplier from the Lockhart-Martinelli parameter:

$$\emptyset_g^2 = 1 + 2.85\chi_{tt}^{0.523} \quad [44]$$

3.8 VOID FRACTION

As we are considering a homogeneously mixed model that is in equilibrium the phase velocities are assumed to be equal. This allows for the most simple void fraction equation to be used:

$$\varepsilon = \frac{\rho - \rho_l}{\rho_g - \rho_l} \quad [45]$$

Where ρ is the average density of the two-phase fluid in a pipe segment, at the average pressure and temperature. The sub-scripts l and g are the densities of the saturated liquid and gas at the average pressure.

3.9 SUMMARY

Now that the relevant correlations for heat transfer and pressure drop along with the conservation equations have been evaluated, the homogeneous model can be developed. It is clear that the model should be able to take the different transition into account as the transient will handle phase change. These changes will have to use different correlations and that this, with the natural instabilities discussed in chapter 3, can result in errors with a numerical approach. From the equations the pipe segments that encounter boiling and dry-out will be cause concern as there will be a large change in fluid properties in these regions. How the model was developed and the different issues encountered addressed will be covered in the next chapter.

CHAPTER 4 – MATHEMATICAL MODEL

4.1 INTRODUCTION

Based on the theory defined in Chapter 3, the methodology used to develop the simulation model will be discussed in this chapter. How this theory was implemented for the simplified homogeneous vertical pipe model will be described. The numerical stability for different time wise integration factors will then be independently evaluated for the primary and secondary sides using a constant heat flux over a length of pipe. The most suited factor will then be used in the setup of the combined model which will also include more detailed correlations for the heat transfer and pressure drop compared to the simplified homogeneous model mentioned above.

4.2 MATHEMATICAL MODEL LAYOUT

As mentioned in the previous chapter, the methodology applied to develop the mathematical model was that of the node and element approach. It should be noted that the geometries and boundary values, used for the model, is arbitrary and not that of a specific SG. This is to ensure that the theory of two-phase flow boiling, in a vertical tube, is correctly implemented.

The model uses the geometry of a single tube and the SG layout will be simplified, for decreased calculation time, to that of a concentric vertical tube-in-tube counter flow heat exchanger. The primary side high pressure water will flow in the annulus and the lower pressure secondary side water will flow in the inner tube. The following geometry and boundary conditions have been used as shown in Table 2:

Table 2 - Boundary conditions for a transient start-up.

	Primary side	Secondary side
Inlet pressure [MPa]	15	5
Inlet temperature [K]	450	400
Mass flow at the inlet[kg/s]	2.75	0.04
Inlet height [m]	25	0
Increments [-]	25	25
Pipe Diameter [mm]	75	25
Wall thickness [mm]	-	5

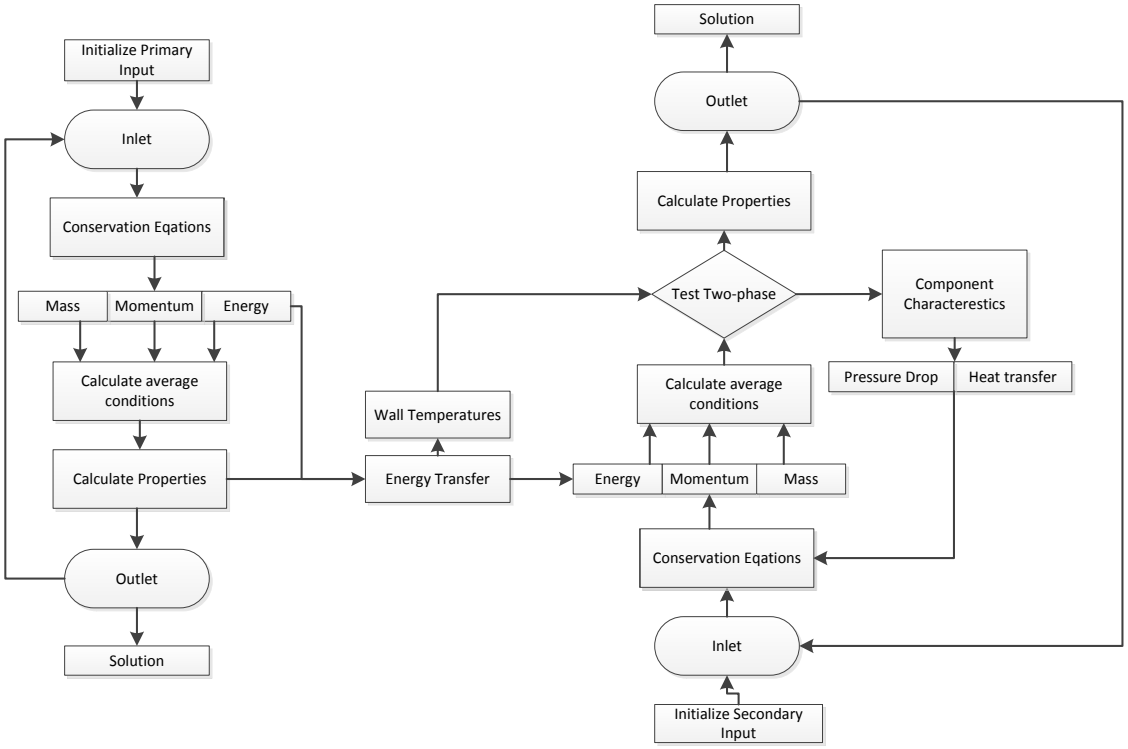

Figure 15 – Mathematical model flow diagram.

The basic flow diagram of the mathematical model is shown in Figure 15, the full EES model can be found in AppendixI. The interactions between the primary and secondary sides are quite complicated, and the results are iterated until convergence has been obtained. For both sides the fluid properties influence the heat transfer that in turn influences the wall temperature. The wall temperature is used to determine if boiling occurs or not.

When boiling occurs the heat transfer increases and it results in a drop in the wall temperature. This cause the energy transfer to be insufficient to sustain boiling and the secondary side will return to a single phase. This then in turn results in an increase of wall temperature, again, to above the boiling criteria (Ishii & Hibiki, 2011). This is called the thermal oscillation as mentioned in Chapter 2 and the effects on the model have to be investigated.

4.3 STABILITY

It was stated in Chapter 2, that transient two-phase flow boiling has natural instabilities with the thermal and pressure wave oscillations that occur. This requires that the stability of the

solver and solution should first be tested to eliminate the possibility that the solver causes problems.

The stabilities on the primary and secondary sides were first tested individually for the fully implicit, the fully explicit, and the Crank-Nichols approaches. The stabilities was then also evaluated for an alpha value of 0.7. For all these scenarios the boundary values were kept constant for a total of 100 runs to see if the source terms diverges, converges or oscillates. This was then followed by another scenario where the boundary values were kept constant for the first 10 runs after which a step input was added to the heat flux value. Once again the trends of the source terms were inspected for 100 runs. If the source terms showed a divergent nature more runs were added to see when the values exceed the set limits. Time steps of 0.01 [s], 0.1 [s], 1 [s] and 10 [s] was tested.

4.3.1 EXPLICIT APPROACH

For the explicit approach the alpha parameter was set to 0. For this caution should be taken in terms of the time step size and segment lengths. For the selected 25 one meter increments the time steps must be very small, 0.00001 [s], and only small changes of 0.0001 [ºC /run] in boundary values can be made. To increase the stability the increment sizes needs to be decreased dramatically to 0.01 [m/increment]. This makes solving the model tedious, time consuming and can also lead to exceeding EES's variable count limitation of 12 000 variables. For this study the explicit method was therefore not further used.

4.3.2 IMPLICIT APPROACH

For the implicit method an alpha of 1 along with the 1 [m] pipe increments was used. The implicit method is unconditionally stable for any time step size, as only the solution at the current time step is used. However, due to this the results obtained may not be very accurate. To verify the stability of the implicit method a couple of time steps were tested for no change in boundary conditions, as well as a case with a step change in the inlet boundary values. For all the cases investigated, the primary side showed stability and converged for all of the selected time intervals. It was found that the larger time steps resulted in smaller source term deviations from zero and faster return times.

The secondary side also showed good stability for the cases of no change in boundary values. The source term values oscillate around zero, but with negligible amplitude. For the case of the step change in the boundary value, the selected time steps also converged. However, for time steps larger than 1 [s], the solutions become inaccurate. This inaccuracy is related to the large velocity increase that occurs due to a decrease in the density. This high velocity requires smaller time steps to capture certain events more accurately inside the 1 [m] pipe increments. These events will otherwise be missed when larger time steps are taken. Please refer to Appendix II for a more detailed discussion along with figures illustrating the results of the implicit investigation.

4.3.3 CRANK-NICHOLSON APPROACH

The Crank-Nicholson approach implies that an Alpha of 0.5 is used. This should provide a good balance between stability and accuracy. However, caution should be taken as too small time steps can lead to the solution diverging. For both the primary and secondary sides the pre-selected increment length of 1 [m] resulted in divergence. The results of this are shown in more detail in Appendix II.

For the case of no change in the boundary values the primary side diverged for all time steps. This resulted in conditions that are beyond the fluid property reference base of EES. It should be noted that the larger time steps took longer to diverge. For the case where a step function was initiated at the boundary value all the selected time steps also diverged.

The secondary side did not give good results for the Crank-Nichols approach either. For both the fixed and stepped boundary values the secondary side source terms also diverged. Smaller the time steps resulted in faster divergence rates, where the larger time steps still diverged but at a much slower rate.

It was concluded that a Crank-Nichols approach will not be adequate for the selected geometry and boundary values. No change in boundary values resulted in a divergence of the source term for all time step sizes and an unstable transient steady state solution. With this in mind, an integration factor with a value of between 0.5 and 1 must be selected that results in a more stable solution.

4.3.4 ALPHA = 0.7 APPROACH

In order to maintain stability throughout the different regions numerous values for Alpha was investigated. The best compromise for stability and accuracy was found to be an Alpha of 0.7. When comparing this to other simulation packages it was found that Flownex (Flownex, 2012) also incorporates this value for its time-wise integration.

4.3.4.1 PRIMARY SIDE

When implementing an alpha of 0.7 on the primary side, stability is achieved for both the cases of fixed boundary value as well as for a step change. This can be seen from Figure 16 and Figure 17 below. A time step of 1 [s] seems to be the best approach as the deviation

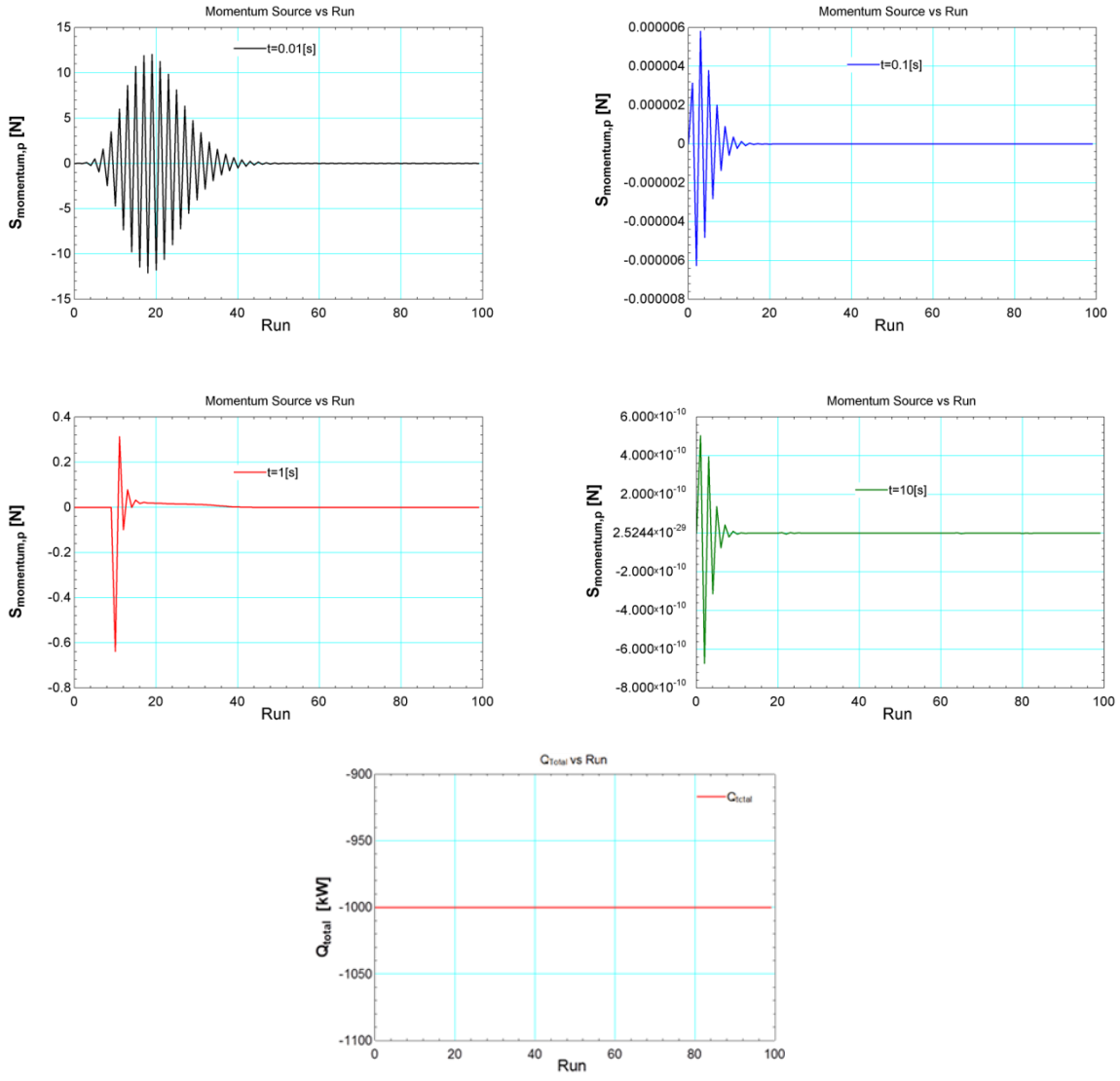

Figure 16 – Alpha of 0.7 primary momentum source term - Constant boundary values.

is small and the source term converges within 15 steps. For the boundary step change scenario of Figure 17, only the 0.01 [s] time step solution did not converge. At first the 10 [s] time step shows better stability than the 1 [s], but with the large time steps certain events can be missed between calculations. Thus the 1 [s] time step showed the best potential to be used in the combined model for stability and capturing events.

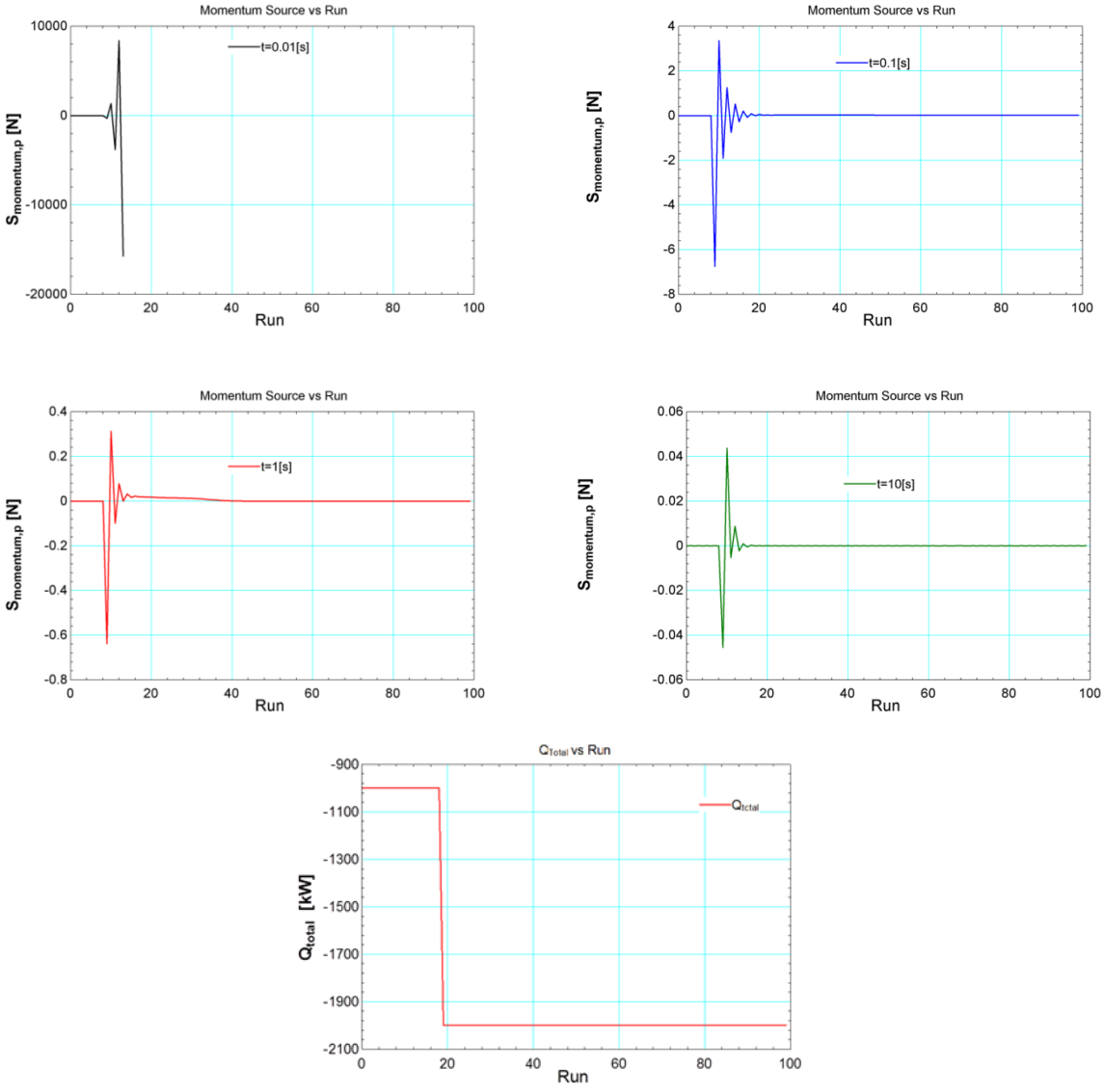

Figure 17 – Alpha of 0.7 primary momentum source term - step increase boundary values.

4.3.4.2 SECONDARY SIDE

The solution on the secondary side with an alpha of 0.7 converges for the case of no change in boundary values, Figure 18, and for a stepped change, Figure 19. The 1 [s] time step interval, identified as the best solution for the primary side, also results in a stable solution for both the scenarios investigated here, thus supporting its implementation in the combined model.

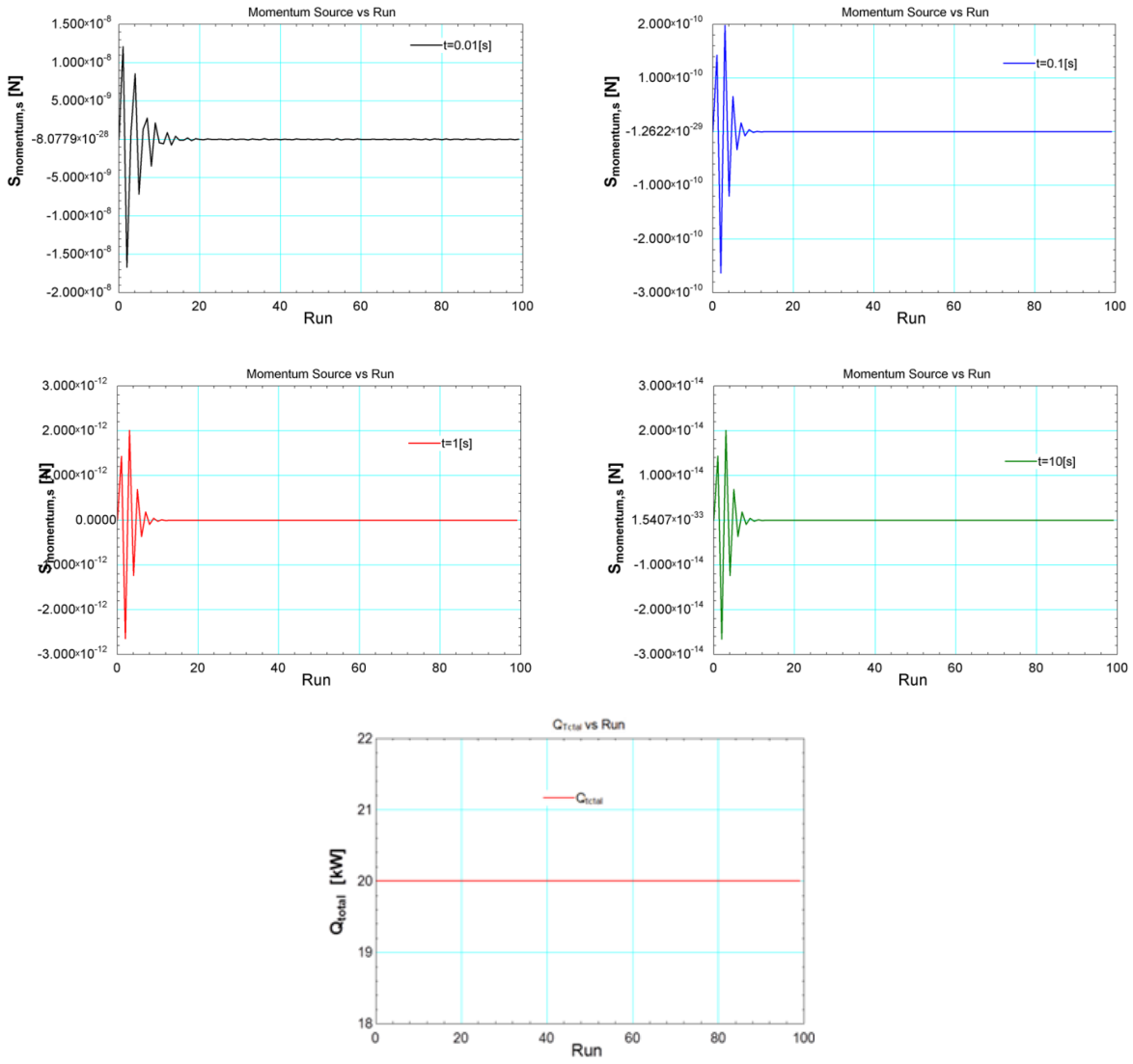

Figure 18 – Alpha of 0.7 secondary momentum source term – constant boundary values.

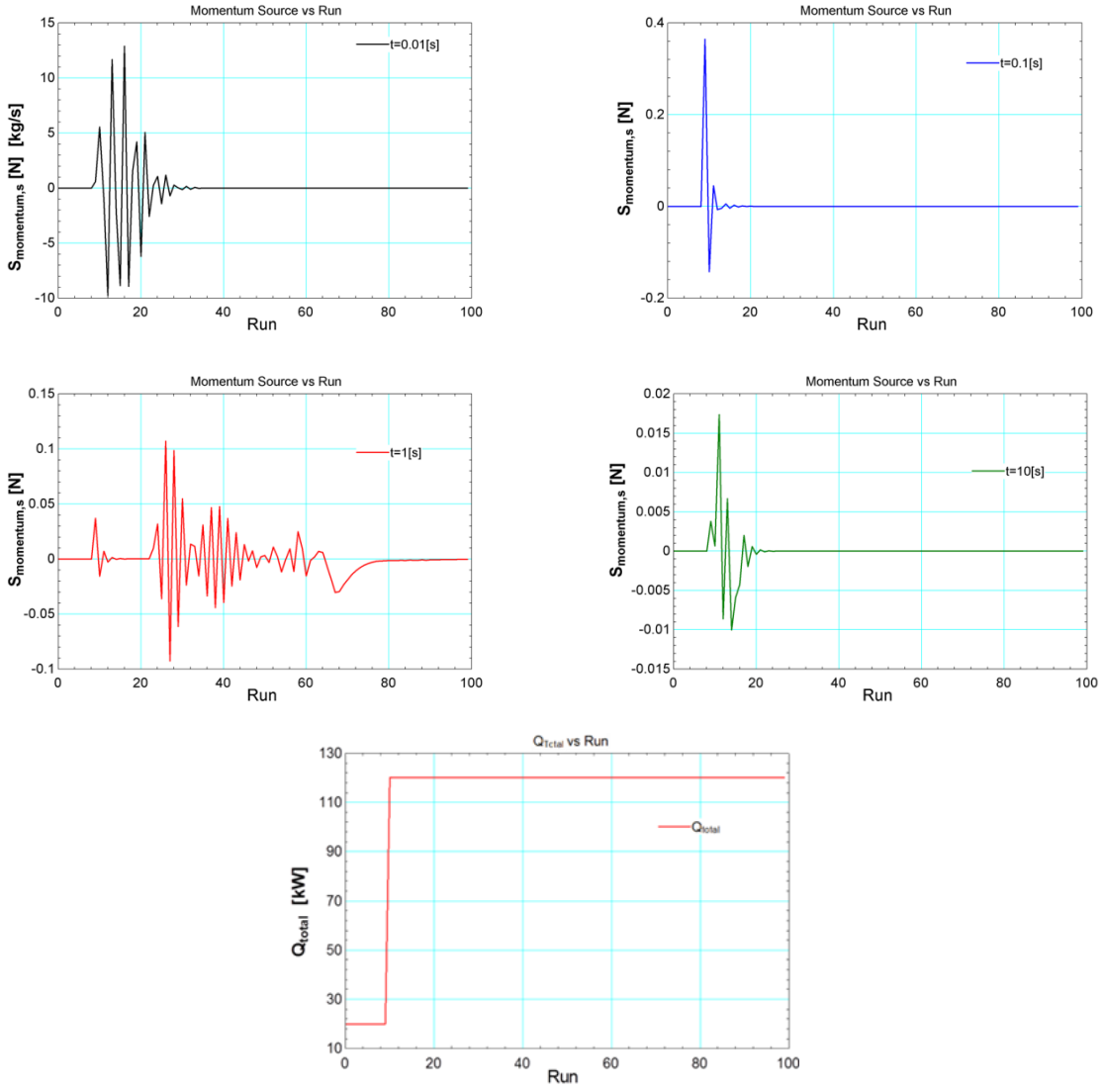

Figure 19 – Alpha of 0.7 secondary momentum source term - step increase boundary values.

4.3.4.3 COMBINED MODEL

With the stabilities of the primary and secondary sides evaluated and proven that an Alpha of 0.7 with a time step of 1 [s] gives reasonable answers, the two sides can now be combined into a single model. For this combined model the boundary values are the inlet pressures, temperatures and mass flow rates as listed in Table 2 above. Figure 20 shows the momentum source terms of the combined model along with the temperature profile over the length of the pipe, for the case of no change in boundary conditions. It can be seen from the third graph in Figure 20 that the primary inlet temperature is kept constant and these results in a constant secondary outlet temperature. In Figure 21 the temperature of the primary inlet side was increased with 0.25 [K] increments for each time step from 450 [K] up to 615 [K] and then

left to stabilize. It is clear, from the last graph of Figure 21, that the model retains stability even as the secondary side crosses over from a sub-cooled liquid into the two-phase region and then over into the super-heated region.

It should be noted that the model at this stage still used an average heat transfer coefficient and fixed pressure drop for the two-phase region, to more easily investigate the stability and transition between regimes. The first two graphs of Figure 21, shows that the source terms converge to zero over time, after the transient has been initiated. The third graph plots the secondary side outlet temperature and total heat transfer over the transient and the last graph is the temperature distribution over the pipe length.

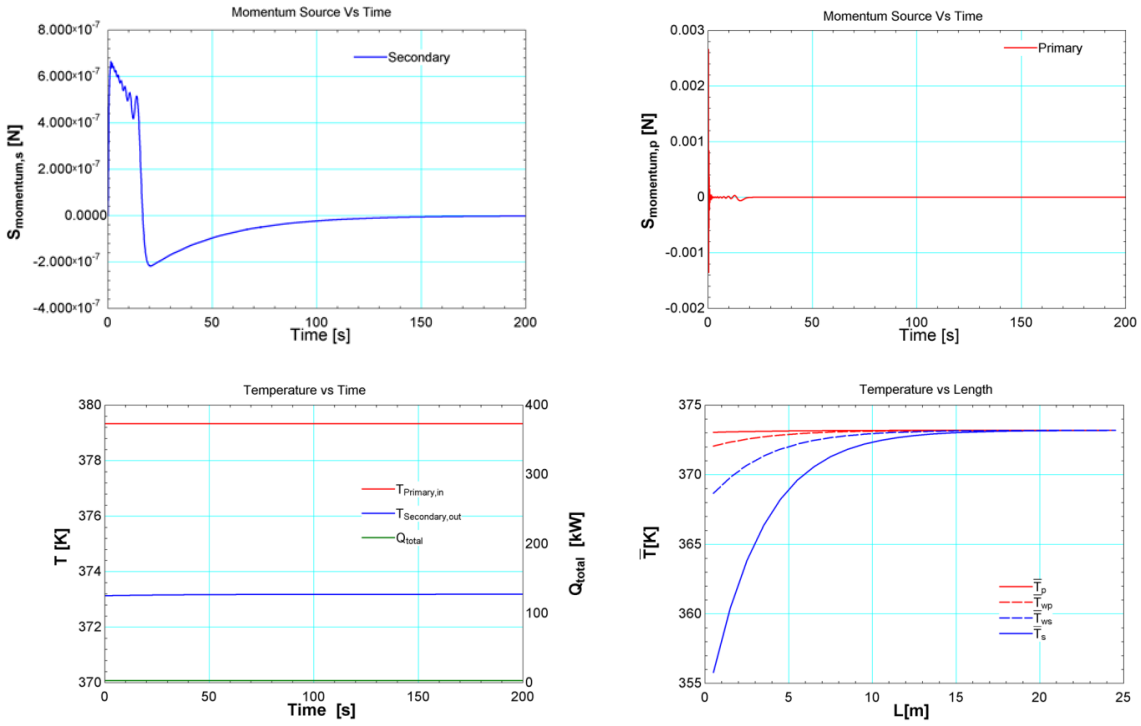

Figure 20 – Alpha of 0.7 momentum source term of combined model – fixed boundary values.

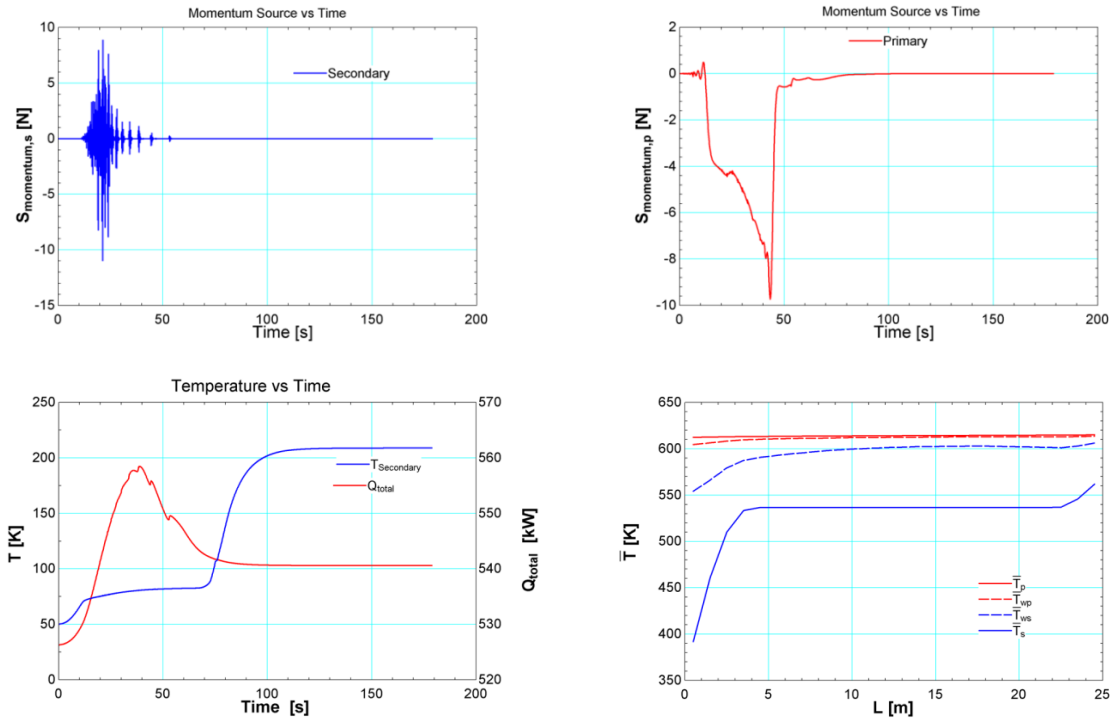

Figure 21 – Alpha of 0.7 source term of combined model - increase boundary values.

4.4 FINAL DETAILED EES MODEL

The next step was to expand the combined model to include the correct single phase and two-phase heat transfer and pressure drop correlations for both sides. As discussed in Chapter 3, the Forster and Zuber (2004) heat transfer correlation should be implemented on the secondary side, with the correlation by Friedel (1979) used for the pressure drop. As the primary side does not undergo any phase change under normal operating conditions the Dittus-Boelter heat transfer and pressure drop correlations will be used. The detailed source code of the final model can be found in Appendix I.

4.4.1 TRANSITION BETWEEN PHASES ON THE SECONDARY SIDE

Figure 22 will be used to illustrate the problems encountered with phase change within a pipe element. For this discussion the pipe consists of five elements and elements one and five contains the transition between two phases. Transition from single phase to two-phase, and

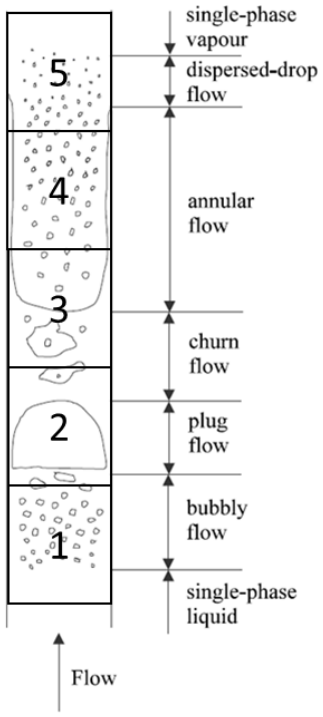

Figure 22 – Element phase change (Wolverine Tube, Inc., 2007).

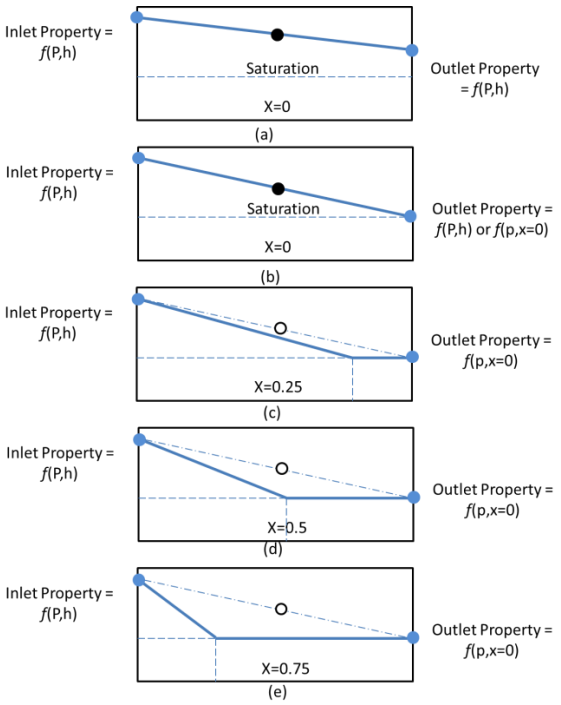

Figure 23 - Normal Average over inlet and outlet per pipe segment.

vice versa, will encounter a sudden change in the respective fluid properties. These fluid properties of the liquid and the gas influence the heat transfer and can cause instabilities in the solver when these are discontinues. To overcome these instability issues, average values are calculated from the known inlet and outlet fluid properties per segment, as illustrated in Figure 23. This approach results in a closer approximation of the actual values and gives EES a slope to work from rather than a discontinued function. The following scenarios can occur in a pipe element, with or without phase change taking place:

- The inlet and outlet conditions both sub-cooled.
- The inlet is sub-cooled with the outlet a saturated liquid.
- The inlet is sub-cooled with the outlet in the two-phase region.
- The inlet is in the two-phase region as well as the outlet.
- The inlet is in the two-phase region and the outlet a saturated vapour.
- The inlet is in the two-phase region and the outlet a superheated vapour.
- Finally, both the inlet and outlet are in the superheated region.

For these seven scenarios the fluid properties is a function of the conditions shown in Table 3. It is know that for sub-cooled liquids and super-heated gasses, the fluid properties change at constant pressure, as the fluid is cooled or heated. For the two-phase region the liquid and gas properties is that of the saturation condition at the local pressure and is thus constant if the pressure remains fixed. Table 3 shows how an arbitrary fluid`s liquid property can change over a pipe segment.

When the mathematical average fluid property for each pipe segment is calculated, it is seen that when no phase change is present, Figure 23(a), the average is calculated correctly from the inlet and outlet conditions. But when the segment contains a phase change, Figure 23(c), (d) and (e), using the mathematical average will result in an incorrect value. The average value remains unchanged regardless of the outlet quality of the pipe segment, even though less liquid is present as the quality increases. In these segments it is assumed that either sub-cooled or saturated liquid is present and thus a weighted average has to be used to calculate the fluid properties.

Table 3 - Segment inlet and outlet scenarios

Inlet Condition	Fluid Properties	Outlet Condition	Fluid Properties
Sub-cooled	Pressure, Enthalpy	Sub-cooled liquid	Pressure, Enthalpy
Sub-cooled	Pressure, Enthalpy	Saturated liquid	Pressure, Enthalpy
Sub-cooled	Pressure, Enthalpy	Two-phase	Pressure, Quality
Two-phase	Pressure, Quality	Two-phase	Pressure, Quality
Two-phase	Pressure, Quality	Saturated gas	Pressure, Enthalpy
Two-phase	Pressure, Quality	Super-heated gas	Pressure, Enthalpy
Super-heated gas	Pressure, Enthalpy	Super-heated gas	Pressure, Enthalpy

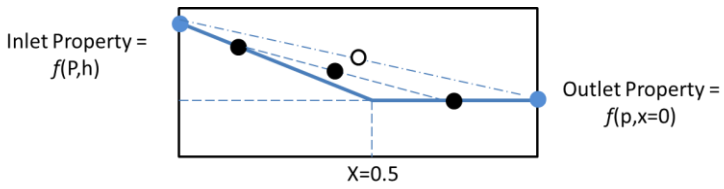

Figure 24 – Quality weighted average over inlet and outlet.

With this phase change inside a segment, even though a homogenous model is used, a boiling point has to be defined. As the model will simulate transient conditions the boiling point will shift from segment to segment depending on the boundary conditions. This result that the boiling point will initiate at the outlet of the segment when saturation is achieved and move through the pipe segment, Figure 23(b). When more heat is added the boiling point will shift more into the pipe segment, Figure 23(c), resulting in a specific outlet quality for the two-phase mixture. If we assume boiling starts a certain fraction form the segment outlet it is known which fraction is sub-cooled and which is in the two-phase region. With the outlet quality known, the boiling initiation point can be determined.

With the precise point where the boiling starts determined, a weighted average for the liquid properties can be calculated. This is done by calculating the areas beneath each of the two distinct phases, as seen in Figure 24, and given by .

$$Average = \Big(0.5 * (Inlet - outlet) * \big(L(1-x)\big)\Big) + (L(1-x) * oulet) + Lx * outlet \quad [46]$$

This averaging method eliminates the discontinuities and smooth out the transition in fluid properties encountered in the segments with phase change. With the smoothed transitions, EES has a slope rather than a discontinuous function to work from and results in the stability of the numerical solver.

4.5 SUMMARY

From this chapter the required time wise integration factor was determined for a stable model. The stabilities of the implicit, Crank-Nichols and an alpha of 0.7 approaches were tested for a set geometry and variable time steps. After the stabilities of the primary and secondary sides were proven, the two models were joined to form a counter-flow heat exchanger and the stability with averaged heat transfer values was inspected. It was indicated that an alpha of 0.7 and any time step larger than 0.01 [s] is satisfactory to ensure stability for

the primary side, the secondary side as well as the combined model. The issue of how to handle the transition between the phases within a segment was also investigated and discussed. In the next chapter the basic vertical tube model will be verified by an appropriate Flownex model.

CHAPTER 5 – VERIFICATION OF THE EES MODEL

5.1 INTRODUCTION

In the preceding chapters we established the required background and theory to ensure that the concepts pertaining to transient homogeneous two-phase flow modelling are understood and modelled correctly. In this chapter the detailed vertical pipe EES model will be verified with an equivalent layout simulated in Flownex. In order to have the relevant comparison with Flownex the EES model`s inlet pressure boundary condition was changed to an outlet boundary condition. This allowed both models to be identical in boundary conditions and geometry so that the results can be compared.

5.2 STEADY-STATE COMPARISON

The first step in verification of the EES model is to determine if a Flownex model with the same inlet conditions and geometry delivers similar results. Figure 25 shows the developed Flownex model of a 25 [m] pipe-in-pipe concentric tube heat exchanger. The relevant geometries given in Table 4 were selected along with the same boundary values as used in the EES model, listed in Table 5. To verify the accuracy of the EES model the Flownex pipe element was also divided into 25 sub elements.

Table 4 - Flownex geometry.

	Primary	Secondary
Hydraulic Diameter [m]	0.04	0.025
Length [m]	25	25
Tube Material	-	AISI 302
Wall thickness [mm]	-	5
Friction Factor	0.01	0.02
Heat Transfer	Dittus-Boelter	Dittus-Boelter

Table 5 - Flownex boundary values.

	Primary	Secondary
Inlet Temperature [K]	450	400
Inlet Mass Flow [kg/s]	1	0.04
Outlet Pressure [MPa]	15.5	5

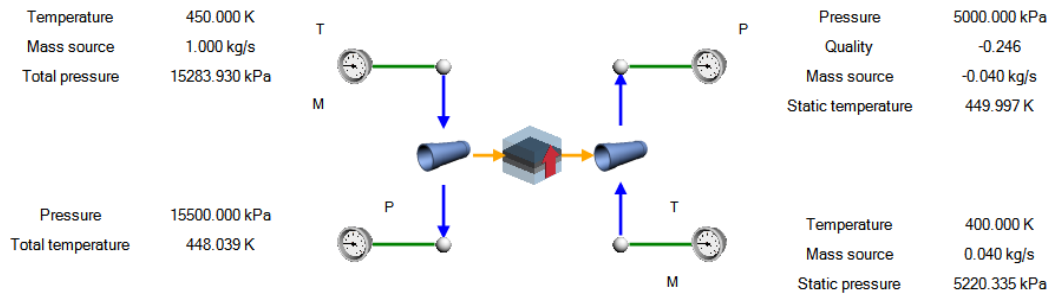

Figure 25 - Flownex model.

The results from both the Flownex and EES models, for a steady state 25 [m] pipe, are compared in Table 6, with the Flownex results used as the reference when values are compared. It can be seen that from the steady state solution the results correspond very well, with a small over-estimation of the total heat transferred to the secondary side of 0.325 [kW] by the EES model. This equates to a 4 [%] over-estimation compared to Flownex. When comparing the calculated heat transfer coefficients, Figure 26, it is seen that both solutions follow the same trend, but that the EES model overestimates the coefficients in the first few increments with a maximum error of 2.2 [%]. This is mainly due to the numerical solution EES employs and the relaxation parameters used in Flownex. Another reason for the variation is due to Flownex calculating the thermal capacity of the wall material, where the EES model does not bring this into consideration.

The calculated inlet pressures, for the fixed outlet pressure defined, correspond with minimal deviation between the two models. It can be concluded that the pressure drop for the single phase flow has been handled correctly in the EES model, the two-phase verification will be handled in the same manner in the next section. The start-up steady state conditions are thus verified with the Flownex network.

Table 6 – Steady state comparison.

	Flownex		**EES**	
	Primary	**Secondary**	**Primary**	**Secondary**
Inlet Pressure [MPa]	15.3	5.2	15.3	5.2
Outlet Temperature [K]	448.1	448.1	447.9	450
Total Heat [kW]	8.3		8.6	

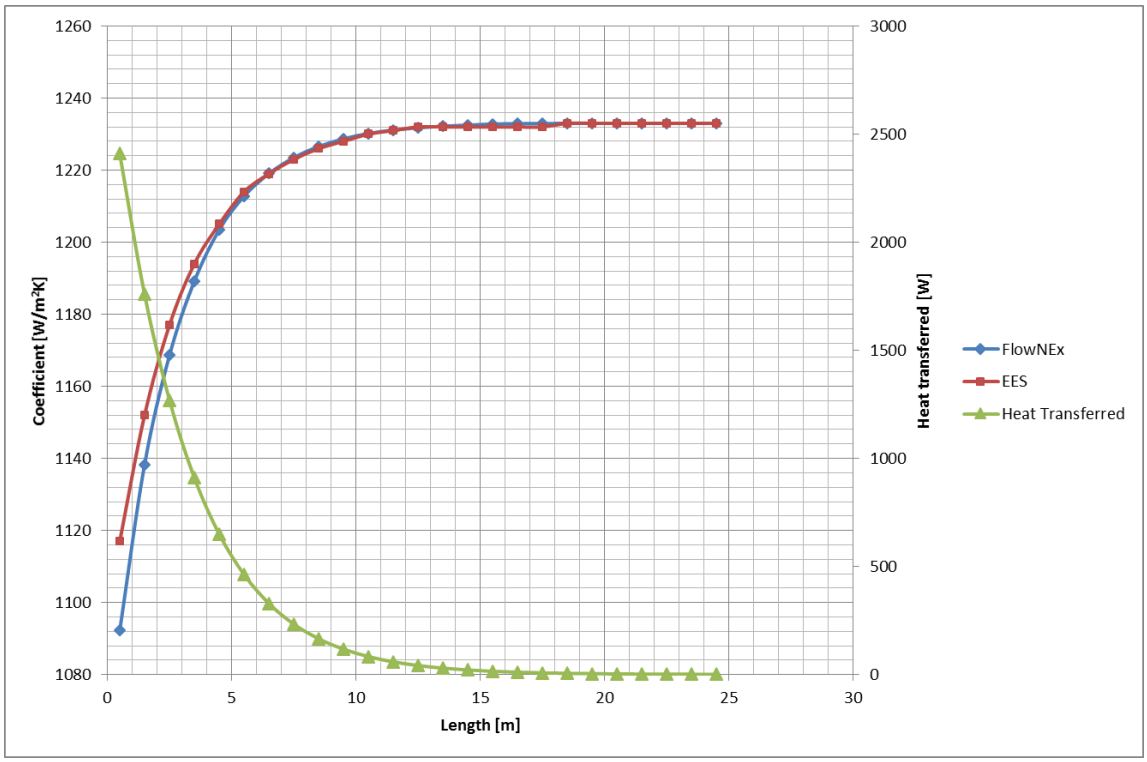

Figure 26 – Single phase heat transfer and heat transfer correlation over length of pipe.

5.3 TRANSIENT COMPARISON

For the transient solution the secondary side undergoes a phase change as the primary side inlet temperature is increased by 0.25 [K/s]. This simulates the effect of the reactor powering up. From literature it is known that the PWR core outlet temperatures are between 570 and 590 [K]. For this transient the inlet temperature was increased from 450 to 580 [K] and the system, then left to stabilize after which the results was compared. Once the scenario has achieved steady state the values are then compared.

For both models the primary inlet temperature was held at 450 [K] for 10[s] before the transient was initiated. The secondary outlet temperature and mass flow along with the inlet pressure were tracked for the duration of the transient. These results are compared, in Table 7 to ensure that the continuity equations were correctly implemented, along with the transition points between phases. These results were then compared to determine the accuracy of the transient EES model. This acts as verification for the EES model and supports the further use of Flownex to investigate the more complex helical SG layout.

Table 7 – Transient comparison.

	Flownex		EES	
	Primary	**Secondary**	**Primary**	**Secondary**
Inlet Pressure [kPa]	15329	5045.1	15320	5049
Outlet Temperature [K]	562.7	578.4	562.3	572.8
Outlet Mass flow [kg/s]	1	0.04	1	0.04
Total Heat [kW]	96.27		96.91	
Time from start [s]	822		822	

To ensure that the two-phase boiling heat transfer correlations were implemented correctly, the Flownex and EES results were compared, as shown in Figure 27. For both cases the boiling starts at around the 2.5 [m] mark. It should be remembered that Flownex uses a relaxation for the two-phase density change and two-phase heat transfer, to compensate for the large changes in properties when boiling occurs. Even with this, the results of the EES and Flownex models only differs with a maximum error of 12.7 [%] in the two-phase region and a 5.7 [%] for the maximum calculated heat transfer coefficient. What is important to note from Figure 27 is that the results of both models follow the same trend line.

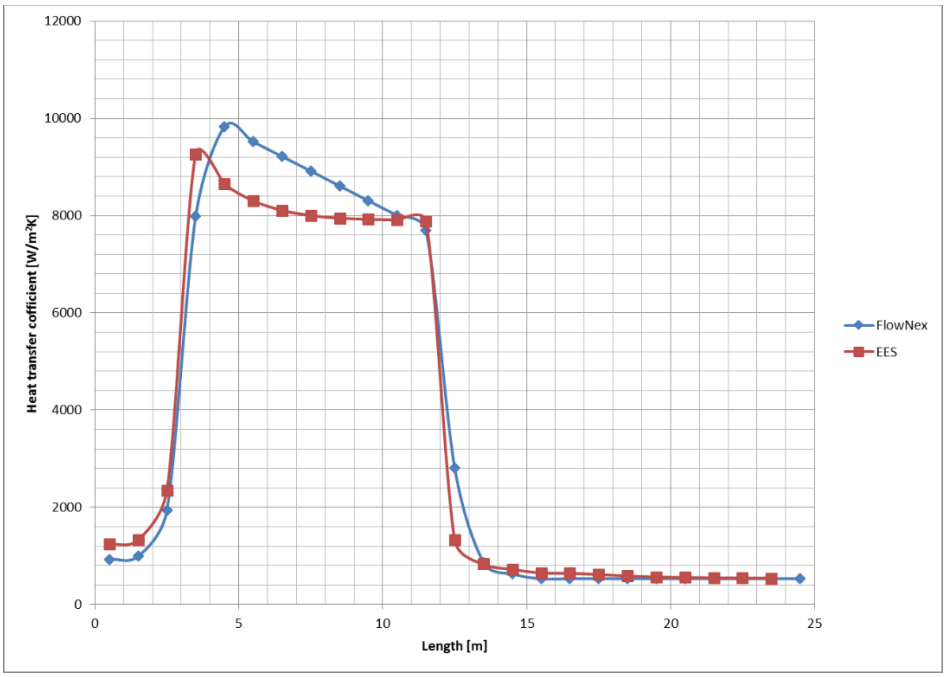

Figure 27 – Single and two-phase heat transfer comparison.

From Figure 28 to Figure 31 for the transient it is clear that for both Flownex and EES the outlet conditions of pressure, temperature, quality and mass flow rate follows the same trend. The EES results for the mass and temperature are more jagged and this is contributed to the numerical Newton-Raphson solver that is used. The results for Flownex are smoother and more gradual; this is due to relaxation parameters that can be specified in the flow solver. The maximum and average errors between the EES and Flownex are given in Table 8.

For Figure 28 there is a 34.01 [%] deviation between the maximum predicted EES and Flownex mass flow rates when boiling initiates. From the Flownex user manual (Flownex, 2012) it was understood that when two-phase liquids are modelled the solver will experience convergence issues. To account for the sudden large density changes, the two-phase density relaxation factor is set as 0.5. This will relax the source term in the mass conservation equation and therefore result in the larger increase in mass for the Flownex network.

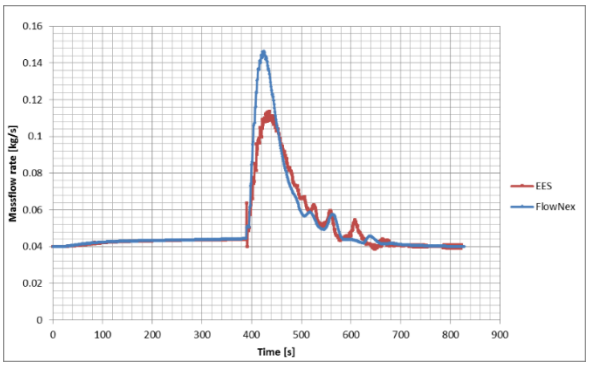

Figure 28 – Comparison of the of the secondary side outlet mass flow rate.

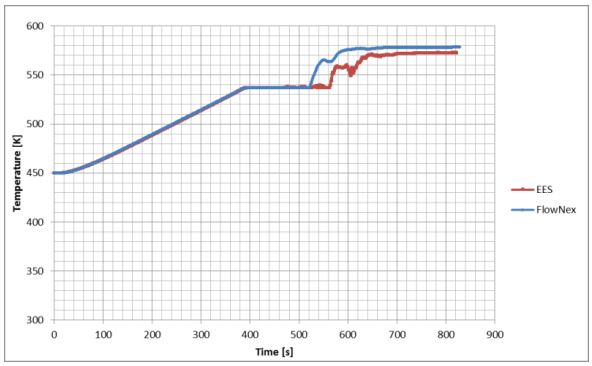

Figure 29 - Comparison of the secondary side outlet temperatures.

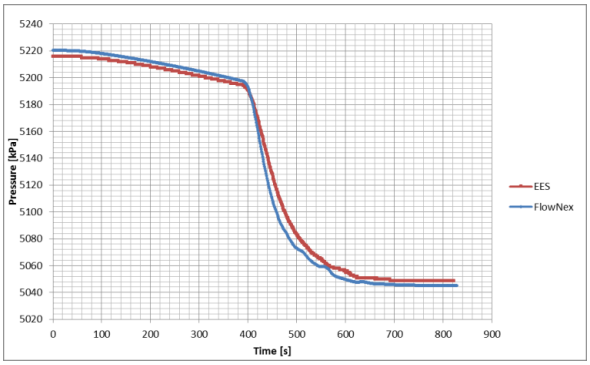

Figure 30 - Comparison of the secondary side outlet pressure.

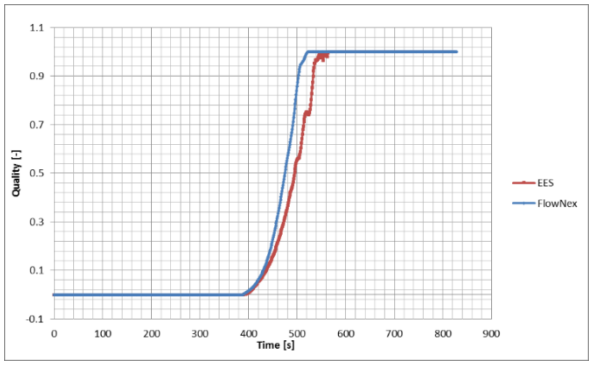

Figure 31 - Comparison of the secondary side outlet quality.

Table 8 - Maximum and average error between EES and Flownex

Secondary Side	Maximum [%]	Average [%]
Mass flow rate	34.01	0.69
Temperature	5	0.71
Pressure	0.37	0.03

With the inlet and outlet conditions verified for the transient simulation a closer look at the property distribution along the length of the pipe can be taken. Figure 32 and Figure 33 shows the property plots of the steam across the length of the pipe as predicted with the EES model. It is shown that the secondary fluid undergoes phase change from a sub-cooled liquid, through the two-phase region, with superheating taking place in the last part of the tube.

To see what effect the two-phase boiling has on the system, the wall surface temperatures and heat flux over the boundaries needs to be plotted. From Figure 34 the effect of the increased heat transfer is clearly seen as the wall temperatures decrease as boiling initiates. When dry out occurs the heat transfer decreases and the resulting increase in wall temperature can be seen.

Figure 35 correspond with the temperature distribution and shows how the heat flux changes over the wall as the phase change takes place. It is clear that in the two-phase region much more heat can be extracted from the wall due to the violent turbulent nature of the boiling within the tube. As soon as dry-out occurs the heat transfer decreases. With the decrease in the heat transfer, the wall temperature increases.

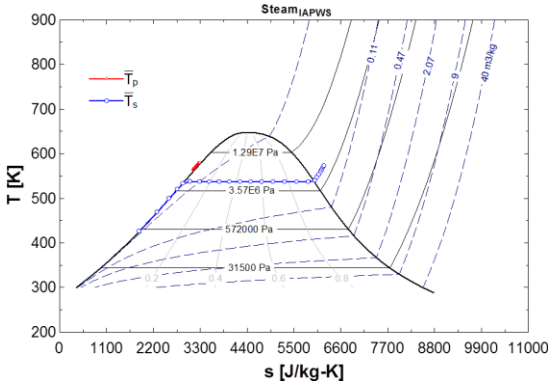

Figure 32 - EES: T-s for primary and secondary side.

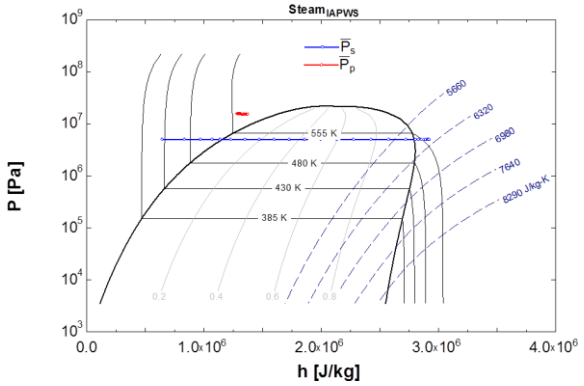

Figure 33 - EES: P-h for primary and secondary side.

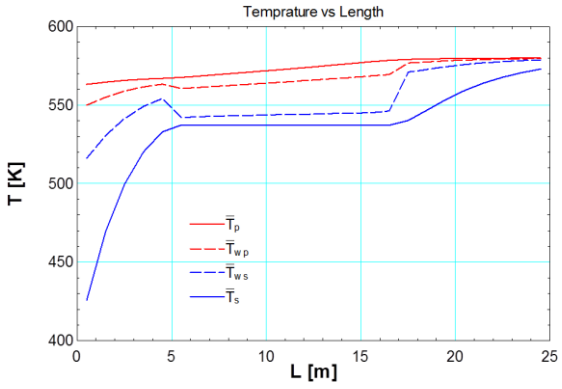

Figure 34 - EES: Temperature change over the length.

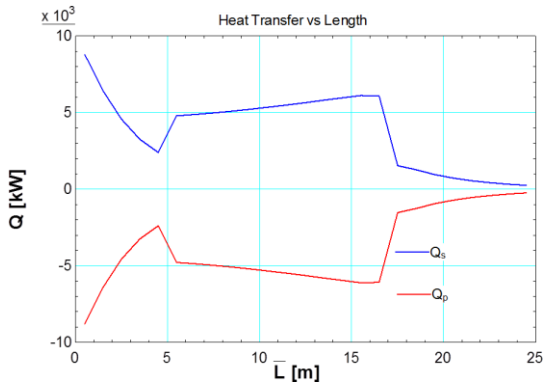

Figure 35 – EES: Change in heat transferred over the length.

As phase change takes place over the length of the tube, it means that as the quality increases liquid will be converted into the gas phase. In Figure 36 the conversion from liquid to gas along the length of the pipe can be clearly seen. From about 5 [m] up to about 16 [m], boiling occurs and the liquid water is converted into steam. Figure 37 shows how the specific heat capacity of the two fluids changes.

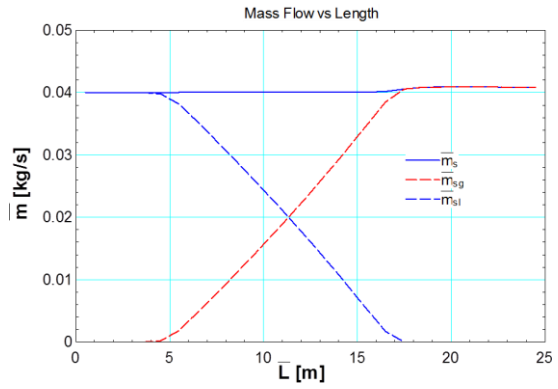

Figure 36 - EES: Change in the mass flow rate over the length.

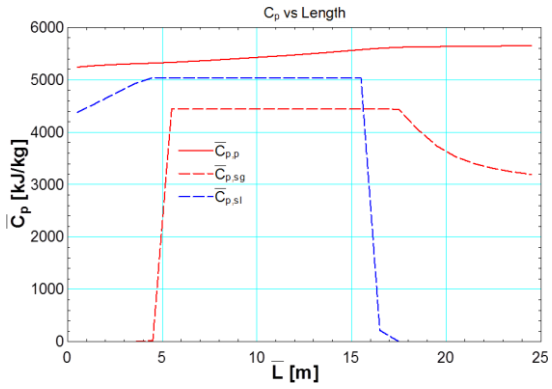

Figure 37 - EES: Change in specific heat over the length.

On the primary side due to phase change, the density of the fluid along the length of the tube decreases, as shown in Figure 38. To satisfy the mass continuity equation the velocity as shown in Figure 39 has to increase. This change in density is also accountable for the increase in mass flow, as seen in Figure 28 during the transient response of the system.

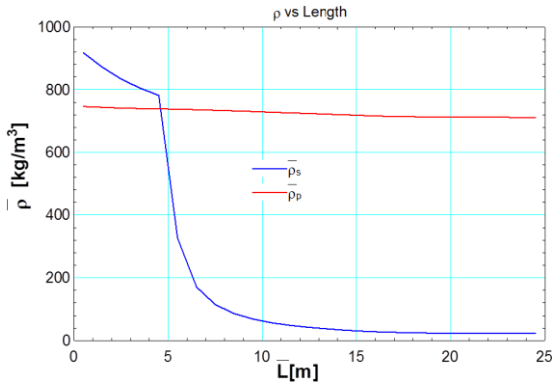

Figure 38 - EES: Density change over the length.

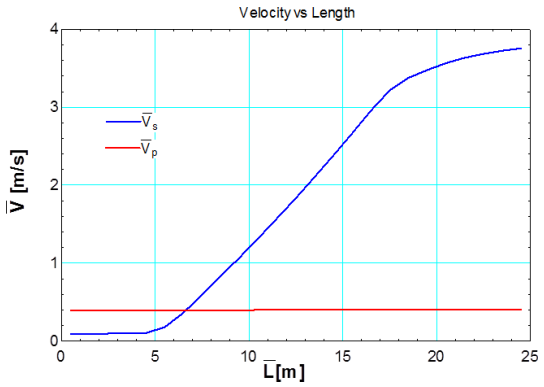

Figure 39 - EES: Velocity change over the length.

5.4 CONCLUSION

In this chapter one scenario`s start-up and transient results of the EES model for a vertical tube with two-phase flow have been compared to that of a Flownex model. From the results it is evident that the theory of two-phase flow heat transfer, pressure drop and transient modelling was implemented correctly. I can be assumed that other normal start-up scenarios should behave in the same manner. It is concluded that an understanding of the theory behind transient two-phase flow modelling has been achieved and that it can now be applied to model an OTHSG. As mentioned earlier in this chapter, due to the advantages of using Flownex, the model developed therein will be further expanded for OTHSG with the SG geometry based on that of the IRIS reactor. In the next chapter the relevant simplifications and enhancement factors will be discussed, and once the geometry has been applied the results will be compared to the test data of Cinott *et al*. (2012).

CHAPTER 6 – HELICAL COIL MODEL

6.1 INTRODUCTION

This chapter will focus on expanding of the Flownex model to simulate an OTHSG with the geometry based on that of the IRIS reactor SG. The relevant simplifications and enhancement factors will be discussed, and the results will be compared to the test data of Cinott *et al*. (2012).

6.2 IRIS REACTOR COIL DATA

According to the IAEA (2012) there are different designs currently under development consisting of multiple configurations and operating conditions. Work done by Cinott et al. (2002 and 2012) simulated the 1000MWt IRIS reactor with its eight integrated once through helical coil steam generators (OTHSG) for licensing purposes as shown in Figure 40. The geometry and boundary conditions taken from their work serves as verification of the Flownex network and the simplifying assumptions made for the model.

Due to the geometrical symmetry and the layout of the eight OTHSGs within the reactor vessel, only one will be modelled within Flownex. The geometrical data and operating conditions of the IRIS OTHSG can be found in Table 9. This includes the coil mean diameter and the average length of the tube bundles. From this the curvature ratio, but more important the amount of coil passes can be determined. This will be used to investigate the effect of tubes in parallel and the influence of the coil passes on tubes downstream from them. From total height of the SG and the total length of the tube it can be calculated that the IRIS SG has at least 6 coil passes.

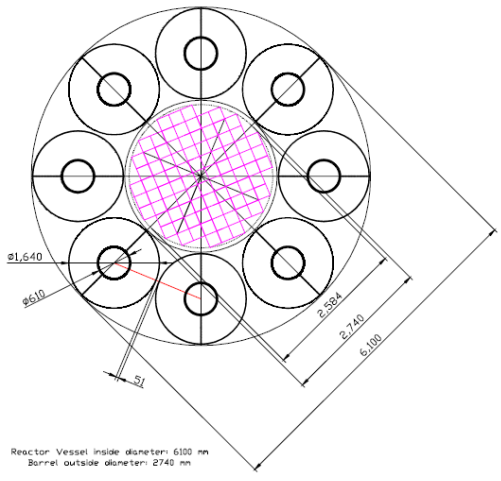

Figure 40 –Top view of IRIS reactor and steam generator layout (Cinotti, et al., 2002).

Table 9 - IRIS SG geometry and operating conditions.

Rated power [MW]	125
Tube outside diameter [mm]	19.05
Tube thickness [mm]	2.26
External shell inside diameter [mm]	1620
Internal shell outside diameter [mm]	610
Number of helical rows	20
Number of tubes	856
Tube bundle average length [m]	32
SG height [m]	10
Coil mean diameter [mm]	1600
Primary inlet temperature [°C]	328.4
Primary outlet temperature [°C]	292
Secondary inlet temperature [°C]	212
Secondary outlet temperature [°C]	317
Primary outlet pressure [MPa]	15.5
Secondary outlet pressure [MPa]	7
Primary mass flow rate [kg/s]	589
Secondary mass flow rate	62.5
Primary pressure loss [kPa]	136
Secondary pressure loss [kPa]	101

6.3 SINGLE PASS WITH A SINGLE COIL

In the previous chapters only a single vertical pipe was considered. Now with the IRIS SG data the effect of the helical coil on the heat transfer have to be investigated. The simplest set-up will be of a single tube with only one coil revolution. From the Figure 40 it is seen that the tubes are coiled within the annulus of the SG and it will be necessary to simplify a three-dimensional geometry to two-dimensions for modelling it in Flownex.

To start the simplification, the annulus can be unfolded and be represented as a rectangular duct as seen in Figure 41. This will be the basis to model the three-dimensional geometry. When the annulus is unfolded the coil flow path becomes a vertically inclining straight tube. It is assumed that the flow in the annulus is evenly distributed. From this it is seen that the flow over the tube has two components, namely a counter flow and a cross flow component. The coil enhancement factor described in Chapter 4 use the counter flow configuration and enhances it to incorporate the cross flow heat transfer as well. Thus the single tube can be modelled as a vertical tube with the enhanced heat transfer due to the coiling and the pressure drop over the tube will be that of the equivalent horizontal tube. This will simplify to a concentric tube-in-tube heat exchanger with the coiling heat transfer in the inner tube and cross flow pressure drop in the annulus.

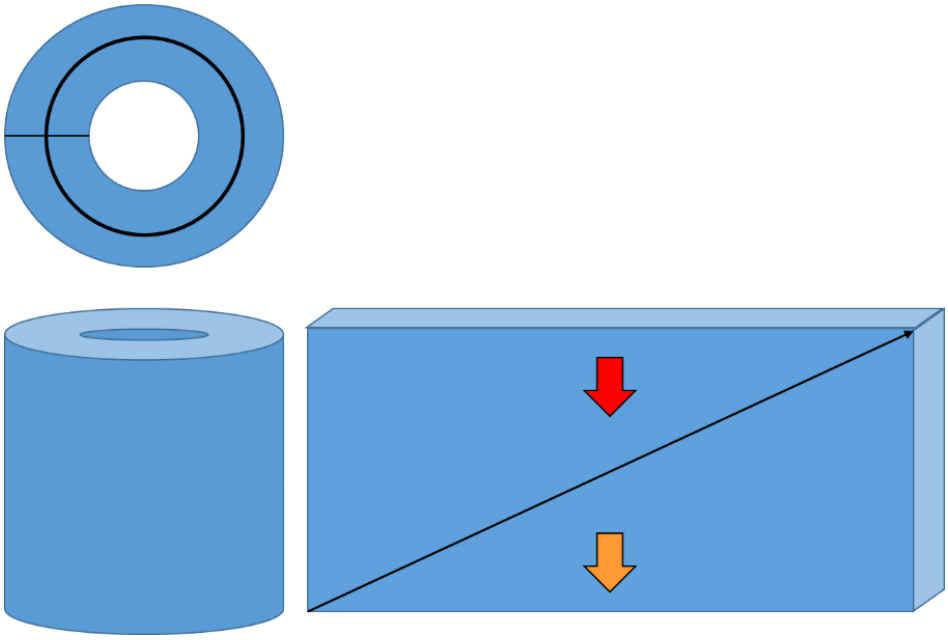

Figure 41 – Representation of a single coil with one pass.

6.4 SINGLE PASS WITH MULTIPLE COILS

When multiple coils in parallel are present, as illustrated in Figure 42 and Figure 43, they start to interfere with one another due to the geometry of the coil. This geometry is used to simplify the model as symmetric regions are present. It is assumed that the coil headers distribute the flow evenly through all the tubes and that the flows inside the annulus is also evenly distributed. Due to the even length of the tubes and the mass flow in and over the tubes the heat transfer and pressure drop will be equal for each tube.

Figure 42 and Figure 43 show the configuration of two and three tubes in parallel with a single revolution. For the two coil scenario of Figure 42 the annulus can be divided into a 2x2 grid and thus the tubes are divided into two increments, namely the lower and upper section. When it is assumed that the flow in the annulus are evenly distributed and the flow within the tubes are balanced a clear pattern can be seen.

The upper sections of both tubes are in contact with the same conditions and equal energy are extracted by both tubes. Because the upper tubes extract the same amount of energy from the fluid, the lower sections, even though in the wake of its neighbouring tube's upper section, experience the same conditions. Figure 44 shows a simplification where the segments of each tube were rearranged, so each coil`s segments are grouped above one another. This is the same configuration as the single tube and simplifies to equivalent vertical tubes. With the simplification and the assumption that the flow is uniform the temperature distribution in the radial direction of the SG is constant for multiple tubes in parallel. The only effect that tubes in parallel has is the increased surface area and thus more energy extracted from the primary fluid. From this coiled tubes in parallel can be simplified to vertical parallel tubes, Figure 44 and the heat transfer enhancement factor compensates for the simplified geometry.

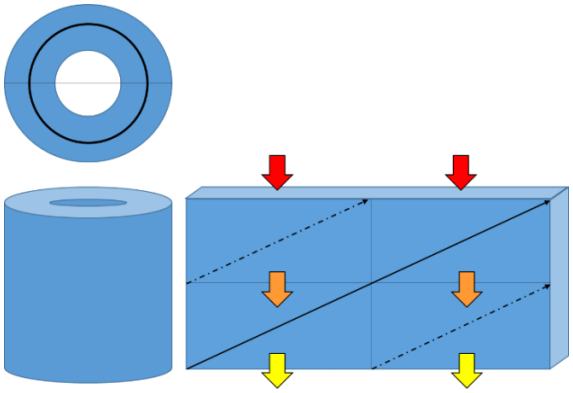

Figure 42 – Representation of two coils with a single pass.

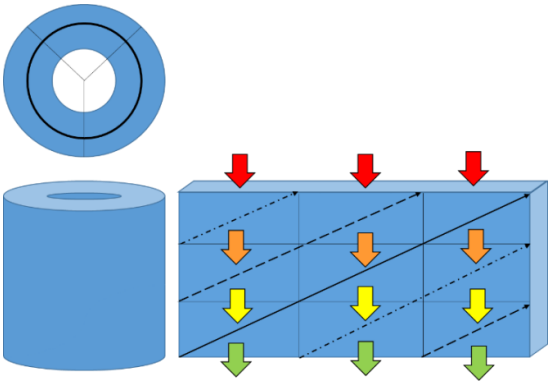

Figure 43 – Representation of three coils with a single pass.

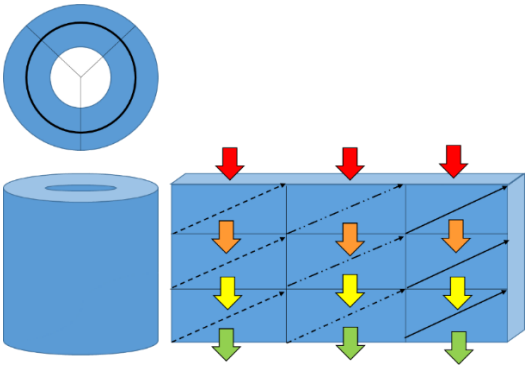

Figure 44 – Simplification of multiple coils with a single pass.

6.5 MULTIPLE PASS WITH MULTIPLE COILS

Now that the simplification of the tube layout in parallel with a single pass has been reviewed, the simplification of multiple passes can also be done as shown in Figure 45 and 46. For multiple passes the height of the SG stays the same but the pitch height and pitch angle of the coil is decreased. With a smaller pitch height, more revolutions can be fitted into the SG. For each pass added the total tube length is doubled. Figure 45 shows two coils in parallel both with two passes. Once again it is seen that, due to the geometry, the radial temperature and flow distribution is constant and the temperature and pressure only varies along the height of the SG. Figure 46 uses the same rearrangement argument as Figure 44 and shows that multiple passes can also be simplified to a single tube, but with a longer length

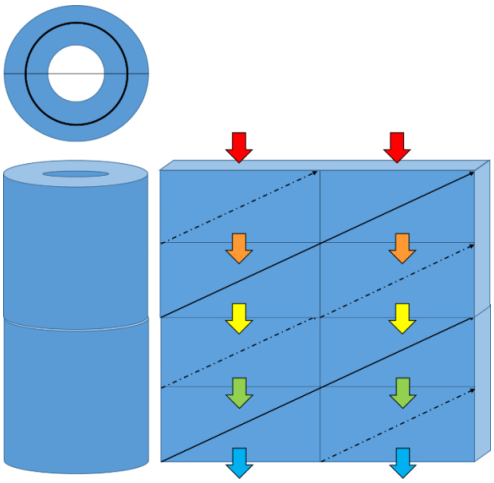

Figure 45 - Representation of two coils with two passes.

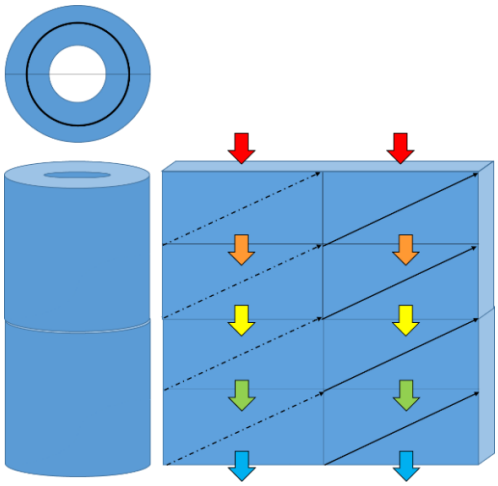

Figure 46 - Simplification of multiple coils with multiple passes.

6.6 FLOWNEX MODEL – FULL POWER COMPARISON

Now with the simplifications for the helical coil covered the geometry listed in Table 9 can be added to the model. The Flownex OTHSG model will now be evaluated with the IRIS experimental data conducted by Cinott *et al.* (2012) to ensure that the helical theory and layout simplifications have been implemented correctly. Once the model has been verified the transient response of the two-phase flow boiling will be modelled. From gathered theoretical background and the geometry of the IRIS SG the following correlations and values was used to model the OTHSG, Table 10 and Table 9.

Table 10 - OTHSG geometry and correlations.

Annulus hydraulic diameter [m]	0.9949
Coil pitch [m]	1.677
Coil revolutions [-]	6
Helix diameter [m]	1.64
Curvature ratio [-]	0.01162
Internal Dittus-Boelter equation with coil enhancement factor	$0.07106Re^{0.74}Pr^{0.3}$
External Dittus-Boelter equation with tube bundle enhancement factor	$0.021Re^{0.84}Pr^{0.36}$
External friction factor	0.454
Internal friction factor	0.03

Figure 47 shows the updated Flownex model that was used to simulate the transient conditions of the IRIS reactor`s SG. The only difference between the vertical and helical model is that of the geometry and the added heat transfer enhancement factor. To verify that the correlations and assumptions were implemented correctly, the boundary values were set to that of Cinott (2012) and the results compared in Table 11. From Table 10 it can be seen that the Flownex model has a very small error percentages when compared to the data of Cinott (2012), except for the primary side pressure loss calculation. The focus of the study was to model the internal flow within the helical coil, thus the simplifications was made regarding the external geometry and flow over the tube banks.

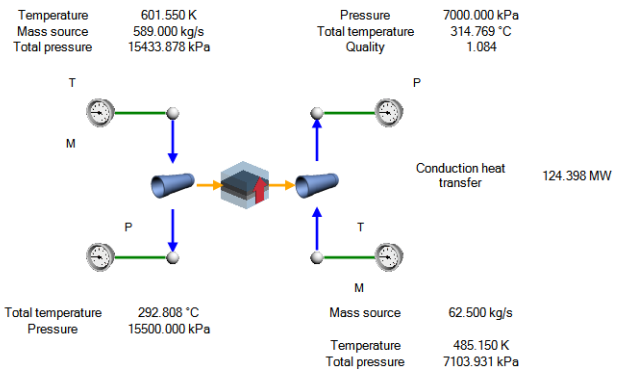

Figure 47- Flownex OTHSG model.

Table 11 – Results comparison between Cinotti and Flownex results.

	Data	Flownex	Error [%]
Rated power [MW]	125	124.4	-0.48
Primary outlet temperature [ºC]	292	292.8	0.27
Secondary outlet temperature [ºC]	317	314.8	-0.69
Primary pressure loss [kPa]	136	66.1	-51.40
Secondary pressure loss [kPa]	101	103.9	2.87

Figure 48 shows the temperature distribution results obtained by Cinotti (2002) and Figure 49 the Flownex model results. From these two figures it can be seen that the Flownex model and Cinotti results correspond with minimal deviation from one another. With these results the Flownex model setup has been verified and the model can now be used to simulate a cold start-up transient scenario.

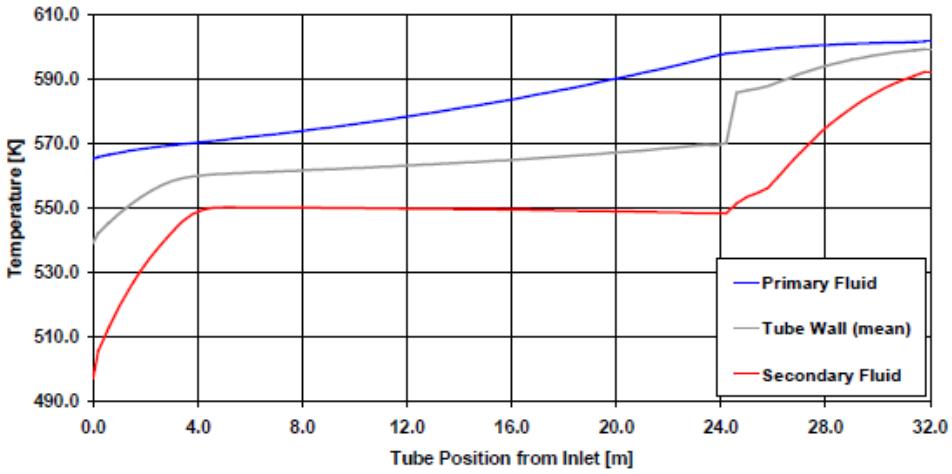

Figure 48 - Temperature distribution of the IRIS SG at 70 bar (Cinotti, et al., 2002).

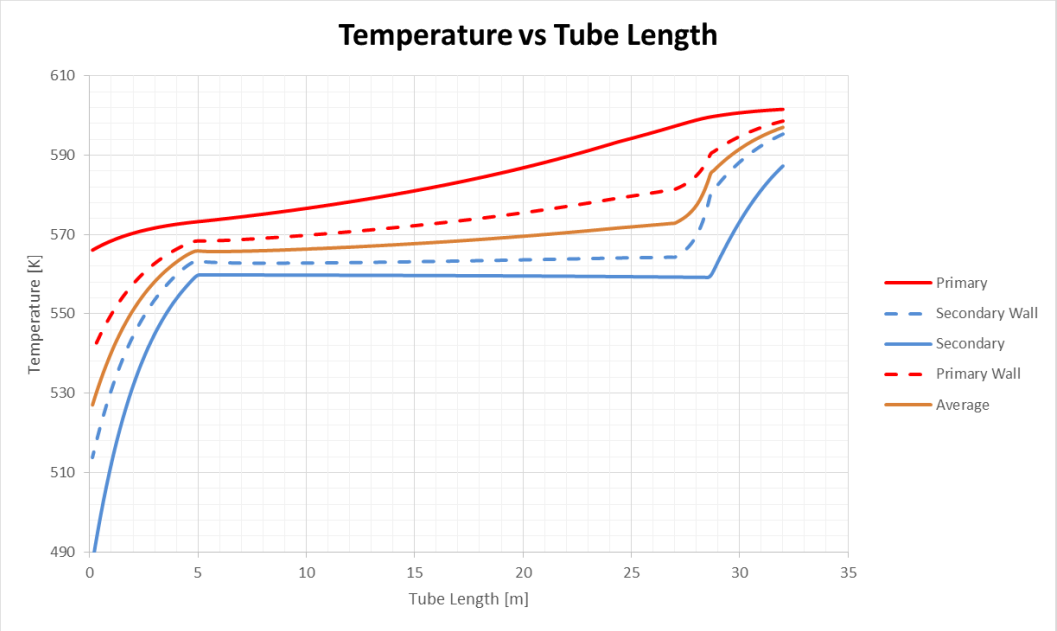

Figure 49 - Temperature distribution of the IRIS Reactor modelled in Flownex.

6.7 FLOWNEX MODEL – TRANSIENT START-UP SCENARIO

The final part of this study focus on a cold start-up transient simulation of the helical coil SG. From the conceptual operating characteristics of the IRIS reactor, the planned load change that the reactor can achieve will be about 5%/minute between 15% and 100% power (International Reactor Innovative & Secure, 2002). Further data regarding the start-up and overall operating characteristics of the reactor is still unknown. As the system is a PWR other similar size PWR plant data can be used for the secondary loop response.

For the transient scenario the reactor will initially be in the cold standby condition. This means the reactor is at zero power, but the primary loop is already at the operating pressure. It will be assumed that both the primary and secondary loops will initially be at room temperature. During the transient start-up of the reactor the outlet temperature will increase by 0.25 [K/s] up to 602 [K] as tested by Cinott (2012). This simulates the 5% power increase per minute that the reactor can achieve. At the beginning of the start-up the secondary loop bypasses the turbines and is directly discarded to the condenser. This is done to protect the turbines from water damage while the secondary loop has not yet achieved the required vapour quality. The discharged water is pumped through the pre-heaters to increase the secondary loop inlet temperature.

To try and simulate this effect, the secondary loop`s inlet temperature will be kept at room temperature, of 25 [C], for the first minute and then gradually increase with 0.1 [K/s] up to 485 [C]. Figure 50 shows the Flownex results of the inlet and outlet temperatures of both the primary and secondary loop over time for the inlet temperatures as explained above. From the figure it is seen that there is no temperature increase of the secondary outlet from 1000 to 1200 [s] as the outlet conditions is two-phase. There is only an increase once the outlet reaches dry out and super-heating occurs.

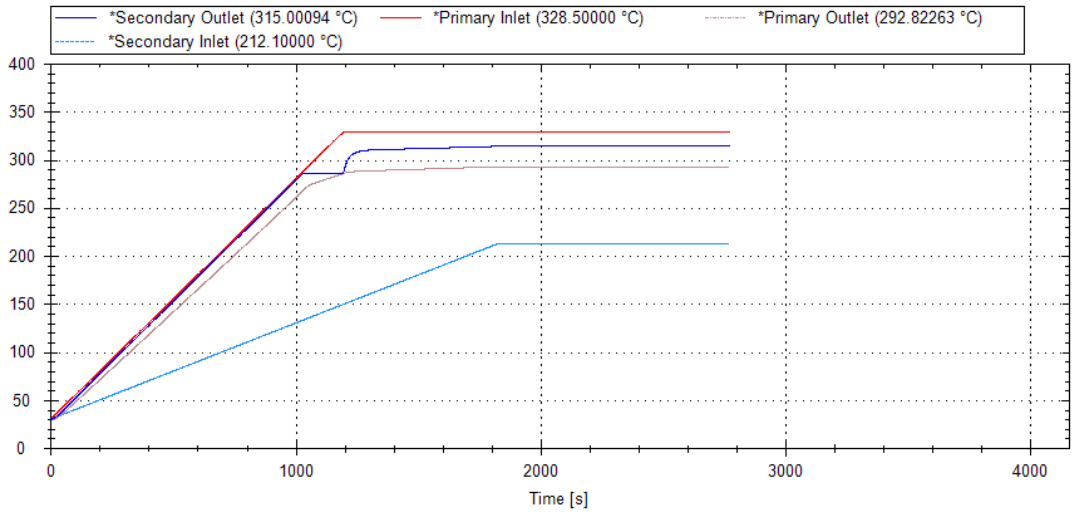

Figure 50 - Temperatures changes over time.

As the primary and secondary side inlet temperatures are increased the secondary side outlet vapour quality gradually increased as more energy is transferred, as seen in Figure 51. Vapour quality is usually defined between 0 and 1, but Flownex on the other hand gives a negative value for sub-cooled liquids and a value larger than 1 for super-heated vapours. This can be seen as Flownex`s way of indicating the degree of sub-cool and super-heating. It is seen that it takes the sub-cooled secondary side about 16.5 minutes to reach saturation from start-up. As soon as boiling starts it only takes 4 minutes for the SG to produce super-heated steam.

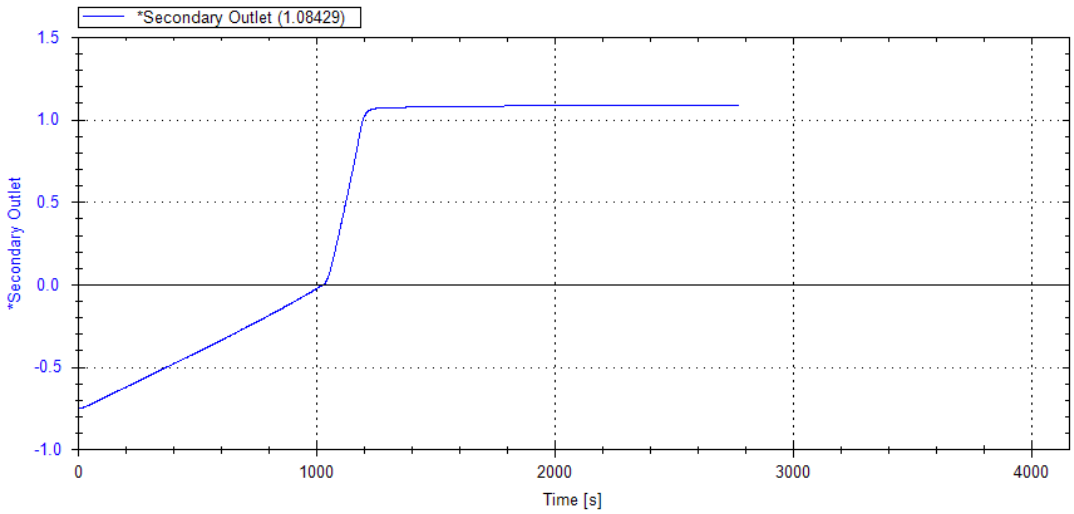

Figure 51 - Secondary side outlet quality over time.

When transition from the sub-cooled to the two-phase region takes place there is a sudden increase in mass flow rate, as seen in Figure 52. This is due to the decrease in fluid density as mentioned before in Chapter 3. This causes the mass flow rate to almost double for a few seconds before returning to the mass flow rate at the inlet. The sudden change can cause unwanted stress, fatigue and vibrations in the SG and further studies can focus in on these effects.

As the density decreases the secondary side inlet pressure also decreases as shown in Figure 53. The secondary side mass flow rate and inlet pressure values return to single phase conditions when the transient reaches steady state and the system stabilizes.

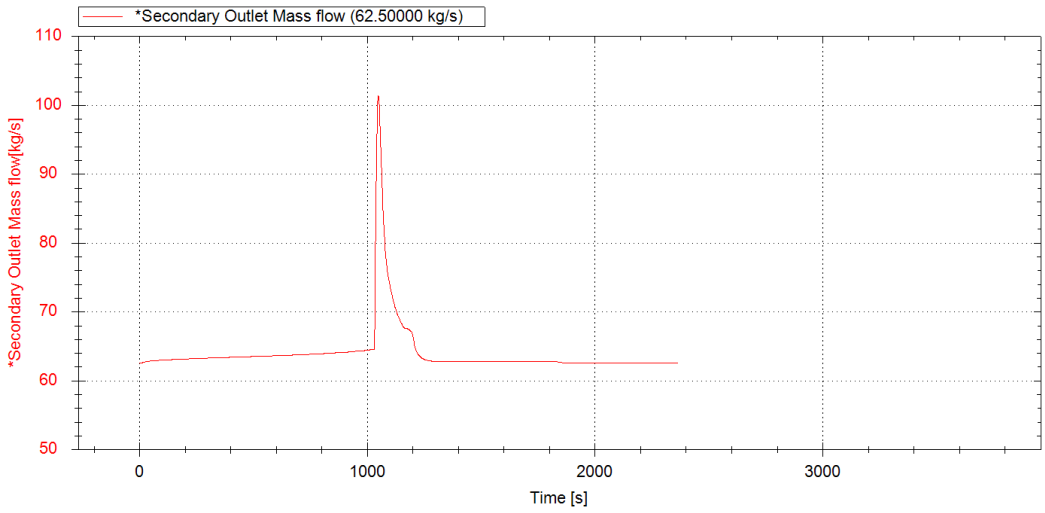

Figure 52 – Change in secondary outlet mass flow over time.

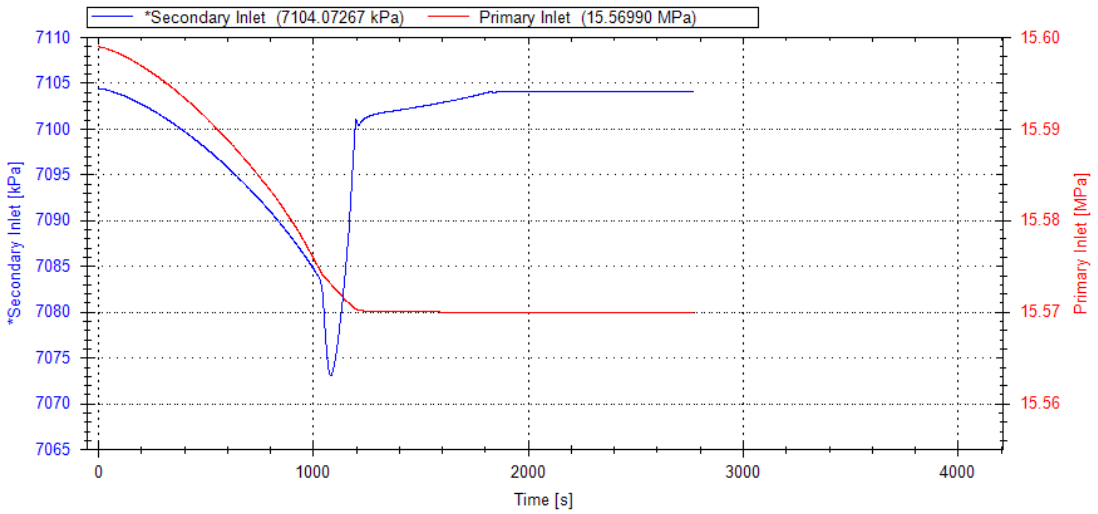

Figure 53 - Inlet pressures changes over time.

With the increase in mass flow rate and the increased heat transfer that can be achieved the energy transferred increases rapidly when boiling starts. This can be seen in Figure 54 after about 1100 [s]. The SG transfers a maximum of 141 [MW] while the outlet vapour quality is still in the two-phase region. As soon as the dry-out condition is achieved the heat transfer decreases to the rated power of the SG. This is due to the sudden decrease in the heat transfer coefficient when the fluid transitions to super-heated steam and dry-out occurs.

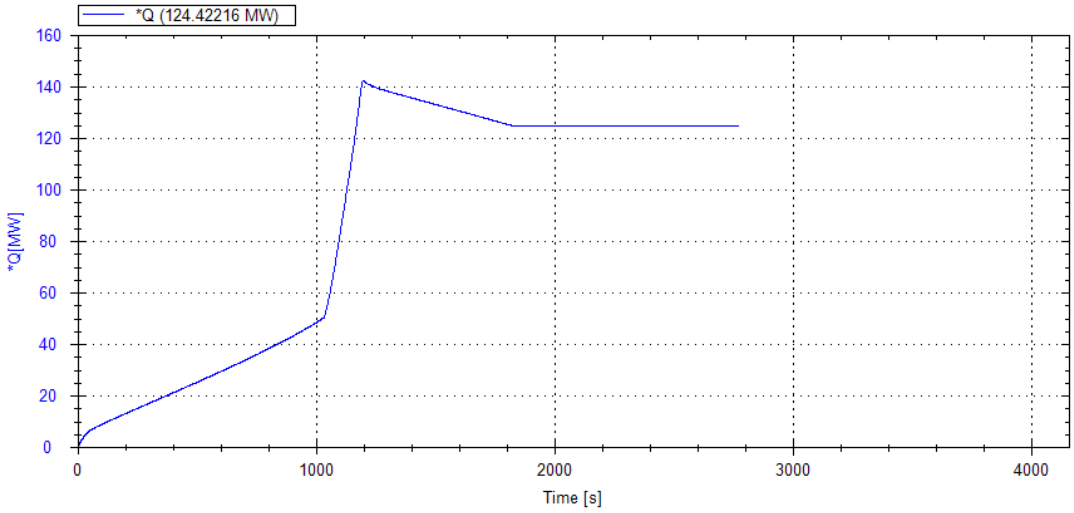

Figure 54 - Heat transferred over time.

The last part of the transient is to see how the heat transfer coefficients change over time at specific points inside the SG. Figure 55 shows the heat transfer coefficients throughout the pipe at certain time intervals from the start of the transient. It can be seen that for the first 17 minutes there is only a small increase in the heat transfer coefficients as the outlet is still sub cooled. After 17 minutes boiling starts to occur. Here it can be seen that the increased boiling heat transfer comes into play, as the secondary outlet vapour quality increases. After about 20 minutes dry out occurs and thereafter is a sudden decrease in the heat transfer coefficient of the superheated region of the last few meters of the tube.

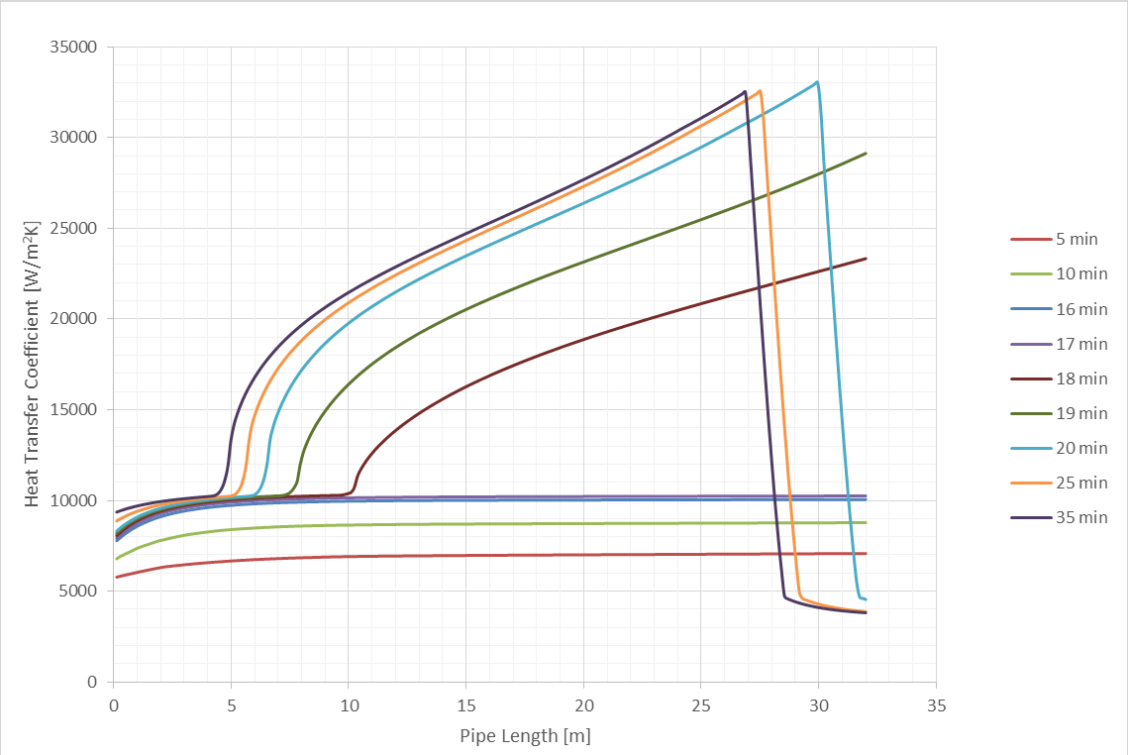

Figure 55 – Change in heat transfer coefficient over time.

6.8 SUMMARY

From this chapter it was shown that to simplify the layout of an OTHSG the annular flow area of the helical SG can be represented as a rectangular channel and that the curved tube will be an equivalent straight diagonal tube. In terms of the internal flow, the heat transfer can be modelled as counter-flow with the proper enhancements applied, along with the pressure drop calculated from a cross flow configuration.

With the simplification of the SG applied, the Flownex model was configured for the test data and geometry of the IRIS SG. For steady state the Flownex model predicted the secondary loop`s outlet temperature with accurately within 0.27 [%]. The energy transferred was also predicted to within 99.5 [%] of the IRIS data.

The transient start-up scenario simulated resulted in a few interesting findings. When the secondary side outlet liquid quality reaches saturation, a sudden increase in mass flow is seen. This increase is due to the rapid decrease in fluid density as the secondary side enters the two-phase region. Due to the increase in mass flow rate the total amount of energy transferred to the secondary side is initially larger than the rated power, but as soon as super heating is achieved the power decreases again to be in line with the rated power.

In the following chapter the study will be concluded and recommendations made for further studies based on the results obtained.

CHAPTER 7 – CONCLUSION

7.1 CONCLUSIONS

The purpose of the study was to model the flow and heat transfer within a helical coil steam generator tube from start-up through boiling and up to super-heated steam conditions. Evidence of such a transient simulation could not be found elsewhere in literature.

From the literature review on current SMR PWRs it was found that the majority of designers are focusing on integrated OTHSG designs. The reason being the compact design of the SG and its ability to produce super-heated steam compared to the conventional UTSG`s saturated vapour. The relevant theory required to model single and two-phase flow and the different modelling approaches were also investigated.

The first goal was to develop a customised homogenous two-phase flow model for a vertical pipe in EES that can simulate steady-state and transient conditions. This was done to cultivate a thorough understanding of the fundamental theory and its application in systems modelling. Different time-wise integration factors were investigated to ensure that the uncoupled models for the primary and secondary loops were numerical stable. A combined model was then expanded to include the correct two-phase flow heat transfer and pressure drop correlations for the different flow regions.

To verify the homogeneous EES model a Flownex network was constructed with the same geometry and boundary values. The results from the two models corresponded with minor deviations. The EES and Flownex secondary side outlet temperature was 0.69 [%] from one another. These deviations are mainly due to the two-phase density and heat transfer relaxation parameters used in Flownex. The relaxation parameters ensure that the rapid change in fluid properties does not affect the solver stability.

Due to the advantages of using Flownex, the model was then expanded to simulate the helical coil of the IRIS reactor's SG. Simplification assumptions were made in terms of the more complex helical coil and tube bundle configuration. The steady state results of the Flownex model were compared to the work done by Cinotti (2002). The results corresponded very well with the pressure drop in the coil having the largest error of 2.9% and the rated power a 0.49 [%] error. With the Flownex model verified for steady state data, the next step was to use the model to simulate a cold start-up transient scenario, as no evidence could be found in literature that this has been done before.

The transient simulation of the cold start-up showed that a sudden increase in mass flow through the SG occurs when boiling occurs. This along with the increased boiling heat transfer, resulted in the SG being able to extract more than the rated power for a short period of time, before it decreased slightly back to the rated power. The change in heat transfer coefficients at different positions inside the pipe was also plotted for selected time steps. This clearly showed the development of the two-phase, dries out and superheated regions as the SG heated up from the initial sub-cooled liquid conditions.

7.3 RECOMMENDATIONS

From this study the following recommendations can be made for future studies:

The current EES model only investigated the homogeneous two-phase flow heat transfer of the helical tubes in the SG, simplified to vertical tubes. The next step will be to expand it to a two-fluid model to investigate the details of the vapour and liquid interactions in the two-phase region. More work can also be done to expand the Flownex two-phase flow approach to a more complex model. This can add to the advantage of the software to model detailed bubble and fluid dynamics. As Flownex is a SFCD simulation package the integration of the current OTHSG model can be implemented into a full scale plant simulation. The influence of different conditions within the power plant and how the SG responds can be investigated.

More detailed investigations of the helical coil itself can be done. CFD and finite element modelling analysis can be done on the helical coil to see what effects the increase in mass flow rate will have on the structure of the coil. This will also give more details on the flow over the coil and forces acting on it during operation. Finally it should be considered to model a complete OTHSG using appropriate simulation tools like Relap, StarCCM+ or other simulation package, where design modifications can be recommended.

BIBLIOGRAPHY

Aakenes, F. (2012). *Frictional pressure-drop models for steady-state and transient two-phase flow of carbon dioxide.* Master Thesis, NOrwegian University of Science and Technology, Trondheim.

Adballa, M. (1993). *A Nonlinear Dynamic Model of a Once-Through, Helical-Coil Steam Generator.* Masters Report, Oak Ridge National Laboratorty, Oak Ridge.

Afrikantov OKB Mechanical Engineering. (2011). *ABV-6M Smaal Power Plants.* Status Report, Afrikantov OKB Mechanical Engineering, Moscow.

Ales, M. (2012). *Generation m Power - Reactor Design Overview.* Presentation, The Babcock & Wilcox Company, Gaithersburg.

Ambroso, A., Chalons, C., & Coquel, F. (2009, December 6). The coupling of homogeneous models for two-phase flows. *International Journal on Finite Volumes, 4*(1).

Annonymous. (2011). *Status Report 72 - Fixed Bed Nuclear Reactor.* Status Report, Federal University of Tio Grande do Sul, Rio Grande do Sul.

Bonavigo, L., & De Salve, M. (2011). *Issues for Nuclear Power Plants Steam Generators.* Articel, inTech, Rijeka.

Borgnakke, C., & Sonntag, R. (2009). Introduction. In *Fundamentals of Thermodynamics* (7th ed., Vol. SI Version, pp. 1-12). Michigan: John Wiley & Sons Pte Ltd.

Carelli, M. (2004). *The Design and saftey features of the IRS Reactor.* Nuclear Engineering and Design, Italy.

Castleberry, G. (2012). *Babcock & Wilcox Pressureized Water Reactors.* Course Notes, PDHcenter, Fairfax.

Chisholm, D. (1973). Pressure Gradients Due to Friction during the Flow of Evaporating Two-phase Mixtures in Smooth Tubes and Channels. *International Heat Transfer Journal, 16*, 347-358.

Cinotti, .., Bruzzone, M., Meda, N., Corsini, G., Lombardi, C., Ricotti, M., & Conway, L. E. (2002). Steam Generator of the International Reactor Innovative and Secure. In ASME (Ed.), *10th International Conference on Nuclear Engineering*, (pp. 1-8). Arlington.

DCNS. (2014). Flexblue. UxC.

Fick, L. (2013). *Application of the rate form of the equation of state for the dynamic simulation of thermal-hydraulic systems.* Master Thesis, North-West University, Potchefstroom.

Fletcher, C., & Schultz, R. (1995). *RELAP5/MOD3 CODE MANUALVOLUME V: USER'S GUIDELINES.* User Manual, Idaho National Engineering Laboratory, Lockhead.

Flownex. (2012). *Two Phase Flow*. Retrieved November 16, 2013, from Flownex Simulation Enviroment: http://www.flownex.com/about-us/2011-08-19-13-59-20/industry-application/item/493-two-phase-flow

Forster, H., & Zuber, N. (2004, 17 June). Dynamics of vapor bubbles and boiling heat transfer. *AIChE, 1*(4), 531-535.

Freidel, L. (1979). Improved Friciton Pressure Drop Correlations for Horizontal and Vertical Two-Phase Pipe Flow. *European Two-Phase Flow Group Meeting.* Ispra, Italy.

Gidropress. (2011). *Satus Report 84 - VVER-300 (V-478) (VVER-300 (V-478)).* Status Report, IAEA.

Gnielinski, V. (1976). *A Study of In-Tube Evaporation Heat Transfer of Carbon Dioxide.* Seoul National University, Seoul.

Green, S., & Hetsroni, G. (1995, February 20). PWR Steam Generators. *Multiphse Flow, 21*, 1-97.

Gungor, K., & Winterton, R. (1986, August 12). A General Correlation for flow boiling in tubes and annuli. *International Journal for Heat Mass Transfer, 29*(3), 351-358.

Gungor, K., & Winterton, R. (1986, August 12). Evaluation of General Correlations for Heat Transfer During Boiling of Saturated Liquids in Tubes and Annul. *International Heat Transfer Journal, 29*(3), 351-358.

Hewitt, G. (2011, February 8). *Thermopedia*. Retrieved March 11, 2015, from Slip Ratio: http://www.thermopedia.com/content/278/?tid=104&sn=1302

Hoffer, N., Sabharwall, P., & Anderson, N. (2011). *Modeling a Helical-coil Steam Generator in RELAP5-3D for the Next Generation Nuclear Plant.* Idaho National Laboratory, Idoha.

Incropera, F., Bergman, T., Lavine, A., & Dewitt, D. (2011). *Fundamentals of Heat and Mass Transfer.* Joahn Wiley & Sons.

INL. (2010). *Next generation Nuclear Plant Steam Generator and Intermediate Heat Excanger Materials Research and Development Plan.* Project, US Department of Energy, Idaho.

International Atomic Energy Agency. (1995). *Integral design concepts of advanced water cooled reactors.* Design Concept, IAEA, Obninsk.

International Atomic Energy Agency. (2012). *Status of Small and Medium Sized Reactor Designs.* Status Report, IAEA, Vienna.

International Reactor Innovative & Secure. (2002). *IRIS Plant Overview.* Plant Overview, Nuclear Energy Research Initiavte.

Invernizzi, C. (2013). The Thermodynamic Properties of theWorking. In *Closed Power Cycles* (p. 95). Hardcover: Springer.

IRSN. (2013). *Enhancing Nuclear Saftey*. Retrieved November 2013, 15, from IRSN: http://www.irsn.fr/EN/Research/Scientific-tools/Computer-codes/Pages/The-CATHARE2-code-4661.aspx

Ishii, M., & Hibiki, T. (2011). Drift-Flux Model. In *Thermo-Fluid Dynamics of Two-Phase Flow* (2 ed., pp. 361-397). New York: Springer.

Ishii, M., & Hibiki, T. (2011). Two-Fluid Model. In *Thermo-Fluid Dynamics of Two-Phase Flow* (2nd ed., pp. 155-217). New York: Springer.

Ishii, M., & Hibiki, T. (2011). Two-Fluid Model. In *Thermo-Fluid Dynamics of Two-Phase Flow* (2nd ed., pp. 155-217). New York: Springer.

Jayakumar, J. (2012). *Helically Coiled Heat Exchangers.* Research Report, Amrita Schoo of Engineering, Kollam.

Kakac, S., & Bon, B. (2007, December 11). A Review of two-phase flow dynamic instabilities in tube boiling systems. *International Journal of Heat and Mass Transfer, 51*, 399-433.

Kandlikar, S. (1983). *A General Correlation for Saturated Two-Phase Flow Boiling HEat Transfer Inside Horizontal and Vertical Tubes.* Mechanical Engineering Department, Rochester Institute of Technology, Rochester.

Lamb, R. (2013). *How Steam Technology Works*. Retrieved November 18, 2013, from How Stuff Works: http://science.howstuffworks.com/steam-technology.htm

Lee, W. (2010). *the SMART Reactor.* Annual Form Report, Asian-Pacific Nuclear Energy Form, Daejeon.

Levy, S. (1999). *Two-phae flow in complex systems.* John Wiley & Sons.

Magana, H., Delmstro, D., & Markieqicz, M. (2010). *CAREM Prototype construction and Licensing Status.* Status Report, Argentina`s National Atomic Energy Commission, Federal Capital.

Mentor Graphics. (2012, June 11). *Mentor Graphics Announces Flowmaster Two-Phase advanced Thermo-Fluid Simulation Software for Power and Energy Markets*. Retrieved November 2013, 16, from Mentor Graphics: http://www.mentor.com/company/news/flomaster-advanced-thermo-fluid-simulation

Mitsubishi. (2011). *Status Report 95 - Integrated Modular Water Reactor.* Status Report, IAEA.

Morin, A. (2013). *A two-fluid four-equation model with instantaneous thermodynamical equilibrium.* Norwegian University of Science and Technology, Trondheim.

Nuclear Energy Agency. (2002, March 14). *NEA-1593 TRAC-PF1/EN MOD 3*. Retrieved November 2013, 15, from NEA: https://www.oecd-nea.org/tools/abstract/detail/nea-1593

Okiishi, M. (2006). *Fundamentals of Fluid Mechanics.* (5th, Ed.) Hoboken: John Wiley & Sons.

Olson, J., Li, X., & Wu, X. (2013, September 19). Tube and shell side coupled thermal analysis of an HTGR helical tube once through steam generator using porous media method. *Annals of Nuclear Energy, 64*(2014), 67-77.

Petukhov, B. (1970). *Heat Transfer and Friction in Turbulent Pipe Flow with Variable Physical Properties.* High Temperature Institute, Moscow.

Rousseau, P. (2014). Thermal-fluid systems modelling I. Potchefstroom: North-West University.

Ruspini, L. (2013). *Experimental and Numerical Investigation on two-phase flow instabilities.* PhD Thesis, Norwegian University of Science and Technology, Trondheim.

Sahin, S. (2007). *The Fixed ben Nuclear Concept.* Concept Report, Gazi University, Ankara.

Seider, E., & Tate, G. (1936). *Heat Transfer and Pressure Drop of Liquids in Tubes.* Publication, Foster Wheeler Corporation, New York.

Shah, M. (1982, January 1). Chart correlation for saturated boiling heat transfer: Equations and further study. *ASHRAE Trans, 88*(1), 158-196.

Stadtke, H. (2006). *Gasdynamic Aspects of Two-Phase Flow.* Wiley.

Stevanovic, V., & Prica, S. (2007, December). Multi-Fluid Model Predictions of Gas-Liquid Two-Phase Flows in Vertical Tubes. *FME Transactions, 35*(2007), 173-181.

Teir, S. (2002). *The History of Steam Generation.* Helsinki University of Technology Department of Mechanical Engineering, Espoo.

The Hong Kong Institution of Engineers. (2008). *Nuclear Power in China*. Retrieved 04 15, 2014, from Qinshan: http://home.pacific.net.hk/~nuclear/info0210.htm

US Nuclear Regulatory Commission. (2014, 02 05). *NuScale Power*. Retrieved 04 2014, 16, from NuScale Power Successfully Complete Helical Coil Steam Generator: http://www.nuscalepower.com/news20140225.aspx

UX Consulting Company. (2012). *UX Consulting*. Retrieved 03 24, 2014, from SMR Research: http://www.uxc.com/s,t/uxc_SMRDetail.aspx?key=RITM-200

VDI - Gesellschaft Verfahrenstechnik und Chemieingenieurwesen. (2010). *VDI Heat Atlas.* Dusseldorf: Springer.

Westinghouse SMR. (2011). Westinghouse SMR. Westinghouse Electronic Company.

Wolverine Tube, Inc. (2007). Two-Phase Flow Patterns. In J. Thome (Ed.), *Engineering Data Book III* (Vol. 3, pp. 12-1 to 12-4). Lausanne: Engineering Thermal Innovation.

Wolverine Tube, Inc. (2007). Two-Phase Flow Patterns. In J. Thome (Ed.), *Engineering Data Book III* (Vol. 3, pp. 12-1 to 12-4). Lausanne: Engineering Thermal Innovation.

Wulff, W. (2010, January 14). Critical review of conservation equations for two-phase flow in the U.S. NRC TRACE code. *ScienceDirect, I*(241), 4237-2371.

Yuming, X. (2010). *World Nuclear News*. Retrieved 02 20, 2014, from CNP-300: www.world-nuclear.org/info/country-profiles/countries-a-f/china--nuclear-power

Zivi, S. (1964, May 1). Estimation of Steady-State Steam Void-Fraction by Means of the Principle of Minimum Entropy Production. *Heat Transfer, 86*(2), 247-251.

Zuber, N. (2014). *Drift-Flux.* Retrieved July 02, 2014, from http://authors.library.caltech.edu/25021/1/chap14.pdf

Zuber, N., & Findlay, J. (1964, September 15). Average Volumetric Concentration in Two-Phase Flow Systems. *Heat Transfer, 87*(4), 453-468.

APPENDIX I – EES Model

In this appendix the source code of the homogeneous two-phase EES model is given. It should be noted that the model is highly dependent on initial guess values and variable limits

```
////////////////////////////////////////////////////////////////////////////////////////////////////////////////////////////////////////////////////////
"Gerrit Botha 2161368"
"Two Phase Transient"
////////////////////////////////////////////////////////////////////////////////////////////////////////////////////////////////////////////////////////
"Nusselt"
FUNCTION Nusselt(Re,Pr,a)
    IF(Re<=0.1) THEN
        Nusselt = 0
    ELSE
        IF (Pr<=0.1) THEN
            Nusselt = 0
        ELSE
            IF (Re < 2e3) THEN
                Nusselt := 7.54
            ELSE
                Nusselt := abs(0.023*abs(Re)^0.8*abs(Pr)^a)
            ENDIF
        ENDIF
    ENDIF
END

"Quality"
FUNCTION MyQ(Fluid$,P,h)
    h_l := Enthalpy(Fluid$,P=P,X=0)
    h_g:= Enthalpy(Fluid$,P=P,X=1)

    IF h<=h_l THEN
        MyQ:=0
    ELSE
        IF h>=h_g THEN
            MyQ := 1
        ELSE
            MyQ:= abs((h-h_l)/(h_g-h_l))
        ENDIF
    ENDIF
END

"Viscosity"
FUNCTION MyVisL(Fluid$,state,P,h,h_sat_l,h_sat_g)
    x_test = quality(fluid$,p=p,h=h)
    IF (h<h_sat_l) and (x_test <= 0) THEN
            MyVisL = abs(Viscosity(Fluid$,P=P,h=h))
    ELSE
        IF (h<h_sat_g) THEN
                MyVisL = abs(Viscosity(Fluid$,P=P,X=0))
        ELSE
            MyVisL = 0
        ENDIF
    ENDIF
END
```

```
FUNCTION MyVisG(Fluid$,state,P,h,h_sat_l,h_sat_g)
    x_test = quality(fluid$,p=p,h=h)
        IF (h>=h_sat_g) and (x_test >=1) THEN
            MyVisG = abs(Viscosity(Fluid$,P=P,h=h))
        ELSE
            IF (h>h_sat_l)  THEN
                MyVisG = abs(Viscosity(Fluid$,P=P,X=1))
            ELSE
                MyVisG = 0
            ENDIF
        ENDIF
END

"Density"
FUNCTION MyDisL(Fluid$,State,P,h,h_sat_l,h_sat_g)
    x_test = quality(fluid$,p=p,h=h)
        IF (h<h_sat_l) and (X_test<=0) THEN
            MyDisL = abs(Density(Fluid$,P=P,h=h))
        ELSE
            IF (h<h_sat_g) THEN
                MyDisL = abs(Density(Fluid$,P=P,X=0))
            ELSE
                MyDisL = 0
            ENDIF
        ENDIF
END

FUNCTION MyDisG(Fluid$,State,P,h,h_sat_l,h_sat_g)
    x_test = quality(fluid$,p=p,h=h)
        IF (h>=h_sat_g) and (x_test >= 1) THEN
            MyDisG = abs(Density(Fluid$,P=P,h=h))
        ELSE
            IF (h>h_sat_l) THEN
                MyDisG = abs(Density(Fluid$,P=P,X=1))
            ELSE
                MyDisG = 0
            ENDIF
        ENDIF
END

"Conductivity"
FUNCTION MyConL(Fluid$,state,P,h,h_sat_l,h_sat_g)
    x_test = quality(fluid$,p=p,h=h)
        IF (h<h_sat_l) and (X_test<=0) THEN
                MyConL = abs(Conductivity(Fluid$,P=P,h=h))
        ELSE
            IF (h<h_sat_g) THEN
                MyConL = abs(Conductivity(Fluid$,P=P,X=0))
            ELSE
                MyConL = 0
            ENDIF
        ENDIF
END
```

```
FUNCTION MyConG(Fluid$,state,P,h,h_sat_l,h_sat_g)
    x_test = quality(fluid$,p=p,h=h)
        IF (h>=h_sat_g) and (x_test >= 1) THEN
            MyConG = abs(Conductivity(Fluid$,P=P,h=h))
        ELSE
            IF (h>h_sat_l) THEN
                MyConG = abs(Conductivity(Fluid$,P=P,X=1))
            ELSE
                MyConG = 0
            ENDIF
        ENDIF
END

"CP"
FUNCTION MyCPL(Fluid$,state,P,h,h_sat_l,h_sat_g)
    x_test = quality(fluid$,p=p,h=h)
        IF (h < h_sat_l) and (x_test<=0) THEN
                MyCPL := abs(CP(Fluid$,P=P,h=h))
        ELSE
            IF (h < h_sat_g) THEN
                MyCPL := abs(CP(Fluid$,P=P,X=0))
            ELSE
                MyCPL := 0
            ENDIF
        ENDIF
END

FUNCTION MyCPG(Fluid$,state,P,h,h_sat_l,h_sat_g)
    x_test = quality(fluid$,p=p,h=h)
        IF (h >= h_sat_g) and (x_test >= 1) THEN
            MyCPG := abs(CP(Fluid$,P=P,h=h))
        ELSE
            IF (h > h_sat_l) THEN
                MyCPG := abs(CP(Fluid$,P=P,X=1))
            ELSE
                MyCPG := 0
            ENDIF
        ENDIF
END

"Prandtl"
FUNCTION MyPr(Cp,Mu,k)
    IF k<=0.001 THEN
            MyPr = 0
    ELSE
        MyPr = abs((Cp*Mu/k))
    ENDIF
END

"Reynolds"
FUNCTION MyRe(m,A,D,mu)
    IF mu<=0.000001 THEN
            MyRe = 0
    ELSE
        MyRe = abs((m*D)/(Mu*a))
    ENDIF
END
```

```
"Multiplier"
FUNCTION Multiplier(Chi,X)
    IF (X<=0.98) THEN
        IF (Chi <= 0.0) THEN
            Multiplier = 1
        ELSE
            IF  (1/CHI <= 0.1) AND (1/Chi <=100) THEN
                Multiplier = 1
            ELSE Multiplier = abs((2.35*(1/Chi + 0.213)^0.736))
        ENDIF
    ELSE
        Multiplier = 1
    ENDIF
END

"Supression"
FUNCTION Suppression(X,Re_f,F)
    IF ( X<=0.001)  THEN
        Suppression = 0
    ELSE
        IF  (X>=0.95) THEN
            Suppression = 0
        ELSE
            Suppression = abs((1+2.53e-6*(abs(Re_f*abs(F)^1.25))^1.17)^(-1))
        ENDIF
    ENDIF
END

"Lockhart-Martinelli"
FUNCTION Lockhart(X,rho_g,Rho_l,Mu_g,Mu_l)
    IF (X<=0.001) THEN
        Lockhart = 0
    ELSE
        IF (Rho_l<=0.01) THEN
            Lockhart = 0
        ELSE
            IF (Mu_g<=0.0000) THEN
                Lockhart = 0
            ELSE
                Lockhart = (abs((1-X)/x))^0.9*(abs(Rho_g/Rho_l))^0.5*(abs(Mu_l/Mu_g))^0.1
            ENDIF
        ENDIF
    ENDIF

END

"Boiling"
FUNCTION Boil(Fluid$,X,T_bulk,T_wall,P,C_pl,Rho_l,k_l,Mu_l,rho_g)

    IF (X>=0.01) AND (X<=0.96) THEN
        DELTAT_sat = T_wall - T_bulk
        DELTAP_sat = P_sat(Fluid$,T=T_wall) - P

        h_lg = Enthalpy(Fluid$,P=P,X=1)-Enthalpy(Fluid$,P=P,X=0)
        Sigma = SurfaceTension(Fluid$,T=T_bulk)

        IF (Mu_l <= 0.0000) THEN
            Boil = 0
```

```
        ELSE
            IF (rho_g <= 0.1) THEN
                Boil = 0
            ELSE
                IF (C_pl <=0.1) THEN
                    Boil = 0
                ELSE
                    IF (rho_l <= 0.1) THEN
                        Boil = 0
                    ELSE
                        IF (k_l <= 0.001) THEN
                            Boil = 0
                        ELSE
                            IF (Sigma <=0) THEN
                                Boil = 0
                            ELSE
                                Boil =
abs((0.00122*(abs(C_pl))^0.45*(abs(rho_l))^0.49*(abs(k_l))^0.79/(((sigma))^0.5*((h_lg))^0.24*(abs(Mu_l))^
0.29*(abs(rho_g))^0.24)*(abs(DELTAT_sat)^0.24)*(abs(DELTAP_sat)^0.75))
                            ENDIF
                        ENDIF
                    ENDIF
                ENDIF
            ENDIF
        ENDIF
    ELSE
        Boil = 0
    ENDIF
END

"TwoPhase"
FUNCTION TwoPhase(X,h_cl,h_cg,h_cboil,F,S)
    IF (X<=0.01) THEN
        TwoPhase = h_cl
    ELSE
        IF (X<=0.93) THEN
            TwoPhase = F*h_cl+S*h_cboil)
        ELSE
            IF (X<= 0.94) THEN
                TwoPhase =F*h_cl+S*h_cboil)*0.75 +h_cg
            ELSE
                IF  (X<= 0.95) THEN
                    TwoPhase =F*h_cl+S*h_cboil)*0.5 +h_cg
                ELSE
                    IF  (X<= 0.96) THEN
                        TwoPhase =F*h_cl+S*h_cboil)*0.25 + h_cg
                    ELSE
                        IF  (X<= 0.97) THEN
                            TwoPhase =F*h_cl+S*h_cboil)*0.1 +h_cg
                        ELSE
                            TwoPhase = h_cg
                        ENDIF
                    ENDIF
                ENDIF
            ENDIF
        ENDIF
    ENDIF
END
```

```
"Phi"
FUNCTION PhiMulti(X,Chi)
    IF (X<=0.001)  THEN
        PhiMulti = 1
    ELSE
        IF Chi <=0.000001 THEN
            PhiMulti = 1
        ELSE
            PhiMulti = abs((1+2.85*Chi^0.523))
        ENDIF
    ENDIF
END

"Pressure Drop"
FUNCTION PressureDrop(X,phi,P_g,P_l)
    IF (X<=0.01)  THEN
        PressureDrop= P_l
    ELSE
        IF (X>=0.95) THEN
            PressureDrop= P_g
        ELSE
            PressureDrop= Phi*P_g
        ENDIF
    ENDIF
END

"Single Phase Pressure Drop"
FUNCTION PDSP(f_s,L,D_h,A_p,m,rho)
        IF rho <= 0.1 THEN
            PDSP = 0
         ELSE
            PDSP = ((f_s*L)/D_h)*((abs(m)*m)/(2*rho*A_p^2))*1000
        ENDIF
END

PROCEDURE Guesses(Counter,Number:NewCounter)
    IF Mod(Counter,Number) = 0 THEN
        NewCounter = 1
        $UpdateGuesses
    ELSE
        NewCounter = Counter +1
    ENDIF
END

////////////////////////////////////////////////////////////////////////////////////////////////////////////////////////////////////////////////////////////
////////////////////////////////////
"Inputs"
////////////////////////////////////////////////////////////////////////////////////////////////////////////////////////////////////////////////////////////
////////////////////////////////////
n = 25                  [Increaments]
freedom = 5
Alpha = 0.7             [Time wise integration factor]
g = 9.81                [m/s^2]

"Secondary"
f_s = 0.02              [-]
T_s0i = 400     [K]
P_s0e =5E6      [Pa]
```

```
m_dot_s = 0.04       [kg/s]
S$ = 'Steam_IAPWS'
"Primary"
f_p = 0.01           [-]
{T_p0i = 300+273.15          [K]}
P_p0e = 15.5E6       [Pa]
m_dot_p = 1          [kg/s]
P$ = 'Steam_IAPWS'

DELTAT = 0.25 [K/s]
Stable = 5
T_p0i_max = 580
T_p0i_min =450
Update = 10
Sample = 2

"Pipe"
Tube$ = 'Stainless_AISI302'
C_th_p = DELTAL*(pi/4*(D_o^2-(D_o-thickness)^2))*Density(Tube$,T=300)*CP(Tube$,T=300)
C_th_s = DELTAL*(pi/4*((D_o-thickness)^2-D_i^2))*Density(Tube$,T=300)*CP(Tube$,T=300)

"Geomerty"
L = 25               [m]
H = L
D_shell = 7.5E-2     [m]
D_i = 25E-3          [m]
thickness = 5E-3     [m]

$IF TableRun# = 1
    Time = 0
    T_p0i = T_p0i_min
    Counter = 1
$ENDIF

////////////////////////////////////////////////////////////////////////////////////////////////////////////////////////////////////////////////////
"Calculations"
////////////////////////////////////////////////////////////////////////////////////////////////////////////////////////////////////////////////////
"Geometery"
DELTAL = L/n
DELTAH = H/n
D_o = D_i+2*thickness
A_s = pi/4*(D_i^2)
Ap_s = pi*D_i*DELTAL
Vol_s = A_s*DELTAL
D_hs = D_i

A_p = pi/4*(D_shell^2-D_o^2)
Ap_p = pi*D_o*DELTAL
Vol_p = A_p*DELTAL
D_hp = 4*A_p/(pi*D_o+pi*D_shell)

"Transient"
$IF TableRun# = 1
Duplicate a = 1,n
    S_mass_s[a] = 0
    S_energy_s[a] = 0
    S_momentum_s[a] = 0
    S_pressure_s[a] = 0
```

```
    S_mass_p[a] = 0
    S_energy_p[a] = 0
    S_momentum_p[a] = 0
    S_pressure_p[a] = 0

    Q_s[a]=Q_w[a]
    Q_p[a] =  -Q_w[a]
END
$ENDIF

$IF TableRun# > 1
    Time = TableValue('Table 1',j,3)+DELTATime
    DELTATime = {abs(DELTAL/(Sample*TableValue('Table 1',j,4)))}1
    T_p0i = IF(j,stable,T_p0i_min,T_p0i_min,IF(T_p0i,T_p0i_max,TableValue('Table
1',j,2)+DELTAT*DELTATime,T_p0i_max,T_p0i_max))
$ENDIF

"Initiate Loop"
z_e[0] = 0
L_e[0] = 0

"Secondary"
        m_se[0] = m_dot_s

        P_s0e[n] = P_s0e
        T_s0e[0] = T_s0i
        h_s0e[0] = Enthalpy(S$,P=P_s0e[0],T=T_s0e[0])

        P_s0e[0] = P_se[0] + (0.5*Rho_se[0]*V_se[0]^2)
        h_s0e[0] = h_se[0] + (0.5*V_se[0]^2)
        T_se[0] = Temperature(S$,P=P_se[0],h=h_se[0])

        Rho_se[0] =Density(S$,P=P_se[0],h=h_se[0])
        V_se[0] = m_se[0]/(Rho_se[0]*A_s)
        X_se[0] =MyQ(S$,P_se[0],h_se[0])
        h_se_satl[0] = Enthalpy(S$,P=P_se[0],X=0)
        h_se_satg[0] = Enthalpy(S$,P=P_se[0],X=1)

        Chi_se[0] = Lockhart(X_se[0],rho_seg[0],Rho_sel[0],Mu_seg[0],Mu_sel[0])
        MF_se[0] = Multiplier(Chi_se[0],X_se[0])
        SF_se[0] = Suppression(X_se[0],Re_sel[0],MF_se[0])
        Phi_se[0] = PhiMulti(X_se[0],Chi_se[0])

    "Liquid"
        m_sel[0] = (1-X_se[0])*m_se[0]
        Mu_sel[0] = MyVisL(S$,1,P_se[0],h_se[0],h_se_satl[0],h_se_satg[0])
        k_sel[0] = MyConL(S$,1,P_se[0],h_se[0],h_se_satl[0],h_se_satg[0])
        C_p_sel[0] = MyCPL(S$,1,P_se[0],h_se[0],h_se_satl[0],h_se_satg[0])
        Re_sel[0] = MyRe(m_sel[0],A_s,D_hs,mu_sel[0])
        Pr_sel[0] = MyPr(C_p_sel[0],Mu_sel[0],k_sel[0])
        Nuss_sel[0] = Nusselt(Re_sel[0],Pr_sel[0],0.4)
        h_c_sel[0] = (k_sel[0]/D_hs)*Nuss_sel[0]
        Rho_sel[0] = MyDisL(S$,1,P_se[0],h_se[0],h_se_satl[0],h_se_satg[0])

    "Gas"
        m_seg[0] = (X_se[0])*m_se[0]
        Mu_seg[0] = MyVisG(S$,2,P_se[0],h_se[0],h_se_satl[0],h_se_satg[0])
```

```
        k_seg[0] = MyConG(S$,2,P_se[0],h_se[0],h_se_satl[0],h_se_satg[0])
        C_p_seg[0] = MyCPG(S$,2,P_se[0],h_se[0],h_se_satl[0],h_se_satg[0])
        Re_seg[0] = MyRe(m_seg[0],A_s,D_hs,mu_seg[0])
        Pr_seg[0] = MyPr(C_p_seg[0],Mu_seg[0],k_seg[0])
        Nuss_seg[0] = Nusselt(Re_seg[0],Pr_seg[0],0.4)
        h_c_seg[0] = (k_seg[0]/D_hs)*Nuss_seg[0]
        Rho_seg[0] = MyDisG(S$,2,P_se[0],h_se[0],h_se_satl[0],h_se_satg[0])

"Primary"
        m_pe[n+1] = m_dot_p

        P_p0e[1] = P_p0e
        T_p0e[n+1] = T_p0i
        h_p0e[n+1] = Enthalpy(P$,P=P_p0e[n+1],T=T_p0e[n+1])

        P_p0e[n+1] = P_pe[n+1] + (0.5*Rho_pe[n+1]*V_pe[n+1]^2)
        h_p0e[n+1] = h_pe[n+1] + (0.5*V_pe[n+1]^2)
        T_pe[n+1] = Temperature(P$,P=P_pe[n+1],h=h_pe[n+1])

        Rho_pe[n+1] =Density(P$,P=P_pe[n+1],h=h_pe[n+1])
        V_pe[n+1] = m_pe[n+1]/(Rho_pe[n+1]*A_p)

"Loop"

DUPLICATE a=1,n
"Inlet"
    z_i[a] = z_e[a-1]
    L_i[a] = L_e[a-1]

    "Secondary "
        m_si[a] = m_se[a-1]

        P_s0i[a] = P_s0e[a-1]
        h_s0i[a] = h_s0e[a-1]

        P_si[a] = P_se[a-1]
        h_si[a] = h_se[a-1]
        T_si[a] = Temperature(S$,P=P_si[a],h=h_si[a])

        rho_si[a] = rho_se[a-1]
        V_si[a] = V_se[a-1]
        X_si[a] = X_se[a-1]
        h_si_satl[a] = h_se_satl[a-1]
        h_si_satg[a] = h_se_satg[a-1]

        Chi_si[a] = Chi_se[a-1]
        MF_si[a] = MF_se[a-1]
        SF_si[a] = SF_se[a-1]
        Phi_si[a] = Phi_se[a-1]

        "Liquid"
            m_sil[a] = m_sel[a-1]
            Mu_sil[a] = Mu_sel[a-1]
            k_sil[a] = k_sel[a-1]
            C_p_sil[a] = C_p_sel[a-1]
            Re_sil[a] = Re_sel[a-1]
            Pr_sil[a] = Pr_sel[a-1]
            Nuss_sil[a] = Nuss_sel[a-1]
```

```
            h_c_sil[a] = h_c_sel[a-1]
            rho_sil[a] = rho_sel[a-1]

        "Gas"
            m_sig[a] = m_seg[a-1]
            Mu_sig[a] = Mu_seg[a-1]
            k_sig[a] = k_seg[a-1]
            C_p_sig[a] = C_p_seg[a-1]
            Re_sig[a] = Re_seg[a-1]
            Pr_sig[a] = Pr_seg[a-1]
            Nuss_sig[a] = Nuss_seg[a-1]
            h_c_sig[a] = h_c_seg[a-1]
            rho_sig[a] = rho_seg[a-1]

    "Primary"
        m_pi[a] = m_pe[a+1]
        P_p0i[a] = P_p0e[a+1]
        h_p0i[a] = h_p0e[a+1]

        P_pi[a] = P_pe[a+1]
        h_pi[a] = h_pe[a+1]
        T_pi[a] = Temperature(P$,P=P_pi[a],h=h_pi[a])

        rho_pi[a] = rho_pe[a+1]
        V_pi[a] = V_pe[a+1]

"Conservation"
    "Secondary"
            {m_se[a] = m_si[a]
            p_s0e[a] = p_s0i[a]
            h_s0e[a] = h_s0i[a]}

            S_mass_s[a] = 1/Vol_s*(m_si[a] - m_se[a])

            S_momentum_s[a] = A_s/(DELTAL)*(DeltaP_s_p[a] + DeltaP_s_z[a] - DeltaP_s0[a] +
DeltaP_s_m[a] - DeltaP_s_rho[a])
                DeltaP_s_p[a] = (P_s0e[a]-P_s0i[a])
                DeltaP_s_rho[a] = 0.5*V_si[a]*V_se[a]*(Rho_se[a]-Rho_si[a])
                DeltaP_s_z[a] = rho_bar_s[a]*g*(Z_e[a]-Z_i[a])
                DeltaP_s_m[a] = DELTAL*V_bar_s[a]*S_mass_s[a]
                DeltaP_s0[a] = PressureDrop(X_bar_s[a],phi_bar_s[a],DeltaP_s0g[a],DeltaP_s0l[a])

            S_energy_s[a] = (1/(Vol_s*rho_bar_s[a]))*(Deltah_s_hi[a]  - Deltah_s_he[a] + Q_s[a] +
Deltah_s_m[a])
                Deltah_s_hi[a] = m_si[a]*(h_s0i[a]+g*z_i[a])
                Deltah_s_he[a] = m_se[a]*(h_s0e[a]+g*z_e[a])
                Deltah_s_m[a] = Vol_s*(S_pressure_s[a]-h_bar_s0[a]*S_mass_s[a])

    "Primary"
        {m_pe[a] = m_pi[a]
        p_p0e[a] = p_p0i[a]
        h_p0e[a] = h_p0i[a]}

        S_mass_p[a] = 1/Vol_p*(m_pi[a] - m_pe[a])

        S_momentum_p[a] =A_p/(DELTAL)*(DeltaP_p_p[a] + DeltaP_p_z[a] - DeltaP_p0[a] +
DeltaP_p_m[a])
            DeltaP_p_p[a] =(P_p0i[a]-P_p0e[a])
```

```
                DeltaP_p_z[a] = rho_bar_p[a]*g*(Z_e[a]-Z_i[a])
                DeltaP_p_m[a] = DELTAL*V_bar_p[a]*S_mass_p[a]
                DeltaP_p0[a]
=((f_p*DELTAL)/D_hp)*((abs(m_bar_p[a])*m_bar_p[a])/(2*rho_bar_p[a]*Ap_p^2))

        S_energy_p[a] = (1/(Vol_p*rho_bar_p[a]))*(Deltah_p_hi[a]  - Deltah_p_he[a] + Q_p[a] +
Deltah_p_m[a])
                Deltah_p_hi[a] = m_pi[a]*(h_p0i[a]+g*z_i[a])
                Deltah_p_he[a] = m_pe[a]*(h_p0e[a]+g*z_e[a])
                Deltah_p_m[a] = Vol_p*(S_pressure_p[a]-h_bar_p0[a]*S_mass_p[a])

        $IF TableRun# >1
                "Secondary"
                (rho_bar_s[a] - TableValue('Table 1',j,0*n+freedom+a))/DELTATime =
alpha*(S_mass_s[a])+(1-alpha)*(TableValue('Table 1',j,1*n+freedom+a))
                (h_bar_s0[a]-TableValue('Table 1',j,2*n+freedom+a))/DELTATime = alpha*S_energy_s[a]+(1-
alpha)*TableValue('Table 1',j,3*n+freedom+a)
                (m_bar_s[a]-TableValue('Table 1',j,4*n+freedom+a))/DELTATime = alpha*S_momentum_s[a]
+ (1-alpha)*TableValue('Table 1',j,5*n+freedom+a)
                S_pressure_s[a] = (P_bar_s[a]-TableValue('Table 1',j,6*n+freedom+a))/DELTATime

                "Wall"
                    Q_s[a]= Q_w[a]
                    Q_p[a] = - Q_w[a]

                "Primary"
                ((rho_bar_p[a]) - (TableValue('Table 1',j,12*n+freedom+a)))/DELTATime =
(alpha)*S_mass_p[a]+(1-alpha)*(TableValue('Table 1',j,13*n+freedom+a))
                (h_bar_p0[a]-TableValue('Table 1',j,14*n+freedom+a))/DELTATime =
(alpha)*S_energy_p[a]+(1-alpha)*TableValue('Table 1',j,15*n+freedom+a)
                (m_bar_p[a]-TableValue('Table 1',j,16*n+freedom+a))/DELTATime =
(alpha)*S_momentum_p[a] + (1-alpha)*TableValue('Table 1',j,17*n+freedom+a)
                S_pressure_p[a] =((P_bar_p[a]-TableValue('Table 1',j,18*n+freedom+a))/DELTATime )
    $ENDIF

"Outlet"
    z_e[a] = z_i[a]+DELTAH
    L_e[a] = L_i[a]+DELTAL

    "Secondary"
    P_s0e[a] = P_se[a] + (0.5*Rho_se[a]*V_se[a]^2)
    h_s0e[a] = h_se[a] + (0.5*V_se[a]^2)
    T_se[a] = Temperature(S$,P=P_se[a],h=h_se[a])

    Rho_se[a] = Density(S$,P=P_se[a],h=h_se[a])
    V_se[a] = m_se[a]/(A_s*rho_bar_s[a])
    X_se[a] = MyQ(S$,P_se[a],h_se[a])
    h_se_satl[a] = Enthalpy(S$,P=P_se[a],X=0)
    h_se_satg[a] = Enthalpy(S$,P=P_se[a],X=1)

    Chi_se[a] = Lockhart(X_se[a],rho_seg[a],Rho_sel[a],Mu_seg[a],Mu_sel[a])
    MF_se[a] = Multiplier(Chi_se[a],X_se[a])
    SF_se[a] = Suppression(X_se[a],Re_sel[a],MF_se[a])
    Phi_se[a] = PhiMulti(X_se[a],Chi_se[a])
```

```
    "Liquid"
        m_sel[a] = (1-X_se[a])*m_se[a]
        Mu_sel[a] = abs(MyVisL(S$,1,P_se[a],h_se[a],h_se_satl[a],h_se_satg[a]))
        k_sel[a] = abs(MyConL(S$,1,P_se[a],h_se[a],h_se_satl[a],h_se_satg[a]))
        C_p_sel[a] = abs(MyCPL(S$,1,P_se[a],h_se[a],h_se_satl[a],h_se_satg[a]))
        Re_sel[a] = MyRe(m_sel[a],A_s,D_hs,mu_sel[a])
        Pr_sel[a] = MyPr(C_p_sel[a],Mu_sel[a],k_sel[a])
        Nuss_sel[a] = Nusselt(Re_sel[a],Pr_sel[a],0.4)
        h_c_sel[a] = (k_sel[a]/D_hs)*Nuss_sel[a]
        Rho_sel[a] = MyDisL(S$,1,P_se[a],h_se[a],h_se_satl[a],h_se_satg[a])

    "Gas"
        m_seg[a] = (X_se[a])*m_se[a]
        Mu_seg[a] = abs(MyVisG(S$,2,P_se[a],h_se[a],h_se_satl[a],h_se_satg[a]))
        k_seg[a] = abs(MyConG(S$,2,P_se[a],h_se[a],h_se_satl[a],h_se_satg[a]))
        C_p_seg[a] = abs(MyCPG(S$,2,P_se[a],h_se[a],h_se_satl[a],h_se_satg[a]))
        Re_seg[a] = MyRe(m_seg[a],A_s,D_hs,mu_seg[a])
        Pr_seg[a] = MyPr(C_p_seg[a],Mu_seg[a],k_seg[a])
        Nuss_seg[a] = Nusselt(Re_seg[a],Pr_seg[a],0.4)
        h_c_seg[a] = (k_seg[a]/D_hs)*Nuss_seg[a]
        Rho_seg[a] = MyDisG(S$,2,P_se[a],h_se[a],h_se_satl[a],h_se_satg[a])

    "Primary"
    P_p0e[a] = P_pe[a] + (0.5*Rho_pe[a]*V_pe[a]^2)
    h_p0e[a] = h_pe[a] + (0.5*V_pe[a]^2)
    T_pe[a] = Temperature(P$,P=P_pe[a],h=h_pe[a])

    rho_pe[a] = Density(P$,P=P_pe[a],h=h_pe[a])
    V_pe[a] = m_pe[a]/(A_p*rho_bar_p[a])

"Averages"
    L_bar[a] = Average(L_e[a],L_i[a])
    Z_bar[a] = Average(Z_e[a],Z_i[a])

    "Secondary"
        m_bar_s[a] = Average(m_se[a],m_si[a])
        P_bar_s[a] = Average(P_se[a],P_si[a])
        h_bar_s[a] = Average(h_se[a],h_si[a])
        h_bar_s_satl[a] = Enthalpy(S$,P=P_bar_s[a],X=0)
        h_bar_s_satg[a] = Enthalpy(S$,P=P_bar_s[a],X=1)

        T_bar_s[a] = Average(T_si[a],T_se[a])
        s_bar_s[a] = Entropy(S$,P=P_bar_s[a],h=h_bar_s[a])
        X_bar_s[a] = Average(X_si[a],X_se[a])
        V_bar_s[a] = Average(V_si[a],V_se[a])
        h_bar_s0[a] = Average(h_s0e[a],h_s0i[a])

        "Primary"
        m_bar_p[a] = Average(m_pe[a],m_pi[a])
        P_bar_p[a] = Average(P_pe[a],P_pi[a])
        h_bar_p[a] = Average(h_pe[a],h_pi[a])
        h_bar_p_satl[a] = Enthalpy(P$,P=P_bar_p[a],X=0)
        h_bar_p_satg[a] = Enthalpy(P$,P=P_bar_p[a],X=1)

        T_bar_p[a] =  Average(T_pi[a],T_pe[a])
        s_bar_p[a] = Entropy(P$,P=P_bar_p[a],h=h_bar_p[a])
        V_bar_p[a] = Average(V_pi[a],V_pe[a])
        h_bar_p0[a] = Average(h_p0e[a],h_p0i[a])
```

```
        Rho_bar_p[a] = Average(Rho_pi[a],Rho_pe[a])

"Properties"
    "Secondary"
        Rho_bar_s[a] = Density(S$,P=P_bar_s[a],h=h_bar_s[a])

        Chi_bar_s[a] = average(Chi_si[a],Chi_se[a])
        MF_bar_s[a] = average(MF_si[a],MF_se[a])
        SF_bar_s[a] = average(SF_si[a],SF_se[a])
        Phi_bar_s[a] = average(Phi_si[a],Phi_se[a])
        rho_bar_s[a] = (1-epsilon_bar_s[a])*rho_bar_sl[a]+(epsilon_bar_s[a])*rho_bar_sg[a]

        h_bar_cboils[a] =
Boil(S$,X_bar_s[a],T_bar_s[a],T_bar_ws[a],P_bar_s[a],C_bar_p_sl[a],Rho_bar_sl[a],k_bar_sl[a],Mu_bar_sl[a],
rho_bar_sg[a])
        h_bar_cs_calc[a] =
TwoPhase(X_bar_s[a],h_bar_c_sl[a],h_bar_c_sg[a],h_bar_cboils[a],MF_bar_s[a],SF_bar_s[a])

        $IF TableRun# = 1
            h_bar_cs[a] = h_bar_cs_calc[a]
        $ENDIF

        $IF TableRun# > 1
            h_bar_cs[a] = TableValue('Table 1',j,19*n+freedom+a) {h_bar_cs[a] = h_bar_cs_calc[a]}
        $ENDIF


    "Liquid"
        m_bar_sl[a] = Average(m_sil[a],m_sel[a])
        Mu_bar_sl[a] = (Max(mu_sil[a],mu_sel[a])-Min(mu_sil[a],mu_sel[a]))*(1-X_bar_s[a])*DELTAL +
Min(mu_sil[a],mu_sel[a])*DELTAL*(1-X_bar_s[a]) +Min(mu_sil[a],mu_sel[a])*DELTAL*(X_bar_s[a])
        Rho_bar_sl[a] = (Max(rho_sil[a],rho_sel[a])-Min(rho_sil[a],rho_sel[a]))*(1-X_bar_s[a])*DELTAL +
Min(rho_sil[a],rho_sel[a])*DELTAL*(1-X_bar_s[a]) +Min(rho_sil[a],rho_sel[a])*DELTAL*(X_bar_s[a])
        k_bar_sl[a] = (Max(k_sil[a],k_sel[a])-Min(k_sil[a],k_sel[a]))*(1-X_bar_s[a])*DELTAL  +
Min(k_sil[a],k_sel[a])*DELTAL*(1-X_bar_s[a])+ Min(k_sil[a],k_sel[a])*DELTAL*(X_bar_s[a])
        C_bar_p_sl[a] =(Max(C_p_sil[a],C_p_sel[a])-Min(C_p_sil[a],C_p_sel[a]))*(1-X_bar_s[a])*DELTAL +
Min(C_p_sil[a],C_p_sel[a])*DELTAL*(1-X_bar_s[a])+Min(C_p_sil[a],C_p_sel[a])*DELTAL*(X_bar_s[a])
        Re_bar_sl[a] = (Max(Re_sil[a],Re_sel[a])-Min(Re_sil[a],Re_sel[a]))*(1-X_bar_s[a])*DELTAL +
Min(Re_sil[a],Re_sel[a])*DELTAL*(1-X_bar_s[a])+Min(Re_sil[a],Re_sel[a])*DELTAL*(X_bar_s[a])
        Pr_bar_sl[a] = (Max(Pr_sil[a],Pr_sel[a])-Min(Pr_sil[a],Pr_sel[a]))*(1-X_bar_s[a])*DELTAL +
Min(Pr_sil[a],Pr_sel[a])*DELTAL*(1-X_bar_s[a])+Min(Pr_sil[a],Pr_sel[a])*DELTAL*(X_bar_s[a])
        Nuss_bar_sl[a] = (Max(Nuss_sil[a],Nuss_sel[a])-Min(Nuss_sil[a],Nuss_sel[a]))*(1-
X_bar_s[a])*DELTAL + Min(Nuss_sil[a],Nuss_sel[a])*DELTAL*(1-
X_bar_s[a])+Min(Nuss_sil[a],Nuss_sel[a])*DELTAL*(X_bar_s[a])
        h_bar_c_sl[a] = (Max(h_c_sil[a],h_c_sel[a])-Min(h_c_sil[a],h_c_sel[a]))*(1-X_bar_s[a])*DELTAL +
Min(h_c_sil[a],h_c_sel[a])*DELTAL*(1-X_bar_s[a])+Min(h_c_sil[a],h_c_sel[a])*DELTAL*(X_bar_s[a])

        DeltaP_s0l[a] = PDSP(f_s,DELTAL,D_hs,Ap_s,m_bar_sl[a],rho_bar_sl[a])

    "Gas"
        m_bar_sg[a] = Average(m_sig[a],m_seg[a])
        Mu_bar_sg[a] = (Max(mu_sig[a],mu_seg[a])-Min(mu_sig[a],mu_seg[a]))*(X_bar_s[a])*DELTAL+
Min(mu_sig[a],mu_seg[a])*DELTAL*(X_bar_s[a]) + Min(mu_sig[a],mu_seg[a])*DELTAL*(1-X_bar_s[a])
        Rho_bar_sg[a] = (Max(rho_sig[a],rho_seg[a])-Min(rho_sig[a],rho_seg[a]))*(X_bar_s[a])*DELTAL +
Min(rho_sig[a],rho_seg[a])*DELTAL*(X_bar_s[a]) +Min(rho_sig[a],rho_seg[a])*DELTAL*(1-X_bar_s[a])
        k_bar_sg[a] = (Max(k_sig[a],k_seg[a])-Min(k_sig[a],k_seg[a]))*(X_bar_s[a])*DELTAL+
Min(k_sig[a],k_seg[a])*DELTAL*(X_bar_s[a]) + Min(k_sig[a],k_seg[a])*DELTAL*(1-X_bar_s[a])
```

```
        C_bar_p_sg[a] = (Max(C_p_sig[a],C_p_seg[a])-
Min(C_p_sig[a],C_p_seg[a]))*(X_bar_s[a])*DELTAL+ Min(C_p_sig[a],C_p_seg[a])*DELTAL*(X_bar_s[a])
+ Min(C_p_sig[a],C_p_seg[a])*DELTAL*(1-X_bar_s[a])
        Re_bar_sg[a] =  (Max(Re_sig[a],Re_seg[a])-Min(Re_sig[a],Re_seg[a]))*(X_bar_s[a])*DELTAL+
Min(Re_sig[a],Re_seg[a])*DELTAL*(X_bar_s[a]) + Min(Re_sig[a],Re_seg[a])*DELTAL*(1-X_bar_s[a])
        Pr_bar_sg[a] =  (Max(Pr_sig[a],Pr_seg[a])-Min(Pr_sig[a],Pr_seg[a]))*(X_bar_s[a])*DELTAL+
Min(Pr_sig[a],Pr_seg[a])*DELTAL*(X_bar_s[a]) + Min(Pr_sig[a],Pr_seg[a])*DELTAL*(1-X_bar_s[a])
        Nuss_bar_sg[a] =  (Max(Nuss_sig[a],Nuss_seg[a])-
Min(Nuss_sig[a],Nuss_seg[a]))*(X_bar_s[a])*DELTAL+
Min(Nuss_sig[a],Nuss_seg[a])*DELTAL*(X_bar_s[a]) + Min(Nuss_sig[a],Nuss_seg[a])*DELTAL*(1-
X_bar_s[a])
        h_bar_c_sg[a] =  (Max(h_c_sig[a],h_c_seg[a])-Min(h_c_sig[a],h_c_seg[a]))*(X_bar_s[a])*DELTAL+
Min(h_c_sig[a],h_c_seg[a])*DELTAL*(X_bar_s[a]) + Min(h_c_sig[a],h_c_seg[a])*DELTAL*(1-X_bar_s[a])

        DeltaP_s0g[a] = PDSP(f_s,DELTAL,D_hs,Ap_s,m_bar_sg[a],rho_bar_sg[a])

    "Primary"
        Mu_bar_p[a] = MyVisL(P$,1,P_bar_p[a],h_bar_p[a],h_bar_p_satl[a],h_bar_p_satg[a] )
        k_bar_p[a] = MyConL(P$,1,P_bar_p[a],h_bar_p[a],h_bar_p_satl[a],h_bar_p_satg[a])
        C_bar_p_p[a] = MyCPL(P$,1,P_bar_p[a],h_bar_p[a],h_bar_p_satl[a],h_bar_p_satg[a])
        Re_bar_p[a] = MyRe(m_bar_p[a],A_p,D_hp,mu_bar_p[a])
        Pr_bar_p[a] = MyPr(C_bar_p_p[a],Mu_bar_p[a],k_bar_p[a])
        Nuss_bar_p[a] = Nusselt(Re_bar_p[a],Pr_bar_p[a],0.3)
        h_bar_cp[a] = k_bar_p[a]/D_hs*Nuss_bar_p[a]

    "Wall"
    k_bar_w[a] = 14
    R_bar_w[a] = ln(D_o/D_i)/(2*pi*k_bar_w[a]*DELTAL)

    "Compenent Char"
    AU_s[a] = h_bar_cs[a]*Ap_s
    AU_p[a] = h_bar_cp[a]*Ap_p

    Q_s[a] = AU_s[a]*(T_bar_ws[a] - T_bar_s[a])
    Q_w[a] = (T_bar_wp[a]-T_bar_ws[a])/R_bar_w[a]
    Q_p[a] = AU_p[a]*(T_bar_wp[a] - T_bar_p[a])

END

T_s_out = T_bar_s[n]
h_s_out = h_bar_s[n]
V_s_out = V_bar_s[n]
P_s_in = P_bar_s[1]
m_s_out = m_bar_s[n]
X_s_out = X_bar_s[n]
V_max = Max(V_bar_s[1..n],V_bar_p[1..n])
Q_s_total = Sum(Q_s[1..n])


$IF TableRun# > 1
    CALL Guesses(Tablevalue('Table 1',j,5),update:counter)
$ENDIF
```

APPENDIX II – Stability

In this appendix the detail and discussions regarding the stability of the different time wise integration approaches is given.

1 IMPLICIT

For the implicit method an Alpha of 1 along with 1 [m] pipe increments were used for to . The implicit method is unconditionally stable for any time step sizes, as only the current solution is used, but the results obtained may lack accuracy. To verify the stability of the implicit method a couple of time steps were tested.

1.1 PRIMARY SIDE

The primary side showed good stability for both the constant and stepped boundary values, as can be seen from Figure 56 and Figure 57. It can be seen from the heat flux vs. time graphs how the fix and stepped change have been implemented. The larger the time step the quicker the source terms returned to zero, as the change in variable divided by a larger time step results in a smaller value. When evaluating the deviation, from zero, of the source term the smaller time steps resulted in larger source terms.

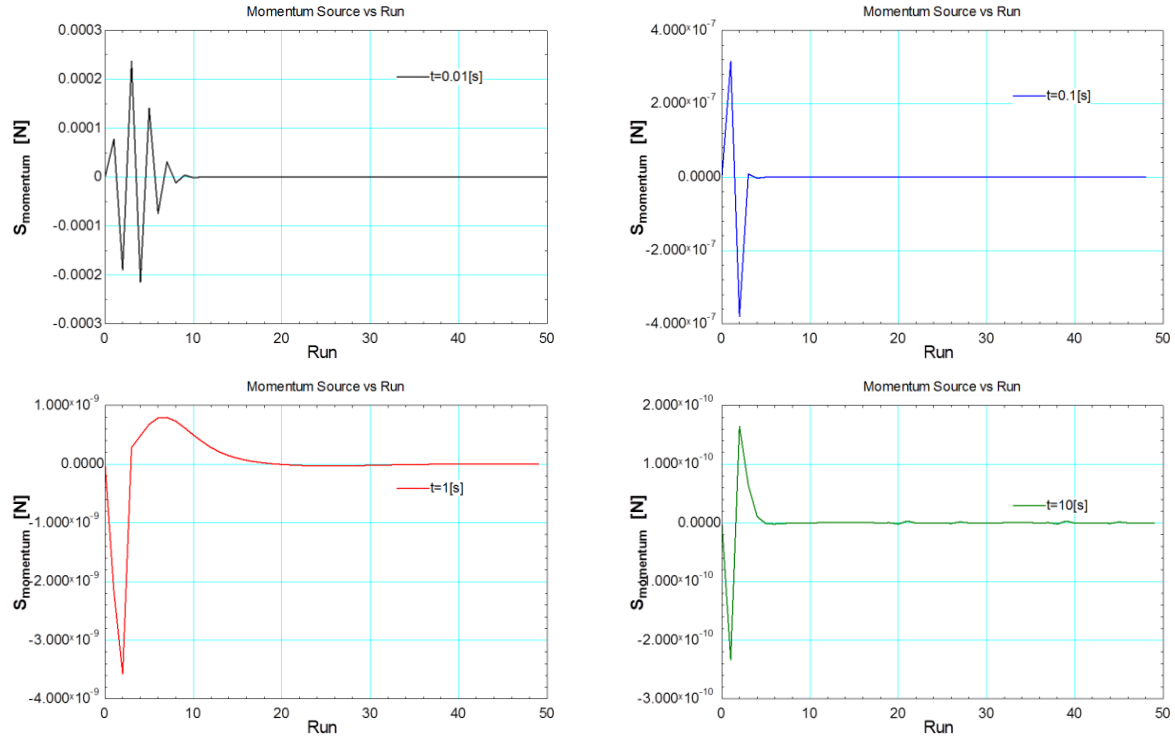

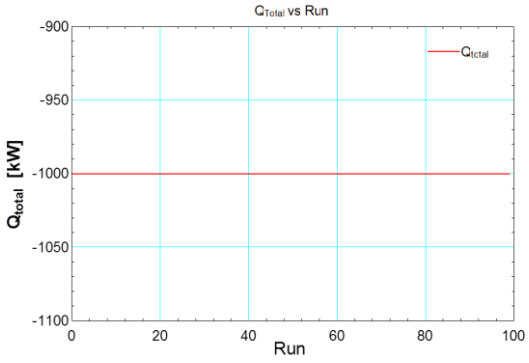

Figure 56 – Implicit primary momentum source term - Constant boundary values.

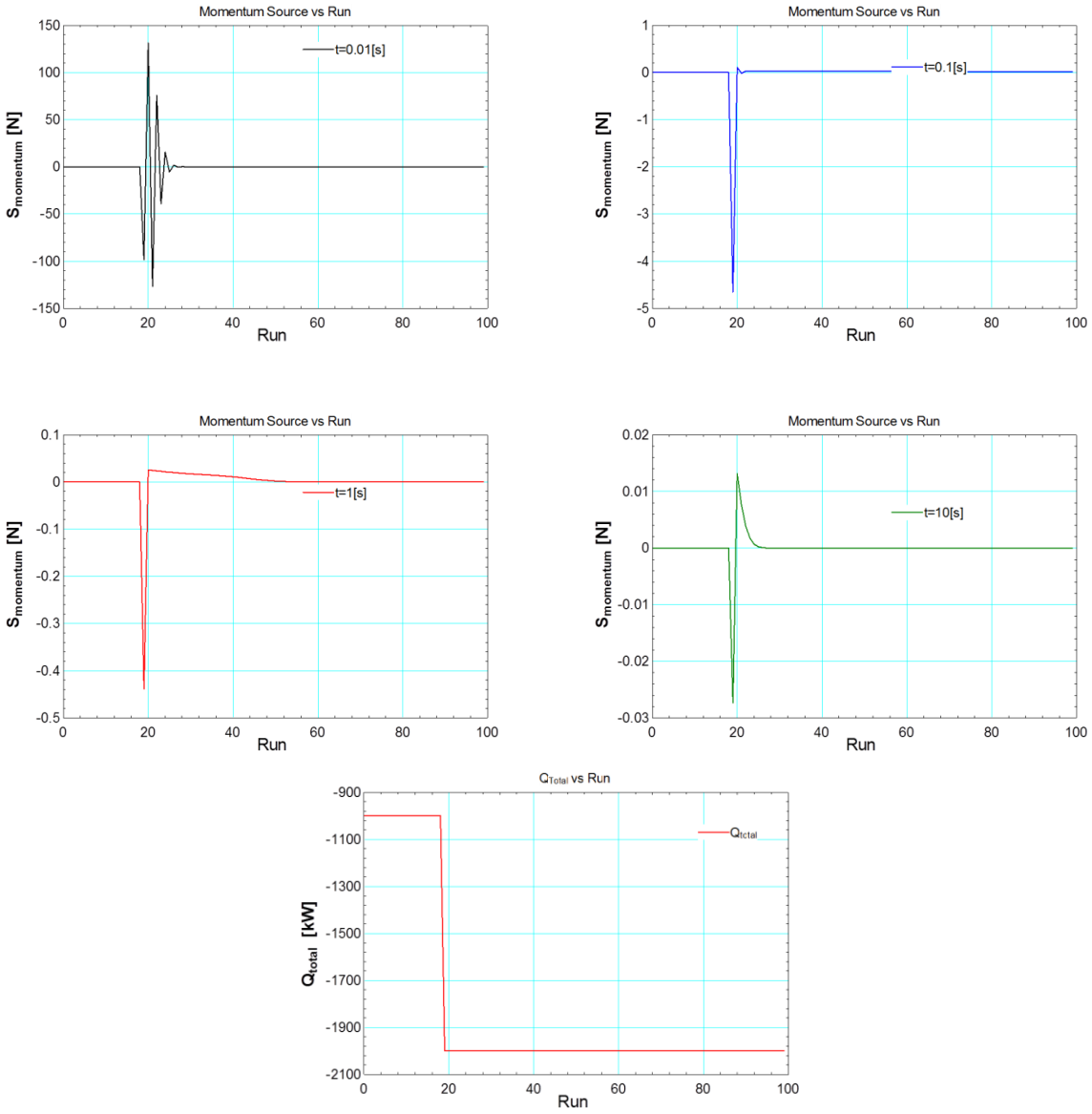

Figure 57 – Implicit primary momentum source term – Step increase in the boundary values.

1.2 SECONDARY SIDE

For the secondary side the constant and stepped boundary values both showed good stability of the source term, as seen from Figure 58 and Figure 59 . It either returned to zero or oscillates around zero, but with a negligible small deviation, as see for the 0.1 [s] and 10 [s] in Figure 59.

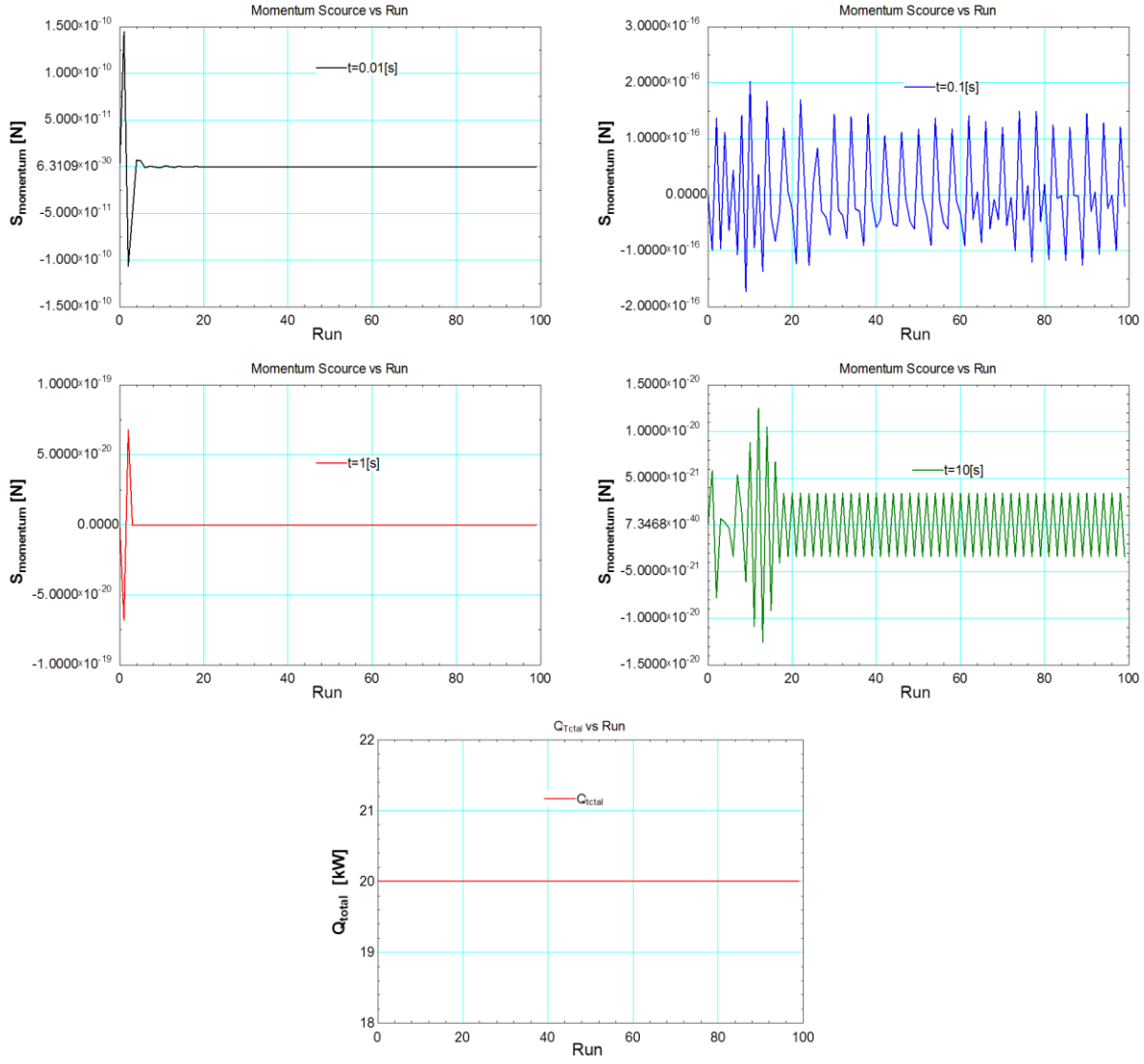

Figure 58 – Implicit secondary side momentum source term - constant boundary values.

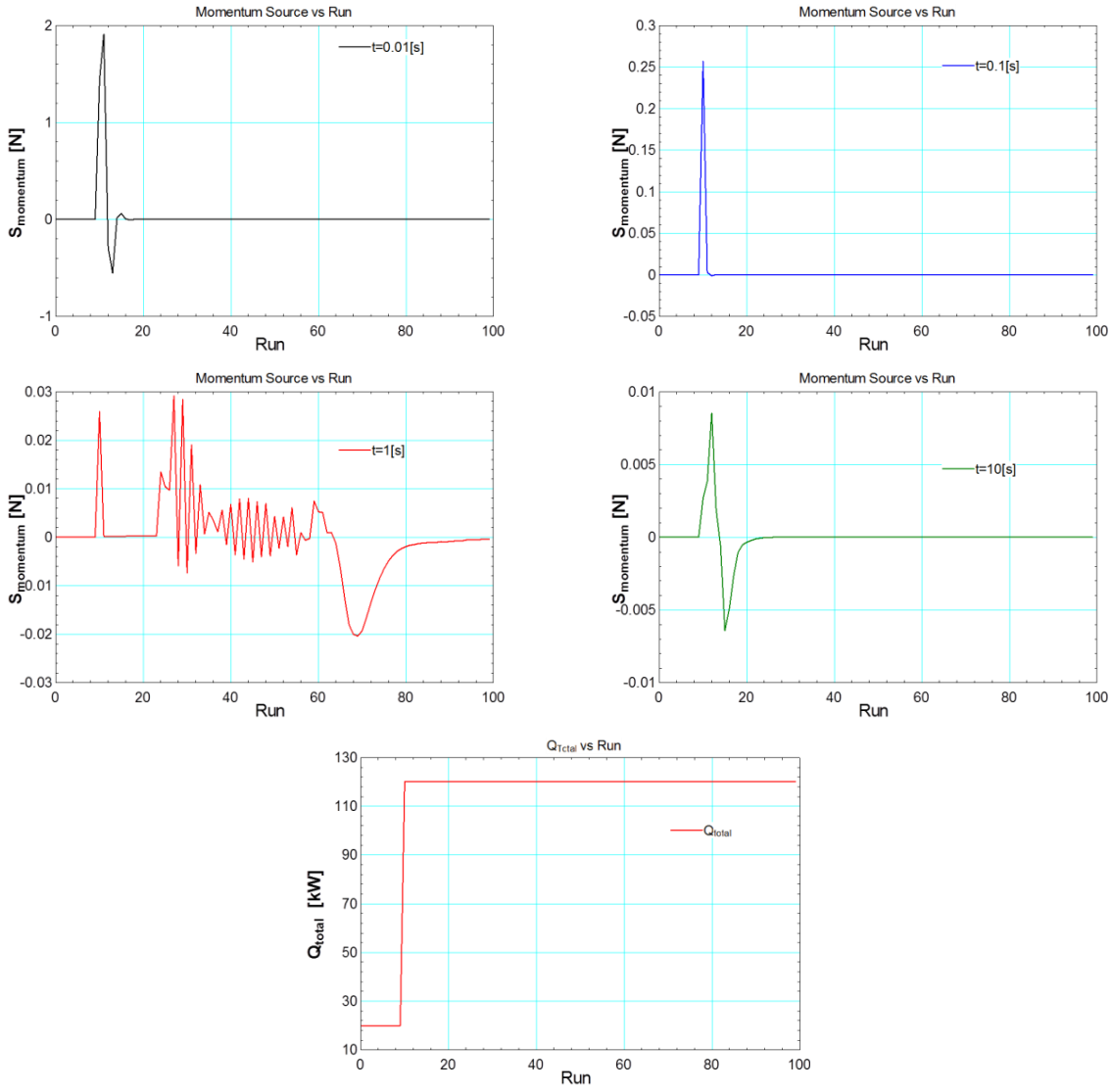

Figure 59 – Implicit secondary side momentum source term – step increase boundary values.

2 CRANK-NICHOLSON APPROACH

The Crank-Nicholson method implies that an Alpha of 0.5 is used in to . It should provide a good balance between stability and accuracy. Caution should be taken as too small time steps can lead to the solutions diverging. For both the primary and secondary sides the pre-selected increment length of 1[m] resulted in the solution diverging.

2.1 PRIMARY SIDE

For no change in the boundary values, the smaller the time step the quicker the primary source terms diverged and the model encountered conditions outside of EES fluid property reference base. From Figure 60 the rate at which the source term starts to diverge can clearly

be seen. For all the selected time steps the source term eventually diverged if the model was left to calculate for more than 100 runs. Figure 60 shows the divergence of the primary side for a stepped input. This also showed that for a larger time step the source term deviation is smaller, but if given time the results will still diverge.

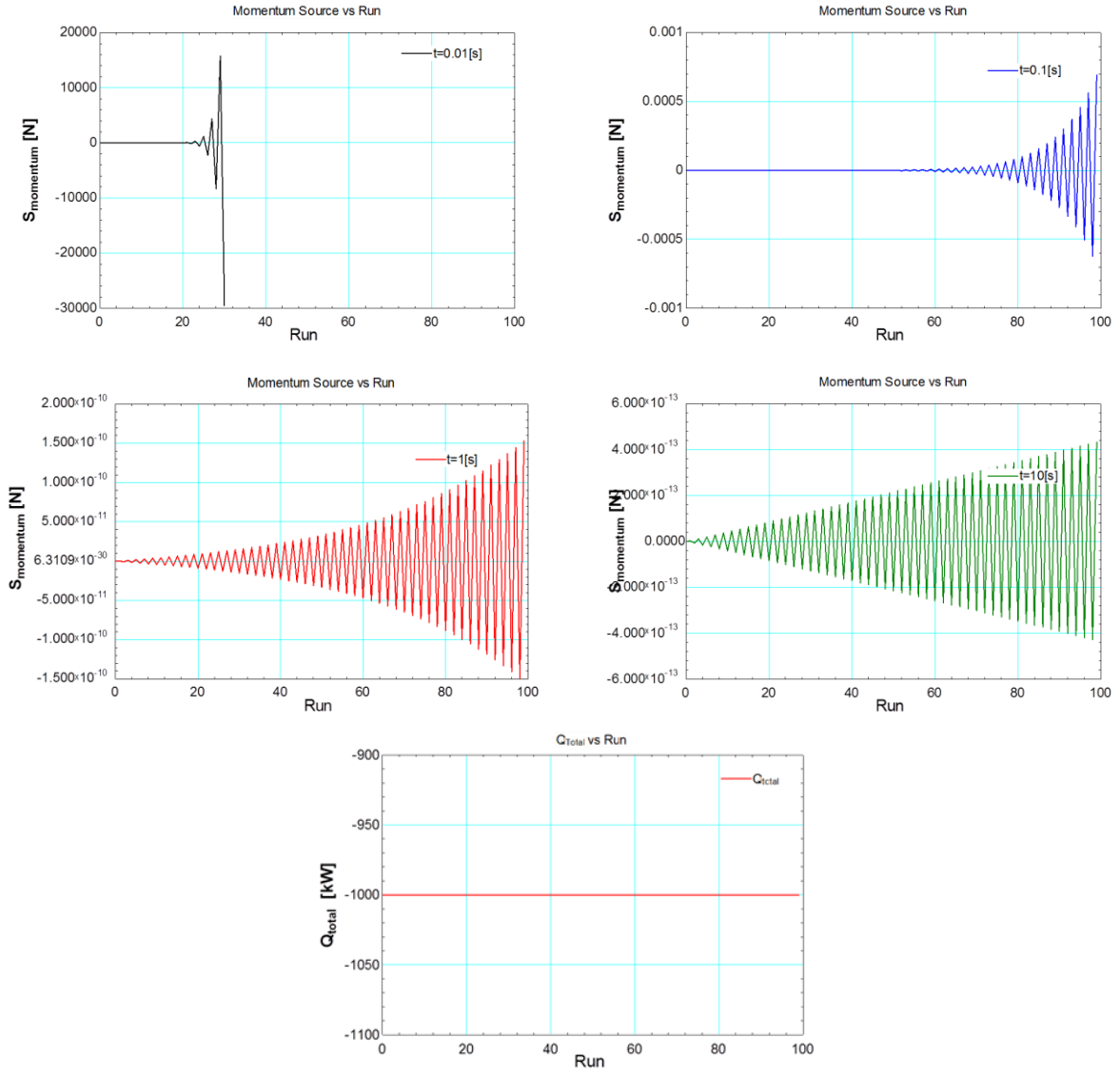

Figure 60 – Crank-Nicholson primary side momentum source term - constant boundary values.

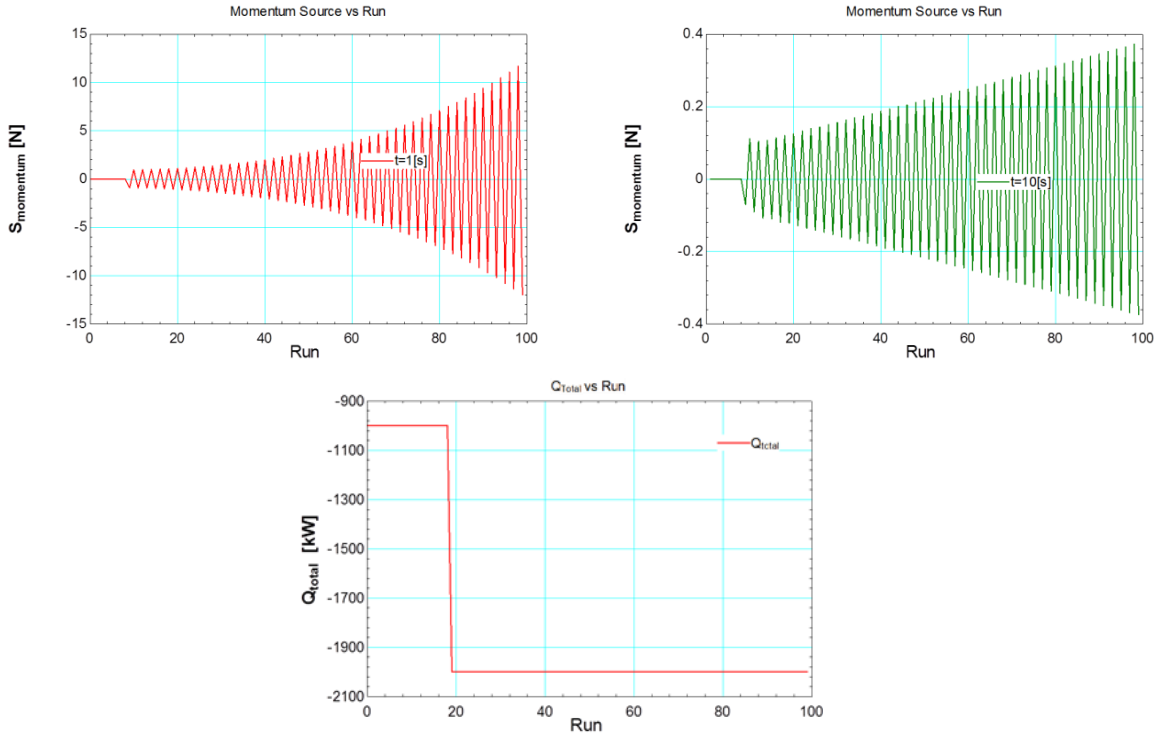

Figure 61 – Crank-Nicholson primary momentum source term - step increase boundary values.

2.2 SECONDARY SIDE

When evaluating the stability of the Crank-Nichols approach for the secondary side it also proved to be unstable, due to the large change in fluid properties when boiling occurs. Figure 62 shows the results for the case of no change in boundary values. For the smaller time steps the model seems to be stable but start to divergence as the source term oscillates around zero. The larger time step`s diverge from the beginning but the source term deviation is small and grows with elapsed time. The stepped input, Figure 17, could not remain stable for the 100 runs. This implies that the segment length is too long.

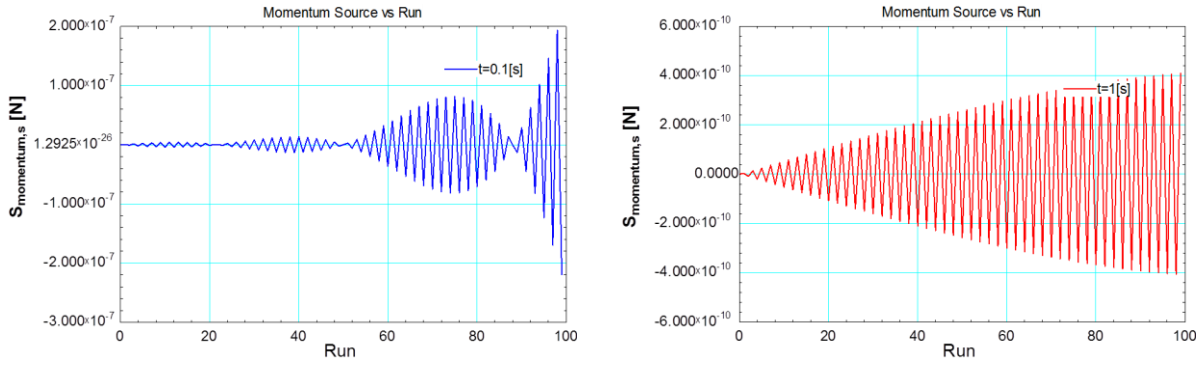

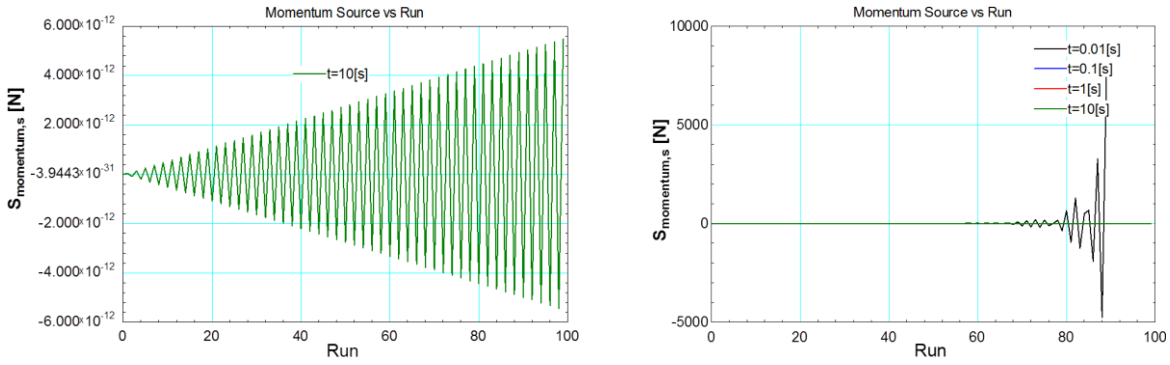

Figure 62 – Crank-Nichols secondary side momentum source term - constant boundary values.

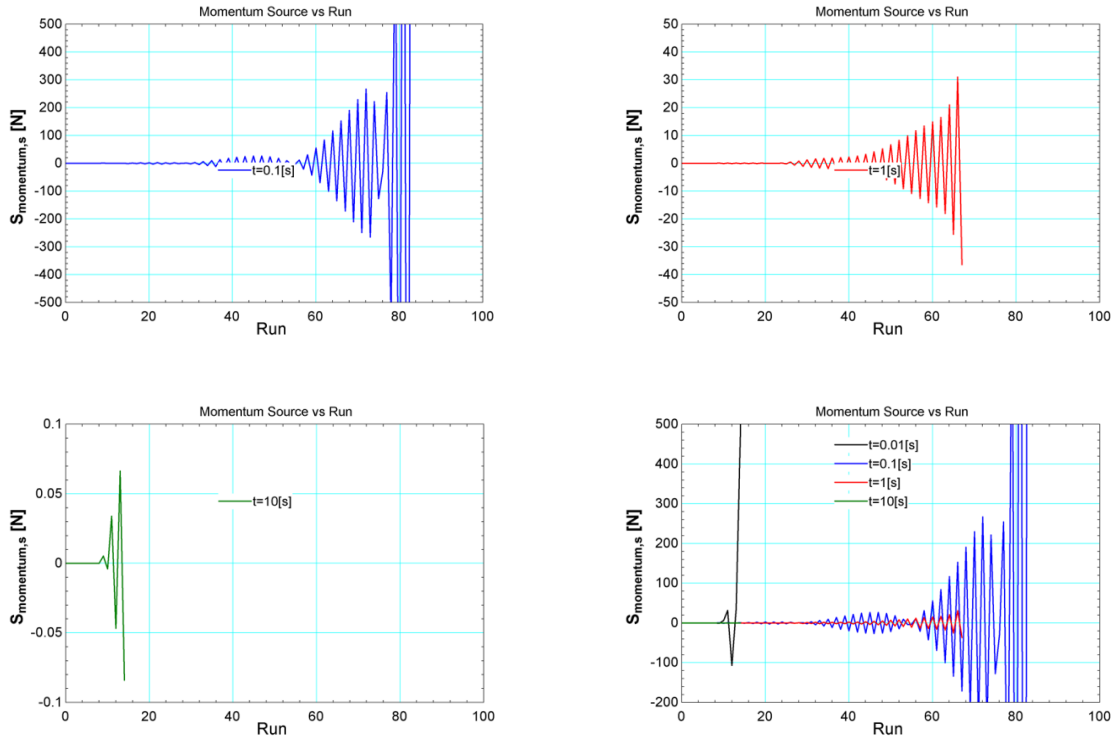

Figure 63 - Crank-Nichols secondary side momentum source term - step increase boundary values.

APPENDIX III – EES Results – Transient

The EES results for the transient that was used to compare with Flownex for verification purpose is given.

i	AU_p[i]	AU_s[i]	Chi_bar_s[i]	Chi_se[i]	Chi_si[i]	C_bar_p_p[i]	C_bar_p_sg[i]	C_bar_p_sl[i]	C_p_seg[i]	C_p_sel[i]	C_p_sig[i]	C_p_sil[i]
	[W/K]	[W/K]	[-]	[-]	[-]	[J/kgK]	[J/kgK]	[J/kgK]	[J/kgK]	[J/kgK]	[J/kgK]	[J/kgK]
0.00				0.00					0.00	4242.82		
1.00	665.60	97.12	0.00	0.00	0.00	5244.00	0.00	4379.56	0.00	4379.56	0.00	4242.82
2.00	666.70	104.70	0.00	0.00	0.00	5272.00	0.00	4554.36	0.00	4554.36	0.00	4379.56
3.00	667.50	109.30	0.00	0.00	0.00	5293.00	0.00	4740.16	0.00	4740.16	0.00	4554.36
4.00	668.10	112.20	0.00	0.00	0.00	5308.00	0.00	4919.81	0.00	4919.81	0.00	4740.16
5.00	668.50	112.80	6.61	13.21	0.00	5319.00	22.60	5036.54	4443.00	5037.14	0.00	4919.81
6.00	669.00	982.90	7.53	1.86	13.21	5333.00	4442.00	5037.11	4442.00	5036.60	4443.00	5037.14
7.00	669.70	910.50	1.41	0.97	1.86	5353.00	4441.00	5036.57	4441.00	5036.32	4442.00	5036.60
8.00	670.50	864.60	0.80	0.62	0.97	5373.00	4440.00	5036.28	4440.00	5036.13	4441.00	5036.32
9.00	671.20	834.70	0.53	0.44	0.62	5394.00	4440.00	5036.09	4440.00	5035.98	4440.00	5036.13
10.00	672.00	814.60	0.38	0.32	0.44	5416.00	4440.00	5035.94	4440.00	5035.87	4440.00	5035.98
11.00	672.80	801.70	0.28	0.24	0.32	5439.00	4440.00	5035.83	4439.00	5035.77	4440.00	5035.87
12.00	673.60	793.60	0.21	0.18	0.24	5464.00	4439.00	5035.73	4439.00	5035.69	4439.00	5035.77
13.00	674.40	788.10	0.15	0.13	0.18	5489.00	4439.00	5035.65	4439.00	5035.62	4439.00	5035.69
14.00	675.30	784.90	0.11	0.09	0.13	5516.00	4439.00	5035.58	4439.00	5035.56	4439.00	5035.62
15.00	676.20	782.00	0.07	0.05	0.09	5545.00	4439.00	5035.51	4439.00	5035.50	4439.00	5035.56
16.00	677.20	767.20	0.04	0.03	0.05	5575.00	4439.00	5035.46	4439.00	5035.45	4439.00	5035.50
17.00	678.20	671.60	0.01	0.00	0.03	5602.00	4438.00	215.58	4434.00	0.00	4439.00	5035.45
18.00	678.90	49.79	0.00	0.00	0.00	5620.00	4434.00	0.00	4051.00	0.00	4434.00	0.00
19.00	679.10	48.87	0.00	0.00	0.00	5627.00	4051.00	0.00	3736.00	0.00	4051.00	0.00
20.00	679.30	45.81	0.00	0.00	0.00	5634.00	3736.00	0.00	3532.00	0.00	3736.00	0.00
21.00	679.50	44.23	0.00	0.00	0.00	5638.00	3532.00	0.00	3397.00	0.00	3532.00	0.00
22.00	679.60	43.26	0.00	0.00	0.00	5642.00	3397.00	0.00	3305.00	0.00	3397.00	0.00
23.00	679.70	42.62	0.00	0.00	0.00	5645.00	3305.00	0.00	3241.00	0.00	3305.00	0.00
24.00	679.70	42.17	0.00	0.00	0.00	5647.00	3241.00	0.00	3195.00	0.00	3241.00	0.00
25.00	679.80	41.85	0.00	0.00	0.00	5649.00	3195.00	0.00	3161.00	0.00	3195.00	0.00
26.00												

Appendix III – EES Raw Results

i	Deltah_p_he[i] [W]	Deltah_p_hi[i] [W]	Deltah_p_m[i] [W]	Deltah_s_he[i] [W]	Deltah_s_hi[i] [W]	Deltah_s_m[i] [W]	DeltaP_p0[i] [Pa]	DeltaP_p_m[i] [Pa]	DeltaP_p_p[i] [Pa]	DeltaP_p_z[i] [Pa]	DeltaP_s0[i] [Pa]
0.00											
1.00	1279000.00	1288000.00	25.98	30254.00	21450.00	0.05	0.01	0.00	-7321.00	7320.68	0.11
2.00	1288000.00	1294000.00	21.97	36670.00	30254.00	0.39	0.01	0.00	-7294.00	7293.51	0.12
3.00	1294000.00	1299000.00	15.05	41242.00	36670.00	0.78	0.01	0.00	-7274.00	7273.71	0.12
4.00	1299000.00	1302000.00	6.46	44489.00	41242.00	1.22	0.01	0.00	-7260.00	7259.53	0.13
5.00	1302000.00	1305000.00	2.68	46884.00	44489.00	1.79	0.01	0.00	-7250.00	7249.24	0.13
6.00	1305000.00	1310000.00	-4.36	51708.00	46884.00	34.01	0.01	0.00	-7237.00	7236.17	0.08
7.00	1310000.00	1314000.00	0.74	56594.00	51708.00	9.33	0.01	0.00	-7219.00	7218.57	0.26
8.00	1314000.00	1319000.00	-6.70	61579.00	56594.00	4.88	0.01	0.00	-7201.00	7200.55	0.55
9.00	1319000.00	1325000.00	8.80	66678.00	61579.00	4.22	0.01	0.00	-7183.00	7182.02	0.92
10.00	1325000.00	1330000.00	-13.53	71901.00	66678.00	3.13	0.01	0.00	-7164.00	7162.97	1.37
11.00	1330000.00	1335000.00	25.47	77261.00	71901.00	3.56	0.01	0.00	-7144.00	7143.30	1.88
12.00	1335000.00	1341000.00	-37.59	82765.00	77261.00	4.25	0.01	0.00	-7124.00	7123.07	2.43
13.00	1341000.00	1346000.00	66.99	88418.00	82765.00	3.85	0.01	-0.01	-7103.00	7102.06	3.03
14.00	1346000.00	1352000.00	-105.39	94227.00	88418.00	3.09	0.01	0.01	-7081.00	7080.54	3.64
15.00	1352000.00	1358000.00	180.02	100197.00	94227.00	3.33	0.01	-0.02	-7059.00	7058.00	4.22
16.00	1358000.00	1364000.00	-293.71	106311.00	100197.00	3.61	0.01	0.03	-7036.00	7035.22	4.70
17.00	1364000.00	1370000.00	-733.25	112697.00	106311.00	733.20	0.01	0.06	-7015.00	7014.43	3.79
18.00	1370000.00	1372000.00	39.61	114952.00	112697.00	1237.00	0.01	0.00	-7001.00	7001.48	4.21
19.00	1372000.00	1373000.00	28.17	116471.00	114952.00	375.70	0.01	0.00	-6996.00	6995.78	4.38
20.00	1373000.00	1374000.00	13.35	117452.00	116471.00	31.28	0.01	0.00	-6991.00	6991.24	4.53
21.00	1374000.00	1375000.00	6.59	118152.00	117452.00	-42.67	0.01	0.00	-6988.00	6987.78	4.65
22.00	1375000.00	1375000.00	3.69	118675.00	118152.00	-48.22	0.01	0.00	-6985.00	6985.13	4.73
23.00	1375000.00	1376000.00	2.22	119071.00	118675.00	-39.82	0.01	0.00	-6983.00	6983.07	4.80
24.00	1376000.00	1376000.00	1.50	119372.00	119071.00	-30.61	0.01	0.00	-6981.00	6981.47	4.85
25.00	1376000.00	1376000.00	0.84	119601.00	119372.00	-23.14	0.01	0.00	-6980.00	6980.22	4.89
26.00											

Appendix III – EES Raw Results

i	DeltaP_s0g[i]	DeltaP_s0l[i]	DeltaP_s_m[i]	DeltaP_s_p[i]	DeltaP_s_rho[i]	DeltaP_s_z[i]	epsilon_bar_s[i]	h_bar_cboils[i]	h_bar_cp[i]	h_bar_cs[i]	h_bar_cs_calc[i]
	[Pa]	[Pa]	[Pa]	[Pa]	[Pa]	[Pa]	[-]	[W/m^2 K]	[W/m^2 K]	[W/m^2 K]	[W/m^2 K]
0.00											
1.00	0.00	0.11	0.00	-8997.00	-0.19	8997.00	0.02	0.00	6053.00	1237.00	1237.00
2.00	0.00	0.12	0.00	-8552.00	-0.17	8552.00	0.02	0.00	6063.00	1333.00	1333.00
3.00	0.00	0.12	0.00	-8183.00	-0.15	8183.00	0.02	0.00	6071.00	1391.00	1391.00
4.00	0.00	0.13	0.00	-7893.00	-0.13	7893.00	0.02	0.00	6076.00	1428.00	1428.00
5.00	0.02	0.13	0.00	-7669.00	-1.03	7668.00	0.01	0.00	6080.00	1436.00	1436.00
6.00	0.01	0.12	-0.01	-3204.00	-4.87	3199.00	0.60	32921.00	6085.00	12515.00	12494.00
7.00	0.06	0.10	-0.01	-1674.00	-5.22	1669.00	0.81	36212.00	6091.00	11593.00	11574.00
8.00	0.16	0.09	0.00	-1128.00	-6.66	1122.00	0.88	38970.00	6098.00	11008.00	10989.00
9.00	0.30	0.07	0.00	-847.20	-7.50	840.70	0.92	41337.00	6104.00	10627.00	10608.00
10.00	0.50	0.06	0.00	-675.60	-8.12	668.90	0.94	43438.00	6111.00	10371.00	10357.00
11.00	0.76	0.04	-0.01	-559.70	-8.63	553.00	0.96	45315.00	6119.00	10208.00	10188.00
12.00	1.08	0.03	-0.01	-476.10	-9.08	469.50	0.97	47038.00	6126.00	10105.00	10078.00
13.00	1.47	0.02	-0.01	-412.90	-9.51	406.50	0.98	48700.00	6134.00	10034.00	10015.00
14.00	1.93	0.01	-0.01	-363.40	-9.91	357.20	0.99	50280.00	6142.00	9993.00	9972.00
15.00	2.47	0.01	-0.01	-323.60	-10.30	317.70	0.99	51902.00	6150.00	9957.00	9943.00
16.00	3.09	0.00	-0.01	-291.10	-10.64	285.30	1.00	54231.00	6159.00	9768.00	9735.00
17.00	3.79	0.01	-1.62	-263.10	-10.02	259.50	0.86	664.40	6168.00	8551.00	679.80
18.00	4.21	0.00	-2.89	-238.40	-3.54	245.30	0.99	0.00	6174.00	634.00	653.50
19.00	4.38	0.00	-0.91	-231.90	-4.19	238.30	0.98	0.00	6176.00	622.30	627.90
20.00	4.53	0.00	-0.08	-225.00	-3.53	231.80	0.99	0.00	6178.00	583.30	601.90
21.00	4.65	0.00	0.11	-219.30	-2.80	226.80	0.99	0.00	6179.00	563.20	583.20
22.00	4.73	0.00	0.12	-215.00	-2.17	223.10	0.99	0.00	6180.00	550.80	570.30
23.00	4.80	0.00	0.10	-211.70	-1.67	220.20	0.99	0.00	6181.00	542.60	561.30
24.00	4.85	0.00	0.08	-209.20	-1.28	218.10	1.00	0.00	6182.00	536.90	554.90
25.00	4.89	0.00	0.06	-207.30	-0.98	216.60	1.00	0.00	6182.00	532.80	550.40
26.00											

Appendix III – EES Raw Results

i	h_bar_c_sg[i]	h_bar_c_sl[i]	h_bar_p[i]	h_bar_p0[i]	h_bar_p_satg[i]	h_bar_p_satl[i]	h_bar_s[i]	h_bar_s0[i]	h_bar_s_satg[i]	h_bar_s_satl[i]	h_c_seg[i]	h_c_sel[i]
	[W/m^2 K]	[W/m^2 K]	[J/kg]	[J/kg]	[J/kg]	[k/kg]	[J/kg]	[J/kg]	[J/kg]	[k/kg]	[W/m^2]	[W/m^2]
0.00											0.00	1065.00
1.00	0.00	1237.00	1284000.00	1284000.00	2596000.00	1630000.00	646294.00	646294.00	2794000.00	1158000.00	0.00	1237.00
2.00	0.00	1333.00	1292000.00	1292000.00	2597000.00	1630000.00	836524.00	836524.00	2794000.00	1157000.00	0.00	1333.00
3.00	0.00	1391.00	1297000.00	1297000.00	2597000.00	1629000.00	973853.00	973853.00	2794000.00	1156000.00	0.00	1391.00
4.00	0.00	1428.00	1301000.00	1301000.00	2597000.00	1629000.00	1072000.00	1072000.00	2794000.00	1156000.00	0.00	1428.00
5.00	0.08	1436.00	1304000.00	1304000.00	2597000.00	1629000.00	1142000.00	1142000.00	2794000.00	1155000.00	16.66	1436.00
6.00	20.05	1432.00	1308000.00	1308000.00	2597000.00	1628000.00	1232000.00	1232000.00	2794000.00	1155000.00	89.06	1351.00
7.00	96.21	1340.00	1313000.00	1313000.00	2598000.00	1628000.00	1353000.00	1353000.00	2794000.00	1155000.00	148.40	1263.00
8.00	159.10	1245.00	1318000.00	1318000.00	2598000.00	1628000.00	1476000.00	1476000.00	2794000.00	1155000.00	203.20	1171.00
9.00	217.50	1145.00	1323000.00	1323000.00	2598000.00	1628000.00	1601000.00	1601000.00	2794000.00	1155000.00	255.60	1075.00
10.00	273.50	1040.00	1328000.00	1328000.00	2598000.00	1627000.00	1730000.00	1730000.00	2794000.00	1155000.00	306.70	974.50
11.00	328.30	928.90	1333000.00	1333000.00	2599000.00	1627000.00	1862000.00	1862000.00	2794000.00	1155000.00	356.90	868.70
12.00	382.50	811.00	1339000.00	1339000.00	2599000.00	1627000.00	1998000.00	1998000.00	2794000.00	1155000.00	406.70	756.50
13.00	436.40	684.80	1344000.00	1344000.00	2599000.00	1626000.00	2137000.00	2137000.00	2794000.00	1155000.00	456.30	636.80
14.00	490.40	548.10	1350000.00	1350000.00	2599000.00	1626000.00	2280000.00	2280000.00	2794000.00	1155000.00	505.90	507.50
15.00	544.50	397.10	1356000.00	1356000.00	2599000.00	1626000.00	2427000.00	2427000.00	2794000.00	1155000.00	555.70	365.30
16.00	598.90	206.40	1362000.00	1362000.00	2600000.00	1626000.00	2578000.00	2578000.00	2794000.00	1155000.00	605.50	182.20
17.00	651.50	7.80	1367000.00	1367000.00	2600000.00	1625000.00	2724000.00	2724000.00	2794000.00	1155000.00	653.50	0.00
18.00	653.50	0.00	1371000.00	1371000.00	2600000.00	1625000.00	2807000.00	2807000.00	2794000.00	1155000.00	627.90	0.00
19.00	627.90	0.00	1372000.00	1372000.00	2600000.00	1625000.00	2834000.00	2834000.00	2794000.00	1155000.00	601.90	0.00
20.00	601.90	0.00	1373000.00	1373000.00	2600000.00	1625000.00	2859000.00	2859000.00	2794000.00	1155000.00	583.20	0.00
21.00	583.20	0.00	1374000.00	1374000.00	2601000.00	1624000.00	2880000.00	2880000.00	2794000.00	1155000.00	570.30	0.00
22.00	570.30	0.00	1375000.00	1375000.00	2601000.00	1624000.00	2896000.00	2896000.00	2794000.00	1155000.00	561.30	0.00
23.00	561.30	0.00	1375000.00	1375000.00	2601000.00	1624000.00	2908000.00	2908000.00	2794000.00	1155000.00	554.90	0.00
24.00	554.90	0.00	1376000.00	1376000.00	2601000.00	1623000.00	2918000.00	2918000.00	2794000.00	1155000.00	550.40	0.00
25.00	550.40	0.00	1376000.00	1376000.00	2601000.00	1623000.00	2925000.00	2925000.00	2794000.00	1155000.00	547.00	0.00
26.00												

Appendix III – EES Raw Results

i	h_c_sig[i]	h_c_sil[i]	h_p0e[i]	h_p0i[i]	h_pe[i]	h_pi[i]	h_s0e[i]	h_s0i[i]	h_se[i]	h_se_satg[i]	h_se_satl[i]	h_si[i]	h_si_satg[i]	h_si_satl[i]
	[W/m^2]	[W/m^2]	[J/kg]	[J/kg]	[J/kg]	[J/kg]	[J/kg]	[J/kg]	[J/kg]	[J/kg]	[J/kg]	[J/kg]	[J/kg]	[J/kg]
0.00							536255.00		536255.00	2794000.00	1158000.00			
1.00	0.00	1065.00	1280000.00	1289000.00	1280000.00	1289000.00	756333.00	536255.00	756333.00	2794000.00	1157000.00	536255.00	2794000.00	1158000.00
2.00	0.00	1237.00	1289000.00	1295000.00	1289000.00	1295000.00	916715.00	756333.00	916715.00	2794000.00	1157000.00	756333.00	2794000.00	1157000.00
3.00	0.00	1333.00	1295000.00	1300000.00	1295000.00	1300000.00	1031000.00	916715.00	1031000.00	2794000.00	1156000.00	916715.00	2794000.00	1157000.00
4.00	0.00	1391.00	1300000.00	1303000.00	1300000.00	1303000.00	1112000.00	1031000.00	1112000.00	2794000.00	1156000.00	1031000.00	2794000.00	1156000.00
5.00	0.00	1428.00	1303000.00	1305000.00	1303000.00	1305000.00	1172000.00	1112000.00	1172000.00	2794000.00	1155000.00	1112000.00	2794000.00	1156000.00
6.00	16.66	1436.00	1305000.00	1310000.00	1305000.00	1310000.00	1292000.00	1172000.00	1292000.00	2794000.00	1155000.00	1172000.00	2794000.00	1155000.00
7.00	89.06	1351.00	1310000.00	1315000.00	1310000.00	1315000.00	1413000.00	1292000.00	1413000.00	2794000.00	1155000.00	1292000.00	2794000.00	1155000.00
8.00	148.40	1263.00	1315000.00	1320000.00	1315000.00	1320000.00	1538000.00	1413000.00	1538000.00	2794000.00	1155000.00	1413000.00	2794000.00	1155000.00
9.00	203.20	1171.00	1320000.00	1325000.00	1320000.00	1325000.00	1665000.00	1538000.00	1665000.00	2794000.00	1155000.00	1538000.00	2794000.00	1155000.00
10.00	255.60	1075.00	1325000.00	1330000.00	1325000.00	1330000.00	1795000.00	1665000.00	1795000.00	2794000.00	1155000.00	1665000.00	2794000.00	1155000.00
11.00	306.70	974.50	1330000.00	1336000.00	1330000.00	1336000.00	1929000.00	1795000.00	1929000.00	2794000.00	1155000.00	1795000.00	2794000.00	1155000.00
12.00	356.90	868.70	1336000.00	1341000.00	1336000.00	1341000.00	2066000.00	1929000.00	2066000.00	2794000.00	1155000.00	1929000.00	2794000.00	1155000.00
13.00	406.70	756.50	1341000.00	1347000.00	1341000.00	1347000.00	2207000.00	2066000.00	2207000.00	2794000.00	1155000.00	2066000.00	2794000.00	1155000.00
14.00	456.30	636.80	1347000.00	1353000.00	1347000.00	1353000.00	2352000.00	2207000.00	2352000.00	2794000.00	1155000.00	2207000.00	2794000.00	1155000.00
15.00	505.90	507.50	1353000.00	1359000.00	1353000.00	1359000.00	2501000.00	2352000.00	2501000.00	2794000.00	1155000.00	2352000.00	2794000.00	1155000.00
16.00	555.70	365.30	1359000.00	1365000.00	1359000.00	1365000.00	2654000.00	2501000.00	2654000.00	2794000.00	1155000.00	2501000.00	2794000.00	1155000.00
17.00	605.50	182.20	1365000.00	1370000.00	1365000.00	1370000.00	2794000.00	2654000.00	2794000.00	2794000.00	1155000.00	2654000.00	2794000.00	1155000.00
18.00	653.50	0.00	1370000.00	1371000.00	1370000.00	1371000.00	2820000.00	2794000.00	2820000.00	2794000.00	1155000.00	2794000.00	2794000.00	1155000.00
19.00	627.90	0.00	1371000.00	1373000.00	1371000.00	1373000.00	2848000.00	2820000.00	2848000.00	2794000.00	1155000.00	2820000.00	2794000.00	1155000.00
20.00	601.90	0.00	1373000.00	1374000.00	1373000.00	1374000.00	2871000.00	2848000.00	2871000.00	2794000.00	1155000.00	2848000.00	2794000.00	1155000.00
21.00	583.20	0.00	1374000.00	1374000.00	1374000.00	1374000.00	2889000.00	2871000.00	2889000.00	2794000.00	1155000.00	2871000.00	2794000.00	1155000.00
22.00	570.30	0.00	1374000.00	1375000.00	1374000.00	1375000.00	2903000.00	2889000.00	2903000.00	2794000.00	1155000.00	2889000.00	2794000.00	1155000.00
23.00	561.30	0.00	1375000.00	1375000.00	1375000.00	1375000.00	2914000.00	2903000.00	2914000.00	2794000.00	1155000.00	2903000.00	2794000.00	1155000.00
24.00	554.90	0.00	1375000.00	1376000.00	1375000.00	1376000.00	2922000.00	2914000.00	2922000.00	2794000.00	1155000.00	2914000.00	2794000.00	1155000.00
25.00	550.40	0.00	1376000.00	1376000.00	1376000.00	1376000.00	2928000.00	2922000.00	2928000.00	2794000.00	1154000.00	2922000.00	2794000.00	1155000.00
26.00			1376000.00		1376000.00									

i	k_bar_p[i]	k_bar_sg[i]	k_bar_sl[i]	k_bar_w[i]	k_seg[i]	k_sel[i]	k_sig[i]	k_sil[i]	L_bar[i]	L_e[i]	L_i[i]	MF_bar_s[i]	MF_se[i]	MF_si[i]
	[W/mK]	[W/mk]	[W/mK]	[W/mK]	[W/mK]	[W/mK]	[W/mK]	[W/mK]	[m]	[m]	[m]	[-]	[-]	[-]
0.00					0.00	0.69				0.00			1.00	
1.00	0.58	0.00	0.69	14.00	0.00	0.68	0.00	0.69	0.50	1.00	0.00	1.00	1.00	1.00
2.00	0.58	0.00	0.68	14.00	0.00	0.66	0.00	0.68	1.50	2.00	1.00	1.00	1.00	1.00
3.00	0.58	0.00	0.66	14.00	0.00	0.64	0.00	0.66	2.50	3.00	2.00	1.00	1.00	1.00
4.00	0.57	0.00	0.64	14.00	0.00	0.62	0.00	0.64	3.50	4.00	3.00	1.00	1.00	1.00
5.00	0.57	0.00	0.62	14.00	0.06	0.60	0.00	0.62	4.50	5.00	4.00	1.00	1.00	1.00
6.00	0.57	0.06	0.60	14.00	0.06	0.60	0.06	0.60	5.50	6.00	5.00	1.45	1.90	1.00
7.00	0.57	0.06	0.60	14.00	0.06	0.60	0.06	0.60	6.50	7.00	6.00	2.33	2.76	1.90
8.00	0.57	0.06	0.60	14.00	0.06	0.60	0.06	0.60	7.50	8.00	7.00	3.20	3.64	2.76
9.00	0.57	0.06	0.60	14.00	0.06	0.60	0.06	0.60	8.50	9.00	8.00	4.12	4.61	3.64
10.00	0.57	0.06	0.60	14.00	0.06	0.60	0.06	0.60	9.50	10.00	9.00	5.16	5.71	4.61
11.00	0.56	0.06	0.60	14.00	0.06	0.60	0.06	0.60	10.50	11.00	10.00	6.37	7.03	5.71
12.00	0.56	0.06	0.60	14.00	0.06	0.60	0.06	0.60	11.50	12.00	11.00	7.87	8.71	7.03
13.00	0.56	0.06	0.60	14.00	0.06	0.60	0.06	0.60	12.50	13.00	12.00	9.83	10.96	8.71
14.00	0.56	0.06	0.60	14.00	0.06	0.60	0.06	0.60	13.50	14.00	13.00	12.64	14.32	10.96
15.00	0.56	0.06	0.60	14.00	0.06	0.60	0.06	0.60	14.50	15.00	14.00	17.28	20.22	14.32
16.00	0.55	0.06	0.60	14.00	0.06	0.60	0.06	0.60	15.50	16.00	15.00	27.71	35.19	20.22
17.00	0.55	0.06	0.03	14.00	0.06	0.00	0.06	0.60	16.50	17.00	16.00	18.09	1.00	35.19
18.00	0.55	0.06	0.00	14.00	0.05	0.00	0.06	0.00	17.50	18.00	17.00	1.00	1.00	1.00
19.00	0.55	0.05	0.00	14.00	0.05	0.00	0.05	0.00	18.50	19.00	18.00	1.00	1.00	1.00
20.00	0.55	0.05	0.00	14.00	0.05	0.00	0.05	0.00	19.50	20.00	19.00	1.00	1.00	1.00
21.00	0.55	0.05	0.00	14.00	0.05	0.00	0.05	0.00	20.50	21.00	20.00	1.00	1.00	1.00
22.00	0.55	0.05	0.00	14.00	0.05	0.00	0.05	0.00	21.50	22.00	21.00	1.00	1.00	1.00
23.00	0.55	0.05	0.00	14.00	0.05	0.00	0.05	0.00	22.50	23.00	22.00	1.00	1.00	1.00
24.00	0.55	0.05	0.00	14.00	0.05	0.00	0.05	0.00	23.50	24.00	23.00	1.00	1.00	1.00
25.00	0.55	0.05	0.00	14.00	0.05	0.00	0.05	0.00	24.50	25.00	24.00	1.00	1.00	1.00
26.00														

i	Mu_bar_p[i] [kg/ms]	Mu_bar_sg[i] [kg/ms]	Mu_bar_sl[i] [kg/ms]	Mu_seg[i] [kg/ms]	Mu_sel[i] [kg/ms]	Mu_sig[i] [kg/ms]	Mu_sil[i] [kg/ms]	m_bar_p[i] [kg/s]	m_bar_s[i] [kg/s]	m_bar_sg[i] [kg/s]	m_bar_sl[i] [kg/s]
0.00				0.00	0.00						
1.00	0.00	0.00	0.00	0.00	0.00	0.00	0.00	1.00	0.04	0.00	0.04
2.00	0.00	0.00	0.00	0.00	0.00	0.00	0.00	1.00	0.04	0.00	0.04
3.00	0.00	0.00	0.00	0.00	0.00	0.00	0.00	1.00	0.04	0.00	0.04
4.00	0.00	0.00	0.00	0.00	0.00	0.00	0.00	1.00	0.04	0.00	0.04
5.00	0.00	0.00	0.00	0.00	0.00	0.00	0.00	1.00	0.04	0.00	0.04
6.00	0.00	0.00	0.00	0.00	0.00	0.00	0.00	1.00	0.04	0.00	0.04
7.00	0.00	0.00	0.00	0.00	0.00	0.00	0.00	1.00	0.04	0.01	0.04
8.00	0.00	0.00	0.00	0.00	0.00	0.00	0.00	1.00	0.04	0.01	0.03
9.00	0.00	0.00	0.00	0.00	0.00	0.00	0.00	1.00	0.04	0.01	0.03
10.00	0.00	0.00	0.00	0.00	0.00	0.00	0.00	1.00	0.04	0.01	0.03
11.00	0.00	0.00	0.00	0.00	0.00	0.00	0.00	1.00	0.04	0.02	0.02
12.00	0.00	0.00	0.00	0.00	0.00	0.00	0.00	1.00	0.04	0.02	0.02
13.00	0.00	0.00	0.00	0.00	0.00	0.00	0.00	1.00	0.04	0.02	0.02
14.00	0.00	0.00	0.00	0.00	0.00	0.00	0.00	1.00	0.04	0.03	0.01
15.00	0.00	0.00	0.00	0.00	0.00	0.00	0.00	1.00	0.04	0.03	0.01
16.00	0.00	0.00	0.00	0.00	0.00	0.00	0.00	1.00	0.04	0.04	0.01
17.00	0.00	0.00	0.00	0.00	0.00	0.00	0.00	1.00	0.04	0.04	0.00
18.00	0.00	0.00	0.00	0.00	0.00	0.00	0.00	1.00	0.04	0.04	0.00
19.00	0.00	0.00	0.00	0.00	0.00	0.00	0.00	1.00	0.04	0.04	0.00
20.00	0.00	0.00	0.00	0.00	0.00	0.00	0.00	1.00	0.04	0.04	0.00
21.00	0.00	0.00	0.00	0.00	0.00	0.00	0.00	1.00	0.04	0.04	0.00
22.00	0.00	0.00	0.00	0.00	0.00	0.00	0.00	1.00	0.04	0.04	0.00
23.00	0.00	0.00	0.00	0.00	0.00	0.00	0.00	1.00	0.04	0.04	0.00
24.00	0.00	0.00	0.00	0.00	0.00	0.00	0.00	1.00	0.04	0.04	0.00
25.00	0.00	0.00	0.00	0.00	0.00	0.00	0.00	1.00	0.04	0.04	0.00
26.00											

Appendix III – EES Raw Results

i	m_pe[i]	m_pi[i]	m_se[i]	m_seg[i]	m_sel[i]	m_si[i]	m_sig[i]	m_sil[i]	Nuss_bar_p[i]	Nuss_bar_sg[i]	Nuss_bar_sl[i]	Nuss_seg[i]	Nuss_sel[i]	Nuss_sig[i]	Nuss_sil[i]
	[kg/s]	[kg/s]	[kg/s]	[kg/s]	[kg/s]	[kg/s]	[kg/s]	[kg/s]	[-]	[-]	[-]	[-]	[-]	[-]	[-]
0.00			0.04	0.00	0.04							0.00	38.77		
1.00	1.00	1.00	0.04	0.00	0.04	0.04	0.00	0.04	260.70	0.00	45.65	0.00	45.65	0.00	38.77
2.00	1.00	1.00	0.04	0.00	0.04	0.04	0.00	0.04	262.30	0.00	50.74	0.00	50.74	0.00	45.65
3.00	1.00	1.00	0.04	0.00	0.04	0.04	0.00	0.04	263.50	0.00	54.75	0.00	54.75	0.00	50.74
4.00	1.00	1.00	0.04	0.00	0.04	0.04	0.00	0.04	264.30	0.00	57.99	0.00	57.99	0.00	54.75
5.00	1.00	1.00	0.04	0.00	0.04	0.04	0.00	0.04	264.90	0.04	59.41	7.54	59.42	0.00	57.99
6.00	1.00	1.00	0.04	0.00	0.04	0.04	0.00	0.04	265.70	9.07	59.25	40.31	55.90	7.54	59.42
7.00	1.00	1.00	0.04	0.01	0.03	0.04	0.00	0.04	266.70	43.55	55.46	67.17	52.25	40.31	55.90
8.00	1.00	1.00	0.04	0.01	0.03	0.04	0.01	0.03	267.80	72.02	51.50	91.98	48.45	67.17	52.25
9.00	1.00	1.00	0.04	0.01	0.03	0.04	0.01	0.03	268.90	98.45	47.37	115.70	44.48	91.98	48.45
10.00	1.00	1.00	0.04	0.02	0.02	0.04	0.01	0.03	270.10	123.80	43.02	138.80	40.32	115.70	44.48
11.00	1.00	1.00	0.04	0.02	0.02	0.04	0.02	0.02	271.20	148.70	38.43	161.60	35.94	138.80	40.32
12.00	1.00	1.00	0.04	0.02	0.02	0.04	0.02	0.02	272.50	173.20	33.56	184.10	31.30	161.60	35.94
13.00	1.00	1.00	0.04	0.03	0.01	0.04	0.02	0.02	273.80	197.60	28.33	206.60	26.35	184.10	31.30
14.00	1.00	1.00	0.04	0.03	0.01	0.04	0.03	0.01	275.10	222.00	22.68	229.10	21.00	206.60	26.35
15.00	1.00	1.00	0.04	0.03	0.01	0.04	0.03	0.01	276.50	246.60	16.43	251.60	15.11	229.10	21.00
16.00	1.00	1.00	0.04	0.04	0.00	0.04	0.03	0.01	278.00	271.20	8.54	274.20	7.54	251.60	15.11
17.00	1.00	1.00	0.04	0.04	0.00	0.04	0.04	0.00	279.40	295.00	0.32	296.00	0.00	274.20	7.54
18.00	1.00	1.00	0.04	0.04	0.00	0.04	0.04	0.00	280.20	296.00	0.00	287.20	0.00	296.00	0.00
19.00	1.00	1.00	0.04	0.04	0.00	0.04	0.04	0.00	280.60	287.20	0.00	277.50	0.00	287.20	0.00
20.00	1.00	1.00	0.04	0.04	0.00	0.04	0.04	0.00	280.90	277.50	0.00	270.10	0.00	277.50	0.00
21.00	1.00	1.00	0.04	0.04	0.00	0.04	0.04	0.00	281.10	270.10	0.00	264.70	0.00	270.10	0.00
22.00	1.00	1.00	0.04	0.04	0.00	0.04	0.04	0.00	281.30	264.70	0.00	260.70	0.00	264.70	0.00
23.00	1.00	1.00	0.04	0.04	0.00	0.04	0.04	0.00	281.40	260.70	0.00	257.70	0.00	260.70	0.00
24.00	1.00	1.00	0.04	0.04	0.00	0.04	0.04	0.00	281.50	257.70	0.00	255.60	0.00	257.70	0.00
25.00	1.00	1.00	0.04	0.04	0.00	0.04	0.04	0.00	281.60	255.60	0.00	253.90	0.00	255.60	0.00
26.00	1.00														

i	phi_bar_s[i]	Phi_se[i]	Phi_si[i]	Pr_bar_p[i]	Pr_bar_sg[i]	Pr_bar_sl[i]	Pr_seg[i]	Pr_sel[i]	Pr_sig[i]	Pr_sil[i]	P_bar_p[i]	P_bar_s[i]	P_p0e[i]	P_p0i[i]
	[-]	[-]	[-]	[-]	[-]	[-]	[-]	[-]	[-]	[-]	[Pa]	[Pa]	[Pa]	[Pa]
0.00		1.00					0.00	1.36						
1.00	1.00	1.00	1.00	0.84	0.00	1.36	0.00	0.99	0.00	1.36	15500000.00	5049000.00	15500000.00	15490000.00
2.00	1.00	1.00	1.00	0.84	0.00	0.99	0.00	0.87	0.00	0.99	15490000.00	5040000.00	15490000.00	15490000.00
3.00	1.00	1.00	1.00	0.84	0.00	0.87	0.00	0.84	0.00	0.87	15480000.00	5032000.00	15490000.00	15480000.00
4.00	1.00	1.00	1.00	0.84	0.00	0.84	0.00	0.83	0.00	0.84	15470000.00	5024000.00	15480000.00	15470000.00
5.00	6.50	11.99	1.00	0.84	0.01	0.83	1.45	0.83	0.00	0.83	15470000.00	5016000.00	15470000.00	15460000.00
6.00	8.47	4.94	11.99	0.84	1.45	0.83	1.45	0.83	1.45	0.83	15460000.00	5010000.00	15460000.00	15460000.00
7.00	4.37	3.80	4.94	0.85	1.45	0.83	1.45	0.83	1.45	0.83	15450000.00	5008000.00	15460000.00	15450000.00
8.00	3.52	3.23	3.80	0.85	1.45	0.83	1.45	0.83	1.45	0.83	15450000.00	5007000.00	15450000.00	15440000.00
9.00	3.04	2.85	3.23	0.85	1.45	0.83	1.45	0.83	1.45	0.83	15440000.00	5006000.00	15440000.00	15430000.00
10.00	2.71	2.57	2.85	0.85	1.45	0.83	1.45	0.83	1.45	0.83	15430000.00	5005000.00	15430000.00	15430000.00
11.00	2.46	2.34	2.57	0.86	1.45	0.83	1.45	0.83	1.45	0.83	15420000.00	5004000.00	15430000.00	15420000.00
12.00	2.24	2.15	2.34	0.86	1.45	0.83	1.45	0.83	1.45	0.83	15420000.00	5004000.00	15420000.00	15410000.00
13.00	2.06	1.97	2.15	0.86	1.45	0.83	1.45	0.83	1.45	0.83	15410000.00	5003000.00	15410000.00	15410000.00
14.00	1.88	1.80	1.97	0.87	1.45	0.83	1.45	0.83	1.45	0.83	15400000.00	5003000.00	15410000.00	15400000.00
15.00	1.71	1.62	1.80	0.87	1.45	0.83	1.45	0.83	1.45	0.83	15400000.00	5002000.00	15400000.00	15390000.00
16.00	1.52	1.42	1.62	0.87	1.45	0.83	1.45	0.83	1.45	0.83	15390000.00	5002000.00	15390000.00	15390000.00
17.00	1.21	1.00	1.42	0.88	1.45	0.04	1.45	0.00	1.45	0.83	15380000.00	5002000.00	15390000.00	15380000.00
18.00	1.00	1.00	1.00	0.88	1.45	0.00	1.36	0.00	1.45	0.00	15370000.00	5002000.00	15380000.00	15370000.00
19.00	1.00	1.00	1.00	0.88	1.36	0.00	1.29	0.00	1.36	0.00	15370000.00	5001000.00	15370000.00	15360000.00
20.00	1.00	1.00	1.00	0.88	1.29	0.00	1.24	0.00	1.29	0.00	15360000.00	5001000.00	15360000.00	15360000.00
21.00	1.00	1.00	1.00	0.88	1.24	0.00	1.22	0.00	1.24	0.00	15350000.00	5001000.00	15360000.00	15350000.00
22.00	1.00	1.00	1.00	0.88	1.22	0.00	1.20	0.00	1.22	0.00	15350000.00	5001000.00	15350000.00	15340000.00
23.00	1.00	1.00	1.00	0.88	1.20	0.00	1.18	0.00	1.20	0.00	15340000.00	5000000.00	15340000.00	15340000.00
24.00	1.00	1.00	1.00	0.88	1.18	0.00	1.17	0.00	1.18	0.00	15330000.00	5000000.00	15340000.00	15330000.00
25.00	1.00	1.00	1.00	0.88	1.17	0.00	1.16	0.00	1.17	0.00	15330000.00	5000000.00	15330000.00	15320000.00
26.00													15320000.00	

i	P_pe[i]	P_pi[i]	P_s0e[i]	P_s0i[i]	P_se[i]	P_si[i]	Q_p[i]	Q_s[i]	Q_w[i]	Re_bar_p[i]	Re_bar_sg[i]	Re_bar_sl[i]	Re_seg[i]	Re_sel[i]	Re_sig[i]	Re_sil[i]
	[Pa]	[Pa]	[Pa]	[Pa]	[Pa]	[Pa]	[W]	[W]	[W]	[-]	[-]	[-]	[-]	[-]	[-]	[-]
0.00			5053000.00		5053000.00								0.00	9266.00		
1.00	15500000.00	15490000.00	5044000.00	5053000.00	5044000.00	5053000.00	-8804.00	8804.00	8804.00	125156.00	0.00	13320.00	0.00	13320.00	0.00	9266.00
2.00	15490000.00	15490000.00	5036000.00	5044000.00	5036000.00	5044000.00	-6417.00	6417.00	6417.00	125936.00	0.00	16184.00	0.00	16184.00	0.00	13320.00
3.00	15490000.00	15480000.00	5028000.00	5036000.00	5028000.00	5036000.00	-4574.00	4574.00	4574.00	126503.00	0.00	18186.00	0.00	18186.00	0.00	16184.00
4.00	15480000.00	15470000.00	5020000.00	5028000.00	5020000.00	5028000.00	-3248.00	3248.00	3248.00	126908.00	0.00	19612.00	0.00	19612.00	0.00	18186.00
5.00	15470000.00	15460000.00	5012000.00	5020000.00	5012000.00	5020000.00	-2397.00	2397.00	2397.00	127203.00	5.84	20170.00	1149.00	20173.00	0.00	19612.00
6.00	15460000.00	15460000.00	5009000.00	5012000.00	5009000.00	5012000.00	-4791.00	4791.00	4791.00	127577.00	1535.00	20104.00	9416.00	18692.00	1149.00	20173.00
7.00	15460000.00	15450000.00	5007000.00	5009000.00	5007000.00	5009000.00	-4878.00	4878.00	4878.00	128081.00	10430.00	18510.00	17827.00	17177.00	9416.00	18692.00
8.00	15450000.00	15440000.00	5006000.00	5007000.00	5006000.00	5007000.00	-4980.00	4980.00	4980.00	128597.00	19506.00	16874.00	26411.00	15630.00	17827.00	17177.00
9.00	15440000.00	15430000.00	5005000.00	5006000.00	5005000.00	5006000.00	-5095.00	5095.00	5095.00	129126.00	28802.00	15199.00	35192.00	14047.00	26411.00	15630.00
10.00	15430000.00	15430000.00	5004000.00	5005000.00	5004000.00	5005000.00	-5221.00	5221.00	5221.00	129671.00	38349.00	13478.00	44188.00	12425.00	35192.00	14047.00
11.00	15430000.00	15420000.00	5004000.00	5004000.00	5004000.00	5004000.00	-5357.00	5357.00	5357.00	130232.00	48171.00	11708.00	53418.00	10762.00	44188.00	12425.00
12.00	15420000.00	15410000.00	5003000.00	5004000.00	5003000.00	5004000.00	-5500.00	5500.00	5500.00	130810.00	58291.00	9884.00	62895.00	9054.00	53418.00	10762.00
13.00	15410000.00	15410000.00	5003000.00	5003000.00	5003000.00	5003000.00	-5651.00	5651.00	5651.00	131407.00	68728.00	8003.00	72631.00	7299.00	62895.00	9054.00
14.00	15410000.00	15400000.00	5003000.00	5003000.00	5003000.00	5003000.00	-5806.00	5806.00	5806.00	132023.00	79496.00	6062.00	82634.00	5497.00	72631.00	7299.00
15.00	15400000.00	15390000.00	5002000.00	5003000.00	5002000.00	5003000.00	-5968.00	5968.00	5968.00	132661.00	90612.00	4059.00	92916.00	3644.00	82634.00	5497.00
16.00	15390000.00	15380000.00	5002000.00	5002000.00	5002000.00	5002000.00	-6111.00	6111.00	6111.00	133316.00	102052.00	1997.00	103443.00	1746.00	92916.00	3644.00
17.00	15380000.00	15380000.00	5002000.00	5002000.00	5002000.00	5002000.00	-6085.00	6085.00	6085.00	133959.00	113425.00	74.77	113872.00	0.00	103443.00	1746.00
18.00	15380000.00	15370000.00	5002000.00	5002000.00	5001000.00	5002000.00	-1533.00	1533.00	1533.00	134363.00	113872.00	0.00	113244.00	0.00	113872.00	0.00
19.00	15370000.00	15360000.00	5001000.00	5002000.00	5001000.00	5001000.00	-1266.00	1266.00	1266.00	134522.00	113244.00	0.00	111437.00	0.00	113244.00	0.00
20.00	15360000.00	15360000.00	5001000.00	5001000.00	5001000.00	5001000.00	-958.80	958.80	958.80	134650.00	111437.00	0.00	109630.00	0.00	111437.00	0.00
21.00	15360000.00	15350000.00	5001000.00	5001000.00	5001000.00	5001000.00	-729.10	729.10	729.10	134747.00	109630.00	0.00	108141.00	0.00	109630.00	0.00
22.00	15350000.00	15340000.00	5001000.00	5001000.00	5000000.00	5001000.00	-554.70	554.70	554.70	134822.00	108141.00	0.00	106980.00	0.00	108141.00	0.00
23.00	15340000.00	15340000.00	5000000.00	5001000.00	5000000.00	5000000.00	-422.10	422.10	422.10	134881.00	106980.00	0.00	106093.00	0.00	106980.00	0.00
24.00	15340000.00	15330000.00	5000000.00	5000000.00	5000000.00	5000000.00	-321.30	321.30	321.30	134926.00	106093.00	0.00	105418.00	0.00	106093.00	0.00
25.00	15330000.00	15320000.00	5000000.00	5000000.00	5000000.00	5000000.00	-244.70	244.70	244.70	134962.00	105418.00	0.00	104905.00	0.00	105418.00	0.00
26.00	15320000.00															

i	rho_bar_p[i]	rho_bar_s[i]	rho_bar_sg[i]	rho_bar_sl[i]	Rho_pe[i]	rho_pi[i]	Rho_se[i]	rho_seg[i]	Rho_sel[i]	rho_si[i]	rho_sig[i]	rho_sil[i]	R_bar_w[i]	SF_bar_s[i]	SF_se[i]	SF_si[i]
	[kg/m^3]	[kg/m^3]	[kg/m^3]	[kg/m^3]	[kg/m^3]	[kg/m^3]	[kg/m^3]	[kg/m^3]	[kg/m^3]	[kg/m^3]	[kg/m^3]	[kg/m^3]	[K/W]	[-]	[-]	[-]
0.00							939.90	0.00	939.90						0.00	
1.00	746.20	917.10	0.00	939.90	747.80	744.70	891.80	0.00	891.80	939.90	0.00	939.90	0.00	0.00	0.00	0.00
2.00	743.50	871.80	0.00	891.80	744.70	742.30	850.30	0.00	850.30	891.80	0.00	891.80	0.00	0.00	0.00	0.00
3.00	741.50	834.20	0.00	850.30	742.30	740.60	817.20	0.00	817.20	850.30	0.00	850.30	0.00	0.00	0.00	0.00
4.00	740.00	804.60	0.00	817.20	740.60	739.40	791.60	0.00	791.60	817.20	0.00	817.20	0.00	0.00	0.00	0.00
5.00	739.00	781.70	0.13	791.50	739.40	738.50	597.50	25.41	777.30	791.60	0.00	791.60	0.00	0.39	0.78	0.00
6.00	737.60	326.10	25.40	777.30	738.50	736.70	224.20	25.40	777.30	597.50	25.41	777.30	0.00	0.70	0.61	0.78
7.00	735.80	170.20	25.39	777.30	736.70	734.90	137.10	25.39	777.40	224.20	25.40	777.30	0.00	0.55	0.50	0.61
8.00	734.00	114.40	25.38	777.40	734.90	733.10	98.16	25.38	777.40	137.10	25.39	777.40	0.00	0.46	0.43	0.50
9.00	732.10	85.70	25.38	777.40	733.10	731.20	76.05	25.38	777.40	98.16	25.38	777.40	0.00	0.40	0.37	0.43
10.00	730.20	68.19	25.37	777.40	731.20	729.20	61.80	25.37	777.40	76.05	25.38	777.40	0.00	0.35	0.33	0.37
11.00	728.20	56.37	25.37	777.40	729.20	727.10	51.83	25.37	777.40	61.80	25.37	777.40	0.00	0.32	0.30	0.33
12.00	726.10	47.86	25.37	777.40	727.10	725.10	44.46	25.37	777.40	51.83	25.37	777.40	0.00	0.29	0.28	0.30
13.00	724.00	41.44	25.37	777.40	725.10	722.90	38.80	25.37	777.40	44.46	25.37	777.40	0.00	0.27	0.26	0.28
14.00	721.80	36.42	25.36	777.40	722.90	720.70	34.31	25.36	777.40	38.80	25.37	777.40	0.00	0.26	0.25	0.26
15.00	719.50	32.38	25.36	777.40	720.70	718.30	30.66	25.36	777.40	34.31	25.36	777.40	0.00	0.25	0.25	0.25
16.00	717.10	29.08	25.36	777.50	718.30	716.00	27.65	25.36	777.50	30.66	25.36	777.40	0.00	0.25	0.26	0.25
17.00	715.00	26.45	25.36	33.28	716.00	714.00	25.35	25.35	0.00	27.65	25.36	777.50	0.00	0.13	0.00	0.26
18.00	713.70	25.01	25.35	0.00	714.00	713.40	24.67	24.67	0.00	25.35	25.35	0.00	0.00	0.00	0.00	0.00
19.00	713.10	24.29	24.67	0.00	713.40	712.90	23.93	23.93	0.00	24.67	24.67	0.00	0.00	0.00	0.00	0.00
20.00	712.70	23.63	23.93	0.00	712.90	712.50	23.34	23.34	0.00	23.93	23.93	0.00	0.00	0.00	0.00	0.00
21.00	712.30	23.12	23.34	0.00	712.50	712.20	22.90	22.90	0.00	23.34	23.34	0.00	0.00	0.00	0.00	0.00
22.00	712.00	22.74	22.90	0.00	712.20	711.90	22.57	22.57	0.00	22.90	22.90	0.00	0.00	0.00	0.00	0.00
23.00	711.80	22.45	22.57	0.00	711.90	711.70	22.33	22.33	0.00	22.57	22.57	0.00	0.00	0.00	0.00	0.00
24.00	711.70	22.24	22.33	0.00	711.70	711.60	22.14	22.14	0.00	22.33	22.33	0.00	0.00	0.00	0.00	0.00
25.00	711.50	22.07	22.14	0.00	711.60	711.50	22.01	22.01	0.00	22.14	22.14	0.00	0.00	0.00	0.00	0.00
26.00					711.50											

Appendix III – EES Raw Results

i	s_bar_p[i]	s_bar_s[i]	S_energy_p[i]	S_energy_s[i]	S_mass_p[i]	S_mass_s[i]	S_momentum_p[i]	S_momentum_s[i]	S_pressure_p[i]	S_pressure_s[i]	T_bar_p[i]	T_bar_s[i]	T_bar_wp[i]	T_bar_ws[i]
	[J/kgK]	[J/kgK]	[W/s]	[W/s]	[kg/m^3 s]	[kg/m^3 s]	[kg/s]	[kg/s]	[Pa/s]	[Pa/s]	[K]	[K]	[K]	[K]
0.00														
1.00	3132.00	1863.00	16.38	0.89	-0.01	0.00	0.00	0.00	-0.45	-109.90	563.10	425.60	549.90	516.20
2.00	3145.00	2289.00	13.68	3.62	0.00	0.00	0.00	0.00	-1.65	-109.90	564.60	469.10	555.00	530.40
3.00	3155.00	2572.00	9.30	5.41	0.00	0.00	0.00	0.00	-2.86	-109.90	565.60	499.40	558.80	541.30
4.00	3162.00	2764.00	4.00	7.01	0.00	0.00	0.00	0.00	-4.08	-109.90	566.40	520.10	561.50	549.10
5.00	3167.00	2897.00	1.68	9.12	0.00	0.00	0.00	0.00	-5.31	-109.80	566.90	532.90	563.30	554.10
6.00	3173.00	3065.00	-2.57	9.18	0.00	-0.06	0.00	0.00	-6.56	-109.50	567.60	537.20	560.40	542.10
7.00	3182.00	3289.00	0.46	3.57	0.00	-0.01	0.00	0.00	-7.80	-109.10	568.50	537.20	561.20	542.50
8.00	3191.00	3518.00	-3.90	1.03	0.00	-0.01	0.00	0.00	-9.04	-108.90	569.40	537.20	562.00	542.90
9.00	3200.00	3753.00	5.14	6.50	0.00	-0.01	0.00	0.00	-10.27	-108.60	570.30	537.20	562.80	543.30
10.00	3209.00	3992.00	-7.76	5.27	0.00	0.00	0.00	0.00	-11.51	-108.40	571.30	537.10	563.50	543.60
11.00	3218.00	4238.00	14.54	20.02	-0.01	0.00	0.00	0.00	-12.72	-108.20	572.30	537.10	564.30	543.80
12.00	3227.00	4491.00	-21.20	44.52	0.01	0.00	0.00	0.00	-13.95	-108.00	573.30	537.10	565.10	544.10
13.00	3237.00	4750.00	37.44	51.17	-0.01	0.00	0.00	0.00	-15.14	-107.80	574.30	537.10	565.90	544.30
14.00	3247.00	5016.00	-58.25	44.60	0.02	0.00	0.00	0.00	-16.38	-107.50	575.30	537.10	566.70	544.50
15.00	3258.00	5290.00	98.44	65.25	-0.04	0.00	0.00	0.00	-17.52	-107.30	576.40	537.10	567.60	544.80
16.00	3268.00	5570.00	-158.90	91.54	0.06	0.00	0.00	0.00	-18.79	-107.10	577.50	537.10	568.50	545.10
17.00	3277.00	5843.00	-399.00	33203.00	0.16	-0.55	0.00	0.00	-20.39	-106.30	578.40	537.10	569.50	546.20
18.00	3283.00	5997.00	21.34	42011.00	-0.01	-0.90	0.00	0.00	-21.10	-100.90	579.00	540.10	576.80	570.90
19.00	3286.00	6046.00	15.13	10209.00	-0.01	-0.27	0.00	0.00	-20.98	-88.34	579.30	546.70	577.40	572.60
20.00	3288.00	6093.00	7.14	864.70	0.00	-0.02	0.00	0.00	-20.91	-74.00	579.50	553.50	578.10	574.40
21.00	3289.00	6130.00	3.50	-1265.00	0.00	0.03	0.00	0.00	-20.88	-61.66	579.70	559.30	578.60	575.80
22.00	3290.00	6159.00	1.95	-1458.00	0.00	0.03	0.00	0.00	-20.86	-50.26	579.80	564.00	579.00	576.80
23.00	3291.00	6180.00	1.16	-1225.00	0.00	0.03	0.00	0.00	-20.85	-39.17	579.90	567.70	579.20	577.60
24.00	3292.00	6197.00	0.77	-954.00	0.00	0.02	0.00	0.00	-20.84	-28.19	579.90	570.60	579.50	578.20
25.00	3292.00	6209.00	0.42	-727.40	0.00	0.02	0.00	0.00	-20.84	-17.26	580.00	572.80	579.60	578.70
26.00														

i	T_pe[i]	T_pi[i]	T_se[i]	T_si[i]	V_bar_p[i]	V_bar_s[i]	V_pe[i]	V_pi[i]	V_se[i]	V_si[i]	X_bar_s[i]	X_se[i]	X_si[i]	Z_bar[i]	z_e[i]	z_i[i]
	[K]	[K]	[K]	[K]	[m/s]	[m/s]	[m/s]	[m/s]	[m/s]	[m/s]	[-]	[-]	[m]	[m]	[m]	[m]
0.00			400.00						0.09			0.00			0.00	
1.00	562.30	564.00	451.10	400.00	0.39	0.09	0.39	0.39	0.09	0.09	0.00	0.00	0.00	0.50	1.00	0.00
2.00	564.00	565.20	487.10	451.10	0.39	0.09	0.39	0.39	0.09	0.09	0.00	0.00	0.00	1.50	2.00	1.00
3.00	565.20	566.10	511.70	487.10	0.39	0.10	0.39	0.39	0.10	0.09	0.00	0.00	0.00	2.50	3.00	2.00
4.00	566.10	566.70	528.50	511.70	0.39	0.10	0.39	0.39	0.10	0.10	0.00	0.00	0.00	3.50	4.00	3.00
5.00	566.70	567.10	537.20	528.50	0.39	0.10	0.39	0.39	0.10	0.10	0.01	0.01	0.00	4.50	5.00	4.00
6.00	567.10	568.00	537.20	537.20	0.39	0.18	0.39	0.39	0.25	0.10	0.05	0.08	0.01	5.50	6.00	5.00
7.00	568.00	568.90	537.20	537.20	0.39	0.36	0.39	0.39	0.48	0.25	0.12	0.16	0.08	6.50	7.00	6.00
8.00	568.90	569.90	537.20	537.20	0.39	0.60	0.39	0.40	0.71	0.48	0.20	0.23	0.16	7.50	8.00	7.00
9.00	569.90	570.80	537.20	537.20	0.40	0.83	0.40	0.40	0.95	0.71	0.27	0.31	0.23	8.50	9.00	8.00
10.00	570.80	571.80	537.10	537.20	0.40	1.07	0.40	0.40	1.20	0.95	0.35	0.39	0.31	9.50	10.00	9.00
11.00	571.80	572.80	537.10	537.10	0.40	1.32	0.40	0.40	1.45	1.20	0.43	0.47	0.39	10.50	11.00	10.00
12.00	572.80	573.80	537.10	537.10	0.40	1.58	0.40	0.40	1.71	1.45	0.51	0.56	0.47	11.50	12.00	11.00
13.00	573.80	574.80	537.10	537.10	0.40	1.84	0.40	0.40	1.97	1.71	0.60	0.64	0.56	12.50	13.00	12.00
14.00	574.80	575.80	537.10	537.10	0.40	2.11	0.40	0.40	2.24	1.97	0.69	0.73	0.64	13.50	14.00	13.00
15.00	575.80	577.00	537.10	537.10	0.40	2.38	0.40	0.40	2.52	2.24	0.78	0.82	0.73	14.50	15.00	14.00
16.00	577.00	578.00	537.10	537.10	0.40	2.66	0.40	0.40	2.81	2.52	0.87	0.91	0.82	15.50	16.00	15.00
17.00	578.00	578.90	537.20	537.10	0.41	2.96	0.40	0.41	3.11	2.81	0.96	1.00	0.91	16.50	17.00	16.00
18.00	578.90	579.20	543.10	537.20	0.41	3.21	0.41	0.41	3.32	3.11	1.00	1.00	1.00	17.50	18.00	17.00
19.00	579.20	579.40	550.30	543.10	0.41	3.38	0.41	0.41	3.43	3.32	1.00	1.00	1.00	18.50	19.00	18.00
20.00	579.40	579.60	556.70	550.30	0.41	3.48	0.41	0.41	3.53	3.43	1.00	1.00	1.00	19.50	20.00	19.00
21.00	579.60	579.70	561.90	556.70	0.41	3.57	0.41	0.41	3.60	3.53	1.00	1.00	1.00	20.50	21.00	20.00
22.00	579.70	579.80	566.10	561.90	0.41	3.63	0.41	0.41	3.66	3.60	1.00	1.00	1.00	21.50	22.00	21.00
23.00	579.80	579.90	569.30	566.10	0.41	3.69	0.41	0.41	3.71	3.66	1.00	1.00	1.00	22.50	23.00	22.00
24.00	579.90	580.00	571.90	569.30	0.41	3.73	0.41	0.41	3.74	3.71	1.00	1.00	1.00	23.50	24.00	23.00
25.00	580.00	580.00	573.80	571.90	0.41	3.76	0.41	0.41	3.77	3.74	1.00	1.00	1.00	24.50	25.00	24.00
26.00	580.00						0.41									